MODELLING THE SPREAD OF ATROPHY IN HUNTINGTON'S DISEASE USING NETWORK DIFFUSION MODEL (NDM)

MADAN K C

~

A thesis submitted in fulfilment of the requirements for the degree of:

Master of Philosophy

Mary MacKillop Institute for Health Research,
Faculty of Health Sciences
Australian Catholic University

Graduate Research Office
250 Victoria Parade
Fitzroy, Victoria, 3065

1st September 2021

Statement of Authorship and Sources

I certify that except where due acknowledgement has been made, the work is that of the author alone; the work has not been submitted previously, in whole or in part, to qualify for any other academic award; the content of the thesis is the result of work which has been carried out since the official commencement date of the approved research program and any editorial work, paid or unpaid, carried out by a third party is acknowledged, and ethics procedures and guidelines have been followed. Unless otherwise stated, all work comprising this thesis has been undertaken by the candidate. This candidature commenced at the Australian Catholic University (ACU) in June 2019.

[signature redacted]

Madan K C

Supervisory Panel

It is acknowledged that the work comprising this thesis was supervised by the following ACU staff members:

Principal Supervisor: Dr. Govinda Poudel (ACU, Melbourne, VIC)

Co-Supervisor: Prof. Ester Cerin (ACU, Melbourne, VIC)

Acknowledgements

This work was carried out in the Mary MacKillop Institute for Health Research Lab, Faculty of Health Sciences, Australian Catholic University, during the years 2019-2021. First and foremost, I would like to thank my supervisor Dr. Govinda Poudel and co-supervisor Prof. Ester Cerin for taking me as their research student. Before I joined the research degree course I had very limited knowledge in computational neuroscience as I majored in Biomedical Engineering. I am forever indebted to my supervisors for what I have achieved while under their supervision. I greatly appreciate the effort with which Dr. Govinda Poudel helped me learn how to plan and perform the research activities described here. I express my sincere thanks to Prof. Ester Cerin for agreeing to act as my co-supervisor. Her guidance, support, and training for statistical approach and other essential suggestions was unforgettable. Dr Govinda Poudel and Prof Ester Cerin not only helped me to perform the study but also to discuss and present the data. Without their continual support and advice throughout my studies I would not have been able to finish my project. Dr Govinda Poudel's broad experience, expertise, wisdom, and kindness never ceased to impress and educate me. Despite his never-ending hectic schedule, his door was always open to me. Thank you, I could not have asked for a better mentor.

I would also like to give special thanks to all staff member of Mary MacKillop Institute for Health Research Lab, Faculty of Health Sciences, Australian Catholic University for their continuous support and guidance wherever needed. Their continuous support made my project so much easier.

A special thanks to the panel members present at my all-candidature review presentations and to their guidelines and suggestions.

Finally, I would like to thank my parents, wife, brother, my wife's family, who have supported us coming abroad to further my education.

Abstract

Huntington's disease (HD) is a progressive neurodegeneration which has symptoms such as movement dysfunction, cognitive abnormalities, and psychiatric disturbances. Neurodegeneration in HD is characterised by pathology that spreads throughout the cortico-striatal network. There is growing recognition that the transfer of mutant huntingtin (mHTT) protein is cellular and shaped by structural organisation of the brain, provides a general framework underlying progressive spread of degeneration in HD. However, relatively little is known regarding how such progression occurs over time. This knowledge is critical to inform future drug discovery efforts where neuroimaging methodology can be used to develop the potential therapeutic compounds in targeting vulnerable neural circuits in HD.

This research aimed to develop and apply a novel graph theoretical network diffusion model to predict how and where in the brain neurodegenerative process is seeded in HD. We used longitudinal MRI scans (N=106 Premanifest HD (pre-HD) and N=89 Healthy Controls), collected 12 and 24 months from the Track-On HD study. We implemented Network diffusion model (NDM), which was previously applied to symptomatic individuals with HD, in the Premanifest HD population.

To evaluate the spatial patterns in change in brain volume of HD brain regions compared to controls, we segmented the T1-weighted structural MRI scans into 82 brain regions using FreeSurfer based tools. A linear mixed-effects model is statistically used to evaluate the brain volume differences (across 82 brain regions) in different time visits. The outcome of this statistical approach revealed that degeneration over time in pre-HD compared to controls shows extensively higher ($p<0.05$). The putamen and caudate showed the highest atrophy sub-cortically. Cortically, the highest atrophy is observed in the visual cortex (lateral occipital) and temporal cortex (superior and middle temporal).

Next, we implemented NDM to simulate the longitudinal pattern of degeneration across the 82 brain regions. The NDM assumes that the linear diffusion of pathological proteins facilitates pathology spread in the HD brain via the brain's structural connectome. Therefore, we used a canonical connectome from the healthy brain (82 x 82 IIT connectome) to simulate the brain's spread process. We found that initiating the diffusion process from pallidum, thalamus, and putamen predicts a pattern of degenerations (predicted atrophy) which is significantly correlated ($p<0.05$, corrected) with longitudinal degeneration measured using MRI scans. However, the predictive ability of NDM was moderate at best (maximum Pearson correlation between predicted and measured atrophy = 0.48, $p <0.0001$). These findings suggest that NDM can only moderately predict the pattern of degeneration in the HD brain.

Overall, this thesis explores how NDM can better understand the progression of degeneration in HD. Our comparative study between healthy and patient's groups statistically showed a progressive pattern of atrophy in the cerebrum. Furthermore, the results from NDM suggests that NDM could be helpful to model the progression of atrophy in subcortical and cortical regions in HD. Thus, NDM may build bio-physically informed machine learning algorithms for predicting future degeneration from baseline MRI scans.

Table of Contents

List of Tables

List of Figures

List of Commonly Used Abbreviations

AD	Alzheimer's disease
ADNI	Alzheimer's Disease Neuroimaging Initiative
AIHW	Australian Institute of Health and Welfare
ALS	Amyotrophic lateral sclerosis
ANOVA	Analysis of Variance
CAG	Cytosine, Adenine, and Guanine
CHDI	Cure Huntington's Disease Initiative
DIAN	Dominantly Inherited Alzheimer Network
DLB	Dementia with Lewy Body
DNA	Deoxyribonucleic Acid
DPS	Disease Progression Scores
DTI	Diffusion Tensor Imaging
DWI	Diffusion-Weighted Imaging
EBM	Event-Based Model
ECM	Extracellular Matrix
EPI	Echo-Planar Imaging
eTIV	Estimated Total Intracranial Volume
FOV	Field Of View
FTD	Frontotemporal Dementia
HD	Huntington's Disease
Pre-HD	Premanifest Huntington's Disease
HDCRG	Huntington's Disease Collaborative Research Group
HPC	High Performance Computing

HTT	Huntingtin
IIT	Illinois Institute of Technology
LBD	Lewy Body Dementia
LME	Linear Mixed Effect
MCI	Mild Cognitive Impairment
mHTT	Mutant Huntingtin
MRI	Magnetic Resonance Imaging
MTL	Mid-Temporal Lobe
NDM	Network Diffusion Model
NITRC	Neuro Imaging Tools & Resources Collaboratory
NPM	Nucleated Polymerization Model
PD	Parkinson's disease
PDE	Partial Differential Equation
PET	Positron Emission Tomography
PSP	Progressive Supranuclear Palsy
REML	Restricted Maximum Likelihood
ROI	Region of Interest
SMRI	Structural Magnetic Resonance Imaging
SPECT	Single-Photon Emission Computed Tomography
SPM	Statistical Parametric Mapping
TIV	Total Intracranial Volume
TSE	Transmissible Spongiform Encephalopathies
TVEM	Time-Varying Effect Model
UHDRS	Unified Huntington Disease Rating Scale Outcomes

Overview of Thesis

The human brain is a dynamic network of ~100 billion neurons, comprising ~100 trillion connections. Signals travel between neuronal cell bodies, which manifest as grey matter, via bundles of axons that form white matter pathways. This complex structure can be damaged in many ways, out of which, one common factor being neurodegenerative disorder. Progressive neurodegeneration, an emerging health threat, mainly due to the rising ageing population and population-level exposure to multiple risk factors. Neurodegenerative diseases kill neural tissues through a progressive neuronal degeneration aggregated over a time frame. The most common neurodegenerative conditions includes Alzheimer's disease (AD), Parkinson's disease (PD), Huntington's disease (HD), transmissible spongiform encephalopathies (TSEs or prion sickness), and multiple sclerosis (MS) (Santa-Cecilia, Leite, Del-Bel, & Raisman-Vozari, 2019). In addition, cognitive and neuropsychiatric dysfunction and a loss of physical functions are common symptoms of neurodegenerative diseases.

Currently, we are lacking behind with the complete cure treatment option for any effects of neurodegenerative diseases (Santa-Cecilia et al., 2019). Notably, the ability to track the atrophy progression is relied upon extensive research and development of noble therapeutic agents, in particular, when therapeutic interventions are necessary during stages of non-symptomatic conditions of the disease (Jedynak et al., 2012). Recent advancements of statistical modelling, computational technology and artificial intelligence provide a new avenue in developing noble biomarkers of neurodegenerative conditions (Neil P. Oxtoby & Daniel C. Alexander, 2017). In this study, we have tried to represent a critical assessment of the role of an advanced computational application, network diffusion model (NDM), in identifying and predicting disease progression in premanifest stage of Huntington's Disease (Pre-HD).

This thesis is compiled with six chapters. Chapter one gives the general overview including background, rationale and aims of the thesis. Chapter two provides a brief introduction to neurodegenerative disease by explaining the fundamental biological process involved in a few common types of these disorders (e.g., AD, PD & HD). Finally, we provide a critical review of neuroimaging techniques focusing on magnetic resonance imaging (MRI), including various advanced MRI systems involved in predicting neurodegeneration.

Chapter 3 is focused on addressing the first aim of this research project. This chapter describes the neuroimaging data, analysis, and results from researching longitudinal changes in brain regions volume in premanifest HD. The MRI scans from a longitudinal study (Track-On HD) were statistically analysed utilising linear mixed effect (LME) approach to derive the longitudinal degeneration and spatial distribution of atrophy in premanifest HD individuals. The next chapter uses these spatial maps to compare against the NDM derived maps of atrophy in HD.

In chapter 4, we implement NDM and use it to predict the pattern of neurodegeneration spread in premanifest HD (Pre-HD). This chapter is focused on the mathematical implementation and application of NDM for predicting longitudinal degeneration in pre-HD compared to healthy controls. We used the empirical data obtained from the previous chapter (Chapter 3) to test the predictive ability of NDM in pre-HD. Furthermore, Chapter 5 includes the general discussion of the study, and Chapter 6 describes the future research avenues in this field.

Figure 1: Summary of the Chapters Included in the Thesis

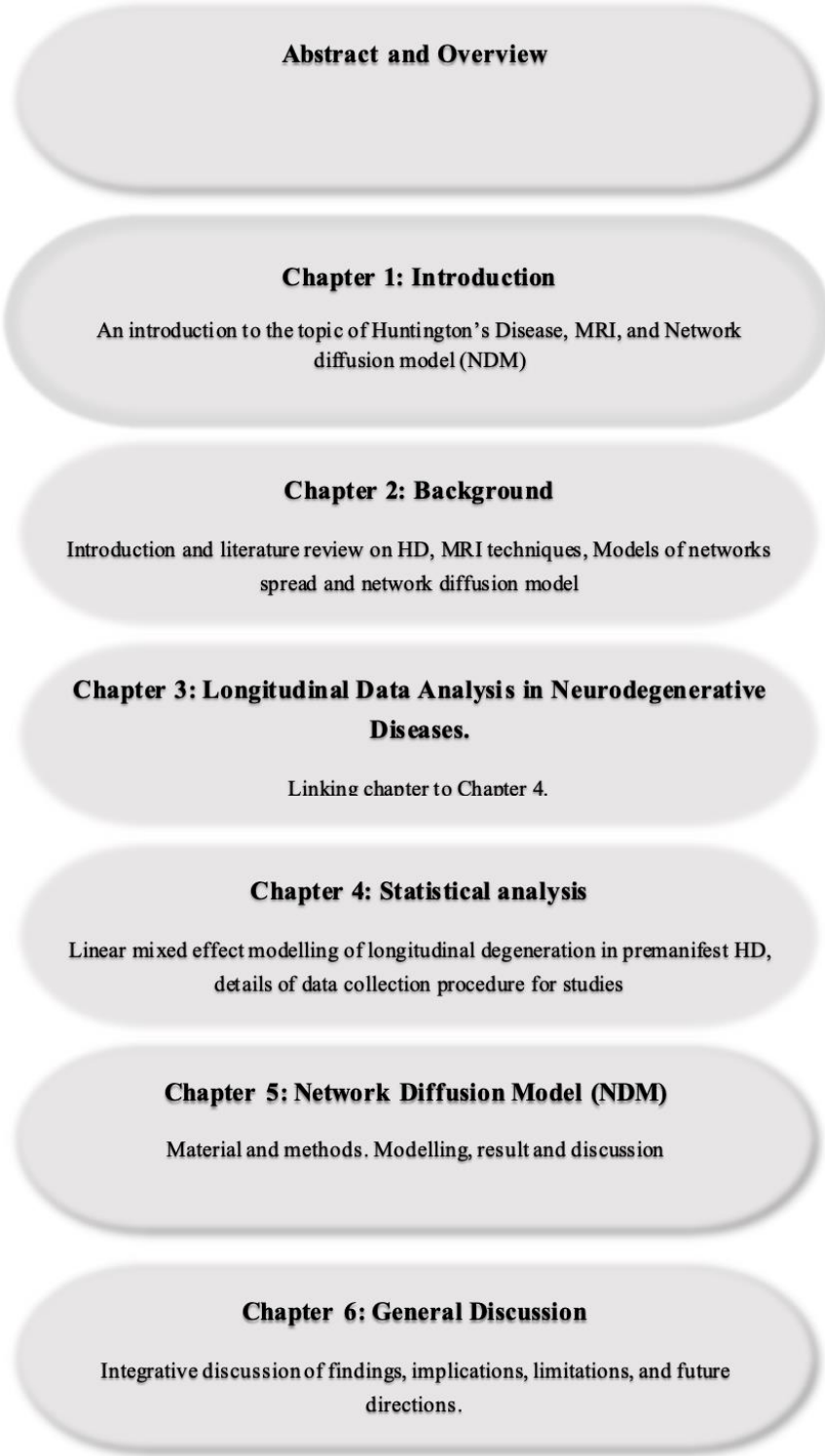

Chapter 1: Introduction

Neurodegenerative diseases caused 16.8% of all deaths globally in 2015 (Feigin et al., (2017). In the same year, in Australia alone, there were 13,496 deaths due to dementia, 1,783 deaths due to Parkinson's disease, 698 deaths due to motor neuron disease, 190 deaths due to multiple sclerosis, and 986 deaths due to other neurological conditions (AIHW, 2018). Globally, more than 50 million people are affected from dementia which is projected to triple by 2050 (AIHW, 2018) . Furthermore, the financial cost of dementia for 2018 was estimated to be 1 trillion US dollars (AIHW, 2018). Despite this threat, we lack robust biomarkers and treatment approaches to address this global health crisis (Santa-Cecilia et al., 2019).

Huntington's disease (HD) is a progressive neurodegeneration which has symptoms such as movement dysfunction, cognitive abnormalities, and psychiatric disturbances. The leading cause of HD is excessive repetition of CAG (cytosine-adenine-guanine) in the huntingtin (HTT) gene, which causes polyglutamine increment in the mutant huntingtin (mHTT) protein (G. R. Poudel, Harding, Egan, & Georgiou-Karistianis, 2019). Chorea which is involuntary motor symptoms due to HD can be diagnosis clinically; although, lack of mental and cognitive dysfunctions takes precedence over motor prodrome.

The prevalence of HD is estimated to be between 5.96 to 13.7 cases per 100,000 members of the population in Australia, northwestern Europe, and North America (Baig, Strong, & Quarrell, 2016). This progressive disorder can begin being symptomatic between 30 to 50 years of age and can last up to 15-20 years after the first clinical diagnosis (Solberg, Filkuková, Frich, & Feragen, 2018). Genetic testing is capable to estimate the number of CAG repeats in total, which can help inform about disease burden and estimated onset time. However, genetic testing alone is not sufficient to track disease progression and the changes occurring in the brain.

Recent advancements in neuroimaging technology (e.g., using high-resolution MRI) have made it possible to visualise structural imbalances and functional changes in regions of the whole

brain, much prior to onset period even in pre symptomatic (pre-HD) stage (Douaud et al., 2006; Georgiou-Karistianis, Scahill, Tabrizi, Squitieri, & Aylward, 2013; N. Z. Hobbs et al., 2010; Müller & Kassubek, 2013; Govinda R. Poudel, Julie C. Stout, et al., 2014). This research has uncovered that sub-cortical region of human brain has highest degeneration making it possible biomarker of atrophy progression. Despite this, our current understanding of how HD pathology spreads in the brain over time remains limited. Furthermore, HD also provides a good model of degeneration that is independent of ageing process.

1.1 Trans-neuronal spread hypothesis

Emerging evidence highlights that neuro-synaptic exchange of mutant huntingtin (mHTT) protein may better clarify the spatial dispersion of pathology in HD brain (G. R. Poudel, Harding, Egan, & Georgiou-Karistianis, 2019). This pathology (mHTT) while examining in mouse model shows trans-synaptic progression (Pecho-Vrieseling et al., 2014). Daniel and Barry (2015) suggested that the trans-neuronal mHTT distribution takes place through the vesicle fusion mechanism across axonal pathways, which leads to the accumulation of mHTT in distant neurons connected by axons. Furthermore, the distribution of pathology in animal models and humans suggests a typical pattern of cortico-striatal spatial progression of degeneration in HD, with the selective early loss of medium spiny projection neurons in the striatal cells (Mitchell, Cooper, & Griffiths, 1999).

Extensive neuronal cell death appears in the other parts of the striatum over time, which further leads to increment of physical structures in the lateral ventricles (Mangiarini et al., 1996). Striatal degeneration is progressive along the dorsomedial to ventrolateral direction (Roos, Pruyt, de Vries, & Bots, 1985; Vonsattel, 2008). Cortical degeneration emerges in close-to-onset premanifest stages of disease, particularly in the regions that are functionally and structurally linked to the striatum (Douaud et al., 2006; Georgiou-Karistianis et al., 2013; Hobbs et al., 2009; Müller & Kassubek, 2013; Govinda R. Poudel, Julie C. Stout, et al., 2014). These disclosures

suggest that normally apparent axonal connections in the frontal cortex may expect an essential part in working with the spread of HD.

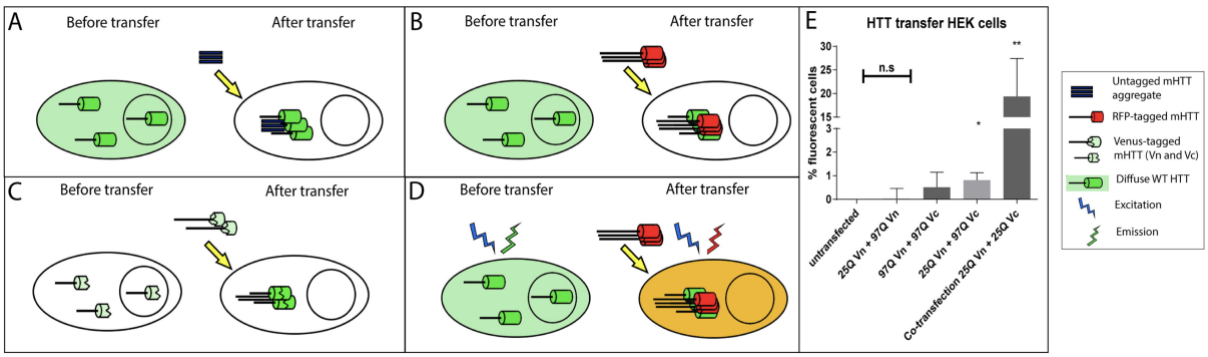

Figure 2: Visualisation of prion-like transfer of mHTT protein as a release and uptake mechanism by donor and acceptor cells respectively in HD

Note: A) shows freely distributed untagged mHTT protein with acceptor cell. B demonstrates the transfer mechanism of both tagged proteins with different fluorophores resulting in co-localisation of both proteins. C: When mixed with two different halves of the fluorophore, transfer mechanism and aggregation of protein result in the complementation of halves of fluorophores. D: an alternative way of visualising sequestration by FRET or FLIM imaging when both proteins are tagged with different fluorophores. E: In vitro quantitative FACS analysis of mHTT transfer in HEK cells (Jansen, Batenburg, Pecho-Vrieseling, & Reits, 2017).

Figure 2 demonstrates the process of prion-like transfer of aggregated proteins between cells HD (Jansen et al., 2017). Overall, various mechanisms have been illustrated to cover the trans-neuronal spread. However, the robust mechanisms of trans-neuronal progression of atrophy and protein aggregation in the HD brain remain to be elucidated.

1.2 Neuroimaging studies of pattern of degeneration in HD

A few large-scale neuroimaging studies in HD have identified patterns of spread of degeneration in an HD brain. Structural MRI studies have illustrated the degeneration progress in the striatum specifically in putamen and caudate is the crucial neuro-pathological feature of HD (Govinda R. Poudel, Julie C. Stout, et al., 2014; Sturrock et al., 2015; S. J. Tabrizi et al., 2009; Sarah J. Tabrizi et al., 2011; Vemuri & Jack, 2010), with other areas outside the striatum demonstrating significant deterioration with disease progression.

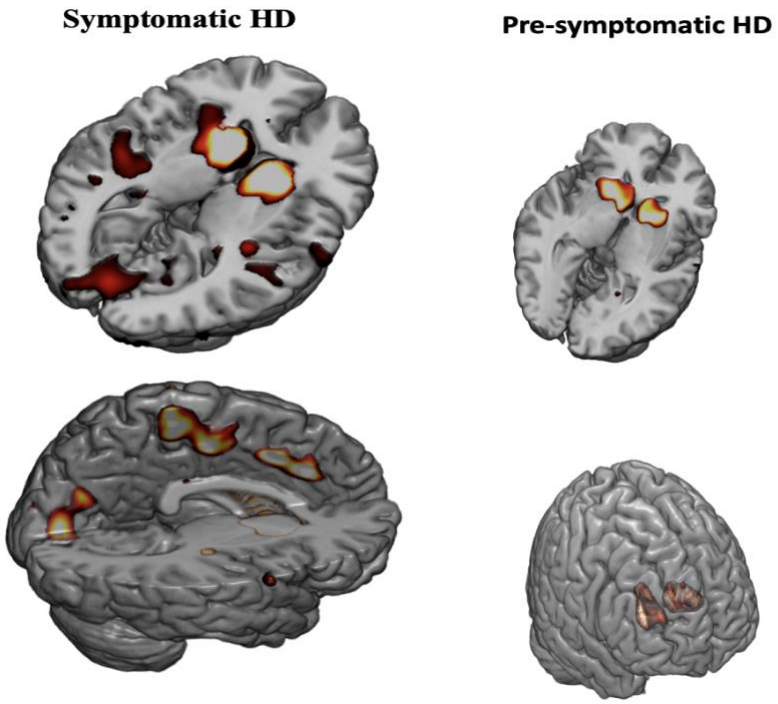

Figure 3: MRI scans show brain degeneration of Pre-Symptomatic and Symptomatic HD with respect to healthy controls (G. R. Poudel, Harding, Egan, & Georgiou-Karistianis, 2019). The red-yellow colours represent degeneration. Degeneration of the striatum is the earliest and most distinctive marker.

MRI is useful for detecting changes in the brain early. These changes have been demonstrated in other neurodegenerative cohorts. For example, brain degeneration can be detected even during mild cognitive impairment (MCI) patients by using advanced machine learning algorithms and combining data with standard neuropsychological test results (Moradi et al., 2015). In addition, data-driven techniques developed for the diagnosis of neurodegenerative diseases (Koikkalainen et al., 2016), including the Bayesian model to "automatically identify distinct latent factors of overlapping atrophy patterns from voxel-wise structural MRIs" (Zhang et al., 2016). Multimodal neuroimaging can also provide better biomarkers for neurodegenerative diseases (Wang et al., 2017); particularly when data-driven models of disease progression is applied (Oxtoby et al., 2017).

Pre-symptomatic HD research have shown intriguing appearance of striatal degeneration as early as twenty years prior to the onset of first visible symptom (motor) (Tabrizi et al., 2009).

Specifically, putamen, caudate as well as globus pallidus regions in sub-cortical brain, reduced volumes have been reported by 25.7%, 30.9% and 29.3% respectively (S. J. Tabrizi et al., 2009). In addition, recent longitudinal data from TRACK-HD and IMAGE-HD have also found that other cortical regions, including the occipital, motor, and prefrontal cortices, also lose volume over time in pre-HD near to onset (Tabrizi et al., 2011, Poudel et al., 2014).

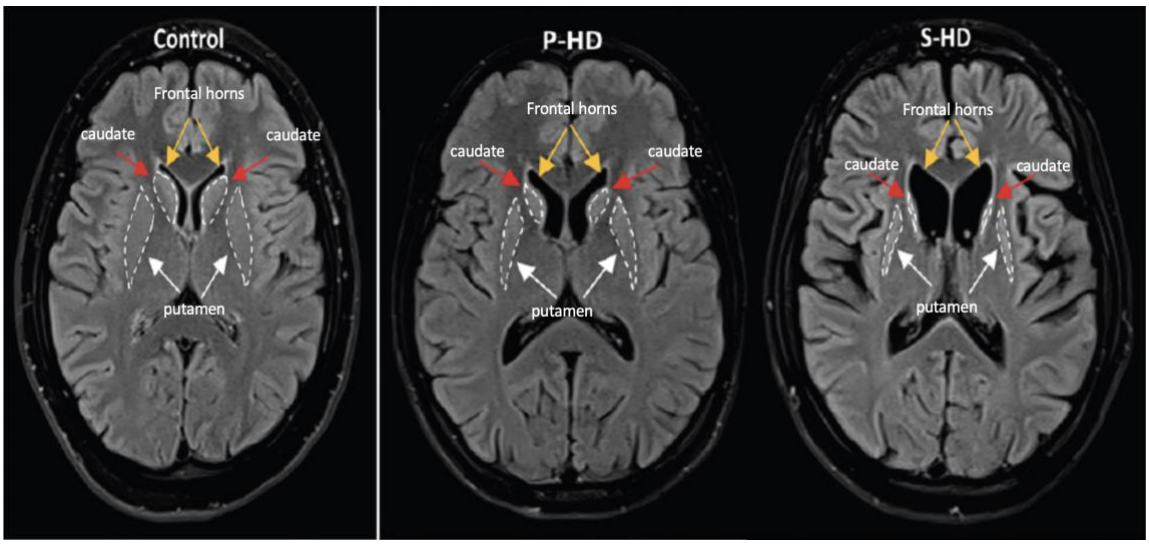

Figure 4: Neuroimaging illustrating structural variations in human brain regions in pre-symptomatic HD and symptomatic HD compared to control.

These neurodegenerative changes are spatially progressive and correlate with clinical measures, such as age at clinical onset, disease duration, and the CAG repeat length. However, these studies can only quantify and visualise the pathology involved. Therefore, we implement NDM in our study to elucidate the progression of atrophy in HD.

1.3 Network Diffusion Model of Trans-Neuronal Spread

Development of network spread models have helped in mapping the epicentres and trajectory of disease spread in neurodegenerative conditions. The network spread model's primary assumption is that the spatial pattern of atrophy in neurodegeneration is structured and driven by a mechanistic process. One mechanistic process that has been well-studied is the

prion-like spread of disease via misfolded protein structures. Neurodegenerative disorders, such as PD, AD, and HD, are believed to be caused by the accumulation of misfolded protein structures, disrupting the function of cells, tissues and other parts of the brain. Payne and Krakauer (1998) first endeavoured to display the procedure of prion accumulation and neuronal degeneration inside the cerebrum using traditional diffusion processes. However, classical diffusion was not preferable due to heterogeneous brain characteristics as it was correctly mapped for modelling the freely moving particles in an analogous medium (Payne & Krakauer, 1998).

First successful model came from Stumpf and Krakauer (2000), who incorporated brain connectivity features into the prion diseases model. However, since it was evident that prion proteins and misfolded proteins spread throughout the nerves and affect neighbouring regions, homogeneous diffusion processes became unrealistic for bigger spaces, such as the whole brain. Keeping this in mind, Matthäus (2006) first introduced the network approach, mathematically representing the network with a set of nodes as neuronal cells, with edges to describe the connections between neuronal cells. This approach was instrumental in identifying the misfolded protein spread and handling the various spatial scales. Further Matthaus (2009) himself suggested a system of reaction-diffusion equations, where the network nodes could represent a distant region to cover larger spaces to overcome the limitation of his previous work.

These initial findings ultimately led to the development of NDM in 2012 (Raj et al., 2012), which modelled the degenerative process as the first order of linear diffusion on the brain's structural connectome (Ashish Raj & Iturria-Medina, 2019). Furthermore, NDM allows for the macroscopic prediction of atrophy patterns by using bigger scale network connectivity for the whole brain (Carbonell, Iturria-Medina, & Evans, 2018). The model proposed by Ashish Raj, Kuceyeski, and Weiner (2012) uses a macroscopic NDM in which disease concentration factor, and the strength of the physical connection between the cells, decides the nature of the misfolded protein spread.

Various neurodegenerative conditions such as, AD, PD, and HD has successfully incorporated NDM to demonstrate the trans-axonal spread of atrophy through the structural connectome of the brain (Sneha Pandya, Mezias, & Raj, 2017; S. Pandya et al., 2019; Govinda R. Poudel et al., 2020; Ashish Raj et al., 2012; A. Raj et al., 2015). The model assumes a linear diffusion of disease factors (e.g., mHTT protein) through the axonal connection. Studies have likewise demonstrated that mHTT attacks areas of the brain that have high network connection, with lower bunching in neighbouring areas (Faria et al., 2016; McColgan et al., 2015). Hence, the NDM application (Ashish Raj et al., 2012) to track the progression of atrophy in HD is a promising tool.

1.4 Aims and Hypotheses

This research aims to develop and apply NDM to predict the spatial pattern of degeneration over time in pre-HD. We used the data from a multi-site international study of HD (Track-On Study) to investigate whether NDM can predict the pattern of degeneration. These data for this study were permitted to use by the CHDI (Cure Huntington's Disease Initiative) foundation as a part of the data use agreement. The anonymised data contains clinical and demographic patient data; cognitive, neuropsychiatric, oculomotor and quantitative motor data; brain imaging (MRI); and blood, tissue, and genetic markers.

Specific aims:

1. Compared to healthy controls, to characterise the longitudinal changes in the cortical and subcortical brain volume in premanifest HD (pre-HD).
2. To implement an NDM for predicting the longitudinal variations in brain volume in pre-HD.

Hypotheses:

1. Premanifest HD will show widespread degeneration in the whole hemispheric brain regions over time, compared to healthy controls.
2. Network diffusion can better predict he longitudinal change in brain volumes in pre-HD, compared to controls.

1.5 Justification

1.5.1 Longitudinal Degeneration in premanifest Huntington's Disease

In the last few years, neuroimaging studies have provided critical new information regarding robust and reproducible structural brain changes in pre-HD, including the IMAGE-HD study, TRACK-HD and PREDICT-HD study. In particular, the TRACK-On HD has reported robust 12- 24 months structural changes in caudate and putamen before (~15 years) symptom onset (Tabrizi et al., 2013; Aylward et al., 2011; Noululous et al., 2010). In addition, whole-brain volumetric changes (and changes in cortical and sub-cortical volumes, separately) have also been reliably documented, including widespread cortical thinning. These early striatal changes, and evolving cortical changes, are now accepted as the hallmark of the disease and hence support the rationale for further investigation of models for the propagation of degeneration in HD.

1.5.2 Considerations of Statistical Analysis Tool

Using appropriate and robust statistical analysis methods is always vital in any research. For example, we have encountered the use of t-test or paired t-test for quantifying degeneration in HD. However, more advanced statistical methods are necessary to model repeated assessments in longitudinal studies. To overcome this challenge, linear mixed effect model (LME) statistical approach was fitted to investigate changes in pre-HD compared to controls.

1.6 Ethical Approval

Ethical approval has been granted by the Australian Catholic University Human Research Ethics Committee (reference number 2019-380N).

Chapter 2: Background

2.1 Huntington's Disease

Huntington's disorder (HD) progressively spread throughout the brain ultimately causing decay of nerve cells mostly in sub-cortical region (basal ganglia). Functional abilities such as movement, cognitive, mental, and psychiatric conditions are deteriorated in span of time as the disease spreads. This inherited disorder can show signs of motor symptoms as early as thirties and forties, though, disease onset may be much prior or later in life. In some cases, HD onset can occur before early twenties called as juvenile HD.

2.2 Symptoms of HD

Movement, cognitive and psychiatric disabilities are most common symptoms in HD. Symptoms appearance can be random depending among HD patients. Some effects of symptoms appear dominating during the progression of disease or on the other hand, significantly affecting functional ability. The following list provides a range of symptoms relevant to HD (adapted from https://www.mayoclinic.org/diseases-conditions/huntingtons-disease/symptoms-causes/syc-20356117).

Muscular: abnormal walking, increased muscle activity, involuntary movements, problems with coordination, loss of muscle, or muscle spasms

Cognitive: amnesia, delusion, lack of concentration, mental confusion, slowness in activity, or difficulty thinking and understanding

Behavioural: compulsive behaviour, fidgeting, irritability, or lack of restraint

Psychological: delirium, depression, hallucination, or paranoia

Mood: anxiety, apathy, or mood swings

Other: difficulty speaking, memory loss, tremor, or weight loss

2.3 Pathology of HD

The primary pathology in HD is found to be decay of specific neurons cells in striatum and cerebral cortex (Mitchell et al., 1999). MRI scans of premanifest HD patients more than 20 years before onset show localised atrophy in the striatum and cerebral cortex (Georgiou-Karistianis et al., 2013; Govinda R. Poudel, Gary F. Egan, et al., 2014). However, atrophy is largely progressed in the manifest stage of the disease, covering the occipital, motor, and frontal areas of the brain, as revealed by the studies of post-mortem brains and MRI scans of manifest HD (G. R. Poudel, Harding, Egan, & Georgiou-Karistianis, 2019). Cognitive, motor, and neuropsychiatric symptoms also increase over time. While early premanifest HD may show subtle changes in motor and cognitive function in laboratory settings, a complex combination of motor, cognitive, and behavioural deficits emerge in manifest HD (G. R. Poudel et al., 2015). Figure 5 shows the general ageing process with abnormal protein accumulation leading to neurodegeneration resulting in various symptoms.

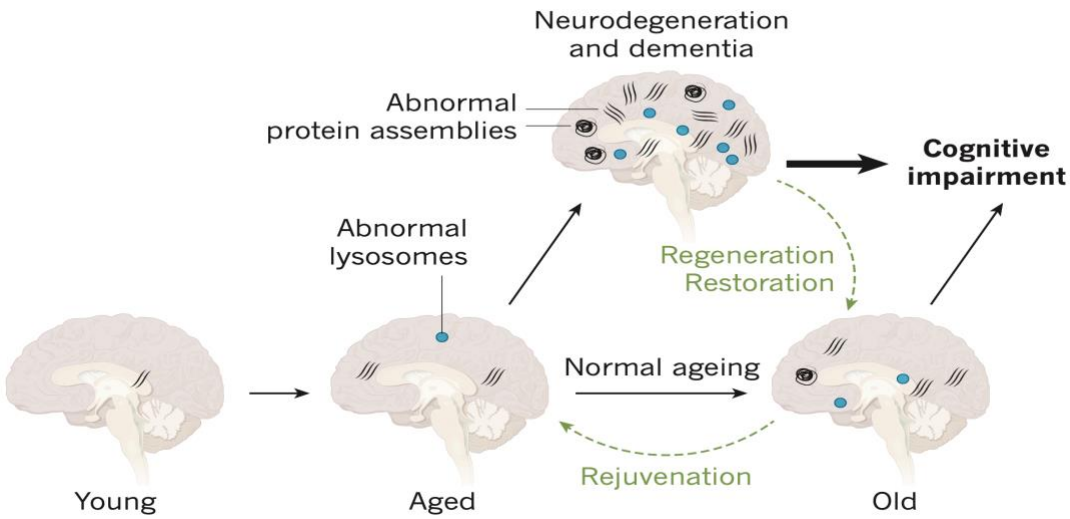

Figure 5: Process of ageing and neurodegeneration and regeneration (Wyss-Coray, 2016).

This review explores the findings from the cellular, animal models and human neuroimaging to better understand HD's neurodegeneration's neurobiological mechanisms and

spatial-temporal modes. We will also review the various findings on protein aggregation, spread mechanism, and patterns of degeneration in HD and broadly describe the NDM implemented for predictions of trans-neuronal spread.

2.3.1 Genetic markers of HD

The HD gene was first mapped using DNA polymorphisms in 1983 (Gusella et al., 1983). After decades of research the HD gene ultimately was recognised in 1993 (Reiner, Dragatsis, & Dietrich, 2011). This study was collaborative research of the Huntington's Disease Collaborative Research Group (HDCRG). Other than in human beings, the HD gene has been identified in several other species such as pig (Matsuyama et al., 2000), mouse (Ambrose et al., 1994; Heinsen et al., 1994), pufferfish (Baxendale et al., 1995), zebrafish (Karlovich, John, Ramirez, Stainier, & Myers, 1998), and Drosophila (Li, Karlovich, Fish, Scott, & Myers, 1999). The examination of CAG rehashes led to the understanding that the CAG tract in the IT15 is polymorphic (Read, 1993), which shows the normal range of CAG repeat numbering 9-11 at the lower end and 34-37 at the higher end. Individuals with a CAG repeat of more than 39 are highly susceptible to developing HD within their lifetime (McNeil et al., 1997). However, there are some exceptions in the late onset of the disease (Andrich et al., 2008; Kenney, Powell, & Jankovic, 2007).

While adult-onset refers to 40-50 repetitions of mutant HD, juvenile-onset HD, defined as onset before 20 years of age, is closely related with CAG repeats of 60 and above (Reiner et al., 2011). In addition, various abnormalities such as chorea, cognitive rigidity, seizures, and psychiatric and behavioural abnormities associated with different CAG repeat scores, which characterise the age of onset groups of HD (Reiner et al., 2011). Furthermore, the CAG repeat expansion increases if transmitted paternally and decreases if transmitted maternally (G. P. Bates, Mangiarini, Mahal, & Davies, 1997; Duyao et al., 1993). Hence, it is evident that understanding the characteristics of CAG expansion is crucial in predicting the progression of atrophy in HD.

2.3.2 Progression of neurodegeneration in HD

Clinical and imaging studies can provide sufficient evidence of brain abnormalities in HD before symptoms appear. Neurodegenerative changes appear to accumulate over cortical and sub-cortical structures, resulting in almost 25% of brain weight loss in the lifetime of an HD patient (Halliday et al., 1998; Reiner et al., 2011). Disease spread leads to extensive neuronal cell death in the striatal part of the basal ganglia, which further increases the size of the lateral ventricles. Striatal degeneration is progressive along the dorsomedial to ventrolateral direction (Roos et al., 1985; Vonsattel, 2008).

MRI studies also show that caudate atrophy is related to CAG repeats and UHDRS motor scores (Nicola Z Hobbs et al., 2010; Jech et al., 2007). In addition, other cortical and subcortical brain regions also degenerate in course of time in HD (Reiner et al., 2011). For instance, loss of volume in the brain regions (20% in the cortex, 30% in cerebral white matter, 60% in the striatum, 55% in the globus pallidus, and 30% in the thalamus) are well evident (Reiner et al., 2011).

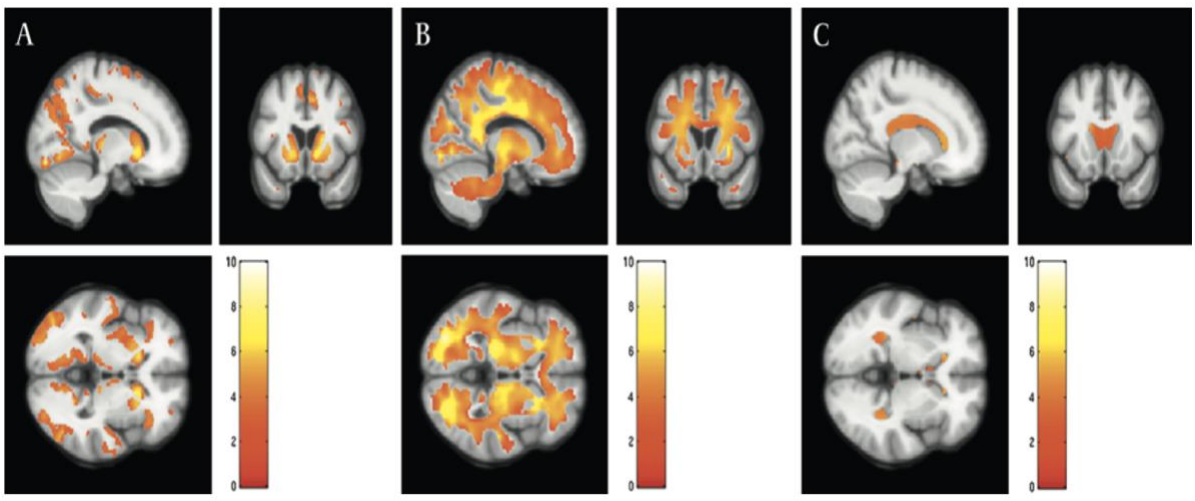

Figure 6: Progression in rates of atrophy in early HD comparing with far onset (predicted) pre-HD cohort (N. Z. Hobbs et al., 2010).

Note: Above statistically mapped brain image shows A. regions of increased grey matter atrophy rates, B. increased white matter atrophy rates, C. progression in ventricular atrophy in early HD compared with pre-HD over the period of two years. Colour bar represents t-score.

Neuroimaging has been used extensively better to characterise the progression of brain pathology in HD. Out of several available neuroimaging techniques, MRI is widely accepted due to being non-invasive (Govinda R. Poudel, Julie C. Stout, et al., 2014; Sturrock et al., 2015; S. J. Tabrizi et al., 2009; Sarah J. Tabrizi et al., 2011; Vemuri & Jack, 2010). Two of the most widely used MRI techniques for visualising changes in the brain's grey and white matter are Diffusion-weighted MRI (DWI) and T1-weighted MRI. The former can visualise general changes (Govinda R. Poudel, Julie C. Stout, et al., 2014); the latter to image microstructural changes (Govinda R. Poudel, Julie C. Stout, et al., 2014). MRI can also be used to detect specific atrophy in the brain's white and grey matter, which is invaluable for clinical research in neurodegeneration (G. R. Poudel et al., 2015). Using MRI, it is also possible to map the functional and structural networks in neurodegenerative conditions (Govinda R. Poudel, Gary F. Egan, et al., 2014). Advanced approaches can be applied to MRI data for generating brain volumes (Agosta, Galantucci, & Filippi, 2017). The National Institute on Aging-Alzheimer's Association has described MRI as a potential biomarker due to its capability to detect pathological changes in the brain without an autopsy (Shimizu et al., 2018). MRI is still playing an essential part to detect and predict several neurodegenerative diseases, including AD, HD, Lewy body dementia (LBD), PD, and frontotemporal dementia (FTD) (Vemuri & Jack, 2010).

2.4 Magnetic Resonance Imaging (Neuroimaging)

Various neuroimaging tools are available at this point to research neurodegenerative conditions. MRI plays a vital role in conducting feasibility studies on several neurodegenerative diseases and detecting specific features that support clinical research. The current availability of advanced MRI technology has made it possible to map neurodegenerative conditions' functional and structural areas. The most commonly used neuroimaging techniques include MRI and radionucleotide imaging (SPECT and PET) (Risacher & Saykin, 2013). The use of MRI and

radionucleotide imaging research in the pathology and progression of neurodegenerative diseases is possible. However, in the context of in vivo neuroimaging techniques, MRI is broadly used for research in anatomical changes and neurodegeneration (Risacher & Saykin, 2013). The utility of MRI in different neurodegenerative conditions is briefly reviewed below.

2.4.1 Alzheimer's Disease (AD)

Structural MRI (SMRI) can be used to investigate structural changes in brain anatomy in neurodegenerative diseases. In one study, regional volumes and regional tissue morphometry extracted from sMRI techniques were able to detect brain atrophy in AD patients (Risacher & Saykin, 2013). The decline of neurons, synapses, and dendritic de-arborisation that occurs on a microscopic level in AD, closely related to grey matter atrophy, can be captured by sMRI (Vemuri & Jack, 2010). Several studies demonstrated mild cognitive impairment (MCI) acts as intermediate atrophy between healthy aging and AD. Increased reduction in density of volume and grey matter is seen in MCI individuals compared to an AD patient, specifically in temporal, parietal, and frontal lobes in focal cortical atrophy. Understanding the progression from MCI to AD through measurement of volume, morphometry, and rate of brain atrophy is possible using sMRI techniques (Risacher & Saykin, 2013). Mid-temporal lobe (MTL) volume loss is recognised as the supporting criteria for a diagnosis of probable AD and MCI due to AD (Agosta et al., 2017). With 65-80% accuracy in predicting the risk of further development of AD in a patient with MCI, using sMRI with advanced machine learning algorithms has become highly acceptable for research (Agosta et al., 2017). Several in vivo biomarkers developed using MRI study are available, including the latest neuroimaging markers of abnormal brain amyloid deposition and neuronal degeneration used for diagnosis of probable AD (McKiernan & O'brien, 2017).

2.4.2 Lewy Bodies Dementia (LBD)

LBD represents 10-15% of all onset dementia cases and is the second most common neuro-disorder. The accumulated α-synuclein within Lewy bodies and Lewy neurites determines the pathological trademark of LBD. However, it is sometimes detected alongside the presence of AD pathology at autopsy in the form of neuritic plaques (Agosta et al., 2017). Specific symptoms, such as fluctuation in executive function, attention, and higher-order visual function, are common in LBD. In addition, researchers have identified widespread structural degeneration in cortical and subcortical regions in the brain.

Furthermore, individuals with LBD show faster rates of cerebral pathology in the medial and lateral temporal lobes areas, including the occipitotemporal areas (Risacher & Saykin, 2013). Observation of α-synuclein protein, referred to as Lewy neurites and Lewy bodies, makes it distinct in pathological terms (Blamire, 2018). However, studies have shown substantial similarities between LBD and AD concerning atrophy in these regions (Agosta et al., 2017).

2.4.3 Parkinson's Disease (PD)

MRI research in PD is mainly focused on the substantia nigra. Due to the lack of a clear outline of the substantia nigra in volumetric studies, the combined use of advanced MRI techniques is prevalent in this research field. Other studies using T2- weighted sequences show an increment of iron content. The nature of the structural combination of the substantia nigra with the thalamus and a volume change determines PD from the control group with a high level of accuracy. Furthermore, sMRI studies have determined the subtle cortical thinning in cognitively intact PD in frontal, temporal, parietal and occipital lobes (Agosta et al., 2017).
In some cases, patients with PD in the absence of dementia showed atrophic and functional brain changes. Additionally, grey matter atrophy in the left anterior cingulate, left gyrus rectus, left parahippocampal gyrus, and the right frontal lobe is shown in PD patients. Overall, various

studies on PD have determined significant atrophic, functional, and molecular brain changes (Risacher & Saykin, 2013).

2.4.4 Huntington's Disease (HD)

HD causes motor and cognitive abnormalities (G. R. Poudel, Harding, Egan, & Georgiou-Karistianis, 2019). The progressive decrement in striatal volume is determined in all stages of HD (pre-HD and symptomatic ("manifest") HD) patients (G. R. Poudel, Harding, Egan, & Georgiou-Karistianis, 2019). Atrophy is seen in the putamen and caudate in the early stages, which later expanded to the nucleus accumbens and globus pallidus parts of the brain (G. R. Poudel et al., 2015). Further, progression of atrophy is identifiable also in grey and white matter in brain of individuals with HD (Govinda R. Poudel, Julie C. Stout, et al., 2014; Risacher & Saykin, 2013). Structural MRI investigations showed the morphological results of the cortico-striatal movement of atrophy in HD (G. R. Poudel, Harding, Egan, & Georgiou-Karistianis, 2019). Reduction of volume in the striatum has been confirmed in MRI neuroimaging, especially from TRACK-HD, PREDICT-HD and IMAGE-HD. Cross-sectional data reported putamen volume reduction is greater than caudate volume in pre-HD and early-stage Symp-HD (S. J. Tabrizi et al., 2009). Overall, structural MRI studies have determined the various microstructural changes in white matter (Govinda R. Poudel, Julie C. Stout, et al., 2014), thalamus, hippocampus and other brain regions in HD patients (Georgiou-Karistianis et al., 2013).

2.5 Diffusion Weighted Imaging (DWI)

DWI has made it possible to characterise the white matter microstructure. The minute changes related to normal brain development, ageing, and various neurological diseases can be determined with the help of DWI (Jelescu & Budde, 2017). In AD, it is reported that white matter alterations take place in the temporal and frontal lobes. In the last few years, DWI has shown early and more accurate diagnosis of AD. Further, DTI studies have shown the capability

to differentiate AD patients from healthy individuals using microstructural measures (Agosta et al., 2017). The intensity of scanned image depends upon strength and direction of the magnetic diffusion gradient (Müller & Kassubek, 2013). A recent longitudinal study suggests that changes in the white matter among LBD and AD patients can be detected over one year, as shown in Figure 6.

One of the most valuable benefits of DWI is its absorbance capability of changes in microscopic level, which are not visible in traditional structural MRI sequences. For example, study of white matter structural connectivity disconnection using DWI, elaborated on existing knowledge about the progression of neurodegenerative pathology (Weston, Simpson, Ryan, Ourselin, & Fox, 2015). In addition, diffusivity changes in the thalamus, which further extended towards putamen and caudate nucleus, correlates with global functional impairment, CAG repeat length, and bicaudate ratio (Seppi et al., 2006).

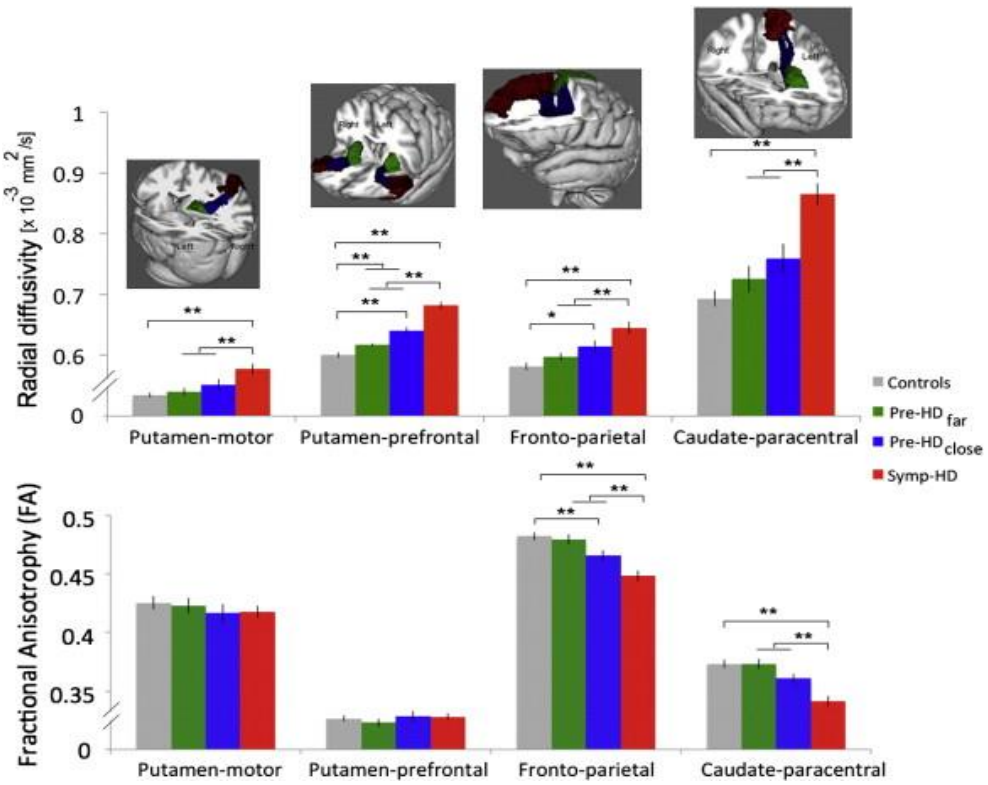

Figure 7: Diffusion-weighted imaging-based microstructural measures show significant variations in tracts of white matter in HD (adapted from Poudel et. al., 2014).

Furthermore, DWI studies showed significant variation in white matter and grey matter degeneration in pre-HD patients (G. R. Poudel, Harding, Egan, & Georgiou-Karistianis, 2019). However, clinical practice is yet to recognise these techniques, and they remain to be subjected to thorough validation (Frisoni, Fox, Jack, Scheltens, & Thompson, 2010).

2.6 Models of Network Spread

The protein misfolding process is a common pathology in various neurodegenerative diseases, including HD. The accumulation in misfolded protein disrupts the function of cells, tissues, and other parts of the brain, ultimately causing cell death. Various studies have attempted to develop a biophysical model for this process so that degenerative processes can be predicted (Ashish Raj & Iturria-Medina, 2019).

2.6.1 One Dimensional Model

Eigen suggested using the mathematical model on prion dynamics to explain the conversion process of a prion protein into a misfolded protein by using ordinary differential equations. This model was called a template-assisted model, or the heterodimer model. However, the model was unable to replicate the long incubation period typically found in prion diseases. Currently, the nucleated polymerisation model (NPM) yields a mathematical formalisation of the prion replication mechanism. However, various modifications and additions to the NPM have been suggested. Later Greer, Pujo-Menjouet, and Webb (2006) suggested a transport partial differential equation (PDE), which showed three-dimensional, epidemiological-like models. PDE was later updated by Pruss (Carbonell et al., 2018).

2.6.2 Spatial Spreading

Payne and Krakauer (1998) attempted to model the process of prion aggregation and neuronal transport inside the brain by incorporating the classical diffusion process. The classical diffusion process in the heterogeneous brain was not preferable due to its suitability for

modelling the freely moving particles in a analogous medium. Among decades of research, it is believed that Stumpf and Krakauer's model was the first successful model to attempt incorporating brain connectivity features into a prion diseases model described by epidemiological-like equations (Carbonell et al., 2018).

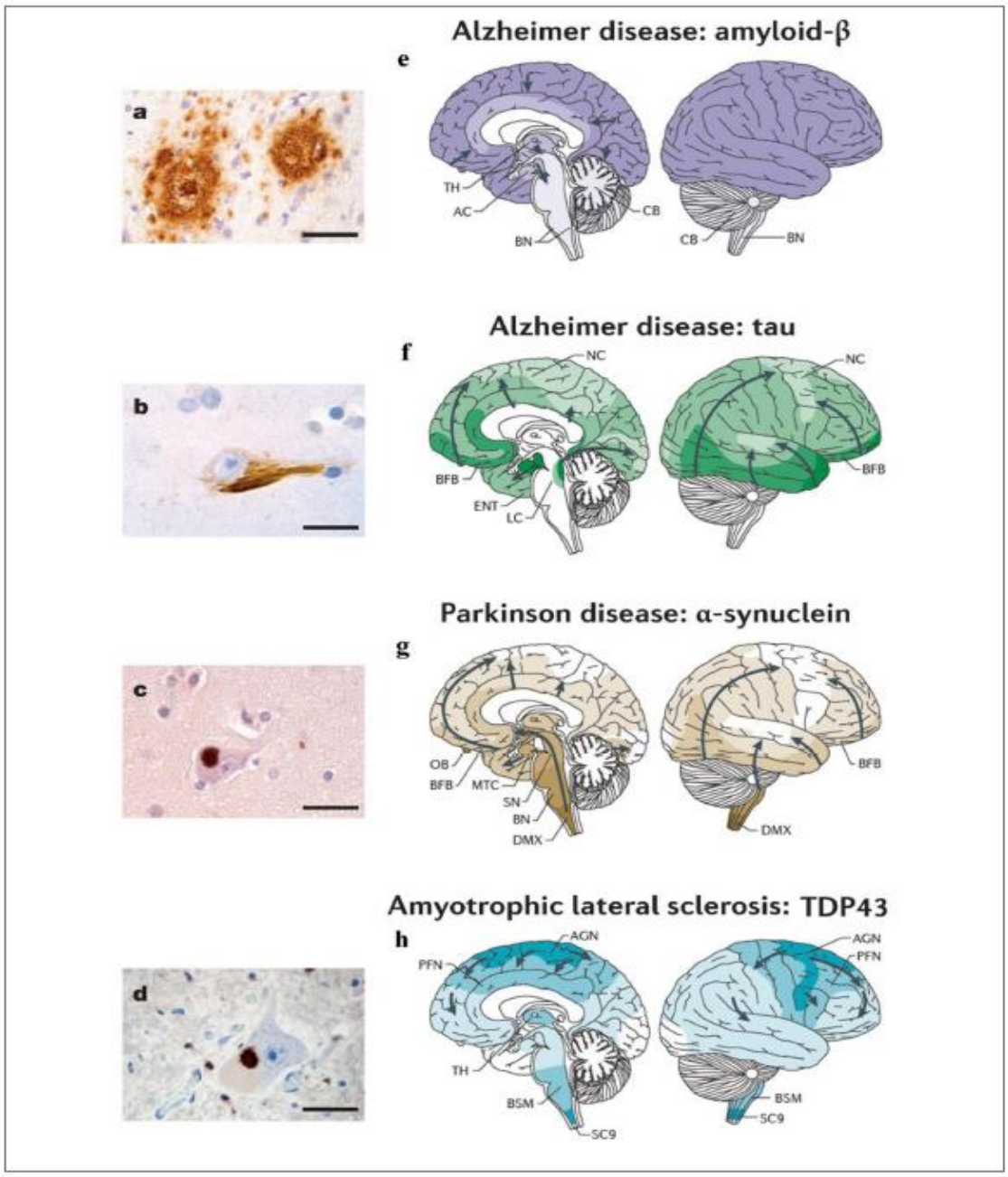

Figure 8: Disease-specific MPs and characteristic anatomical progression patterns

Note: (A) Aβ plaques in the cortex of an Alzheimer's disease (AD) patient. **(B)** Tau neurofibrillary tangle in a neuron of an AD patient. **(C)** α-synuclein inclusion in a neuron from a

Parkinson's disease (PD) patient. **(D)** TDP-43 inclusion in a motoneuron of the spinal cord from a patient with ALS (Carbonell et al., 2018).

Table 1: Mathematical Modelling research on Neuro-disorder (Protein Aggregation and Network Spread) as suggested review (Ashish Raj & Powell, 2018)

Name and Reference	Description	Comments	Validation
Protein Aggregation Models			
Heterodimer Model: Prusiner *et al.* (57)	Original landmark, template-driven heterodimer model of prion spread	Local protein aggregation, not network based	In vitro
Nucleated Polymerization Model: Masel *et al.* (58)	Monte Carlo discrete event simulations to model prion aggregation	Local protein aggregation, not network based	In vivo (animal)
Smoluchowski Aggregation: Bertsch *et al.* (60)	Smoluchowski's coagulation equation describes time evolution of concentration of polymers as they coagulate	Local protein aggregation, not network based; simultaneously modeled amyloid-β cascade and prion hypotheses	N/A
Heterodimer Model: Payne *et al.* (61)	Prion aggregation described utilizing concentration dynamics of two strains of prions undergoing competition	Local protein aggregation, not network based	In vivo (animal)
Matthäus: Matthäus *et al.* (62)	Applied classic epidemic spread models of networks to recapitulate prion-like disease	Used synthetic lattice networks	In vitro
Network Spread Models			
NDM: Raj *et al.* (39)	Applied graph diffusion to model AD progression on large-scale brain networks	Real human connectomes; suggested spatially distinct eigenmodes, which mediate network vulnerability	In vivo (human neuroimaging); validation limited to 2- to 4-year follow-up
NDM vs. Gene Expression: Acosta *et al.* (70)	Compared graph diffusion against innate regional vulnerability (given by healthy regional gene expression) as predictors of the observed cross-sectional atrophy patterns in AD	Found that NDM is a far better predictor of AD topography than innate regional vulnerability is	Validation on cross-sectional regional atrophy data obtained from in vivo human MRI
Epidemic Spreading Model: Iturria-Medina *et al.* (25)	Interrelating structural connectivity and in vivo amyloid-β in AD	Explicit amyloid-β production/clearance terms	In vivo (human neuroimaging) validation on amyloid-β PET
General Graph Theory Models			
Graph Spread: Avena-Koenigsberger *et al.* (71), Mišić *et al.* (72)	Models of graph spread, based on cooperative and competitive spreading dynamics on human connectomes	Model uses general principles of spread rather than biophysical modeling of pathology	In vivo (human neuroimaging)

2.6.3 The Network Approach

Matthaus (2009) developed a system of reaction-diffusion equations to overcome the limitation of his previous work. Since earlier research was more concentrated on a microscopic level (neuronal level), macroscopic studies, which include more considerable scale network connectivity of the whole brain, have been introduced (Carbonell et al., 2018). Ashish Raj et al.

(2012) proposed the macroscopic NDM, in which disease concentration factor and strength of the physical connection between the cells decides the nature of the spread of misfolded protein. NDM has been further extended to identify the brain atrophy regions and sources comparing brain connectivity networks (Carbonell et al., 2018).

2.6.4 Network Diffusion Model (NDM)

NDM models the spread of neurodegenerative disorder in the cerebrum. Given the hypothesis that misfolded protein in this disease spreads via neuronal connections instead of nearness, NDM provides a tool to model this behaviour. The current model for the spread of neurodegeneration through network diffusion was developed by utilising the model of random dispersion for misfolded protein in the cerebrum from higher to lower degrees of concentration (Ashish Raj, 2015). This model has been proven to identify the spread of degeneration and has been suggested to predict the future long-term atrophy pattern. Furthermore Abdelnour, Voss, and Raj (2014) suggest that the predictability of correlation structures of NDM is far better than others when applied in the structural brain networks.

A recent study in HD suggests that the NDM can be used to determine the pattern of grey matter degeneration and white matter disconnection (G. R. Poudel, Harding, Egan, & Georgiou-Karistianis, 2019). Cross-sectional studies of imaging data of AD patients found that NDM successfully identifies the pattern of brain atrophy and metabolism (Ashish Raj et al., 2012). Furthermore, it was suggested that NDM has greater predictability on longitudinal progression when observing a patient's baseline pattern (Ashish Raj et al., 2012; A. Raj et al., 2015). Apart from prediction and pattern recognition, NDM was used successfully to identify from which various seed regions the tau pathology of AD patients was originating (Torok, Maia, Powell, Pandya, & Raj, 2018). The same study showed that many AD seeds are situated in the hippocampus, entorhinal cortices, and neighbouring brain areas. Subsequently, NDM was used in PD to establish the probable pathology seed regions and patterns of disease spread (Freeze,

Pandya, Zeighami, & Raj, 2019a). In other studies, NDM was used to predict progressive supranuclear palsy (PSP) atrophy (Sneha Pandya et al., 2017). Figure 8 below shows the images of time resolved NMD seeded at the hypothalamus, showing progressive atrophy of subcortical and temporal areas.

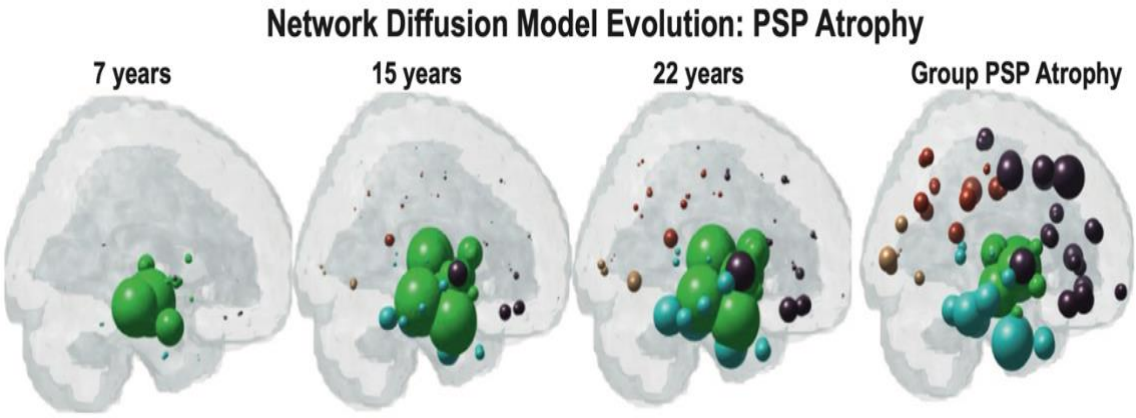

Figure 9 Demonstration of an NDM in predicting progressive supranuclear palsy (PSP) atrophy.

Note: Spheres are colour-coded by lobe (Green = subcortical, blue = temporal, brown = frontal, red = parietal, yellow = occipital). Spheres are sized according to regional atrophy (Sneha Pandya et al., 2017).

2.7 Network Spread of Degeneration in HD

Distinct anatomical patterns of degeneration can be observed in different stages of disease in HD. These anatomical patterns suggest that disease follows a specific cortico-striatal pattern, potentially spreading between neighbouring cells or along axonal pathways (Brundin, Melki, & Kopito, 2010). Research in protein aggregates in HD suggests prion-like transmission, moving from vulnerable to less vulnerable areas (Brundin et al., 2010). In vitro studies of the cell models found intracellular coagulation led by the aggregation of PolyQ in the form of wild-type huntingtin when collectively induced in the cells. Studies conducted in vivo in Drosophila have shown extensive inter-neuronal spread, and with evidence of spread also found in glia cells (Ren et al., 2009; Trevino et al., 2012).

When studied in animal models such as mice, research indicated that aggregation of huntingtin leads to progressive diseases that can spread quickly (Daniel & Barry, 2015; Pearce, Spartz, Hong, Luo, & Kopito, 2015). Furthermore, a study of three patients suggested that mutant forms of huntingtin, introduced as allografts in an intracerebral part of striatal tissue, were also found on extracellular covering (matrix) of the transplanted tissue and even in the host brain. These aggregates were seen on neutrophils, ECM (Extracellular matrix), neurons, blood vessels, and so on (Cicchetti et al., 2014; Jeon et al., 2016). Therefore, it was concluded that the transfer of aggregates of mutant huntingtin could take place among the host cells and allografts, and in-depth research is necessary to test aggregates of huntingtin so that its characteristics can be better validated (Brundin et al., 2010).

There are plenty of evidence to suggest that atrophy has prion-like properties and can seed pathology in neighbouring cells, including distantly associated healthy neuronal cells (Masnata & Cicchetti, 2017). Trans-neuronal spreading in HD is further validated by the study conducted by Pecho-Vrieseling et al. (2014), which investigated the transsynaptic propagation theory.

Table 2 In vitro evidence of m HTT spreading capacities (Masnata & Cicchetti, 2017).

Mechanism	Protein form	Cell model	Observations	References
Transynaptic propagation	Endogenous mHTT from R6/2 mice	*Ex vivo* mixed cortico-striatal cultures from R6/2 or wild type mice	Propagation of mHTT from R6/2 cortical to wild-type striatal neurons Significant vulnerability of striatal neurons in comparison to cortical neurons	Pecho-Vrieseling et al., 2014
	Endogenous mHTT from R6/2 mice	Human ESCs and human iPSC differentiated into neurons transplanted into organotypic brain slices of R6/2 mice	Propagation of endogenous mHTT from murine host tissue to grafted hGFP neurons followed by progressive neurodegeneration of recipient hGFP neurons	
TNTs	Transfection with GFP-480-68Q (donor); mCherry (acceptor)	Co-culture of CAD transfected cells (68Q or mCherry) Co-culture of transfected primary CGNs (68Q or mCherry)	Transfer of GFP-480-68Q to both CAD and CGN neuronal cells via TNTs	Costanzo et al., 2013
Vesicular transport				
Exosome	HD143F-derived exosomes	Co-culture of HD143F and NSCs	Spread of mHTT from HD143F to NSCs	Jeon et al., 2016
		NSCs exposed to HD143F-derived exosomes	Spread of exosomes-containing mHTT in NSCs	
Exopher	Genetically-engineered expression of Q128	*C. elegans*	Q128 gene expression increases the production of exophers Exopher content, including organelles, protein and mHTT, is found in remote cells of the *C. elegans*	Melentijevic et al., 2017
Endocytosis	Fibrillar Alexa488-HTTExon1Q44 and/or polyQ44	Undifferentiated and differentiated mouse and human neuroblastoma cells (N2A and SH-SY5Y)	Internalization and intracellular localization of HTTExon1Q44 and PQ44 fibrils in both types of neuroblastoma cells Fibrillar HTTExon1Q44 uptake via clathrin-dependent endocytosis No mechanisms evaluated for PQ44 fibrils	Ruiz-Arlandis et al., 2016
Direct penetration of plasma membrane	Synthetic K2Q44K2 fibrils	HEK; HeLa; Cos-7; CHO; N2A	Breach plasma membranes by K2Q44K2 fibrils in all cell types tested	Ren et al., 2009
	Transfection with ChFP-HTTQ25 and synthetic K2Q44K2 fibrils	HEK	Recruitment of soluble HTT forms into IBs by synthetic K2Q44K2 fibrils in transfected HEK cells	
	Chemically synthesized Q42, NLS-Q42 and NLS-Q20 fibrils	Cos-7; PC-12	In the nuclei, smaller aggregates are more toxic than larger ones in both cell types tested	Yang et al., 2002
Unknown	Transfection with 25/103QHTT-V1 and 25/103QHTT-V2	Co-culture of H4 cells expressing 103QHTT-V1 and HEK cells expressing 103QHTT-V2	Polymerization and cell-to-cell transmission of HTT oligomers	Herrera et al., 2011
	Exposure to conditioned medium derived from GFP-mHTT-Q19 or GFP-mHTT-Q103 transfected HEK cells	SH-SY5Y cells	Presence of exogenous mHTT protein (Q19 and Q103) within recipient SH-SY5Y cells	Jeon et al., 2016

CAD, mouse catecholaminergic neuronal cell line; CGNs, cerebellar granule neurons; CHO, epithelial-like cell line from Chinese hamster ovary; Cos-7, fibroblast like cell lines derived from monkey kidney; ESCs, embryotic stem cells; H4, human brain neuroglioma cells; GFP, green fluorescent protein; HD, Huntington's disease; HD143F, human fibroblast derived from Huntington's disease patient carrying 143 polyglutamine repeats; HEK, human embryonic kidney cells; HeLa, human uterine cervical carcinoma cells; hGFP neurons, human GFP positive neurons; HTT, huntingtin; IBs, inclusion bodies; iPSC, induced pluripotent stem cells; mHTT, mutant huntingtin; NSCs, neural stem cells; N2A, mouse neuroblastoma cell line; NLS, nuclear localization signals; PC-12, cell line from pheomochromocytoma of the rat adrenal medulla; PolyQ, polyglutamine; SH-SY5Y, human neuroblastoma cell line; TNTs, Tunneling nanotubes; V1, Venus protein half; V2, Venus protein half 2.

Chapter 3: Longitudinal Data Analysis in Neurodegenerative Diseases

This chapter addresses the advanced factual way to deal with the longitudinal data analysis in neurodegenerative sicknesses. Understanding movement of atrophy in neurodegenerative disorder is vital for restorative intercessions just as creating critical clinical preliminaries for medicines. Longitudinal information concentrates on giving the admittance to atrophy movement by contrasting results more than once over the long run and regard to change in variables. Thusly, this chapter will dissect as of now accessible current available modern statistical modelling in relation to disease progression in HD and clarify the purpose for implementing linear mixed effect modelling in this study. This chapter is the linking chapter to Chapter 4.

3.1 Challenges

Although longitudinal data give access to the temporal disease trajectories, statistical analysis is far more complex due to complicated correlation, irregular visits dates, missing data, and a mix of time-varying and static covariates (Garcia & Marder, 2017). These factors make longitudinal data analysis more complicated, primarily related to neuroimaging data, leading to inaccurate data analysis. Longitudinal data have more statistical power with less variability than cross-sectional data (Zeger & Liang, 1992). In the longitudinal study, research conducted several observations of the same subjects over a period of time. A fixed example of population elements is measured repeatedly on the same variable. Correlated data, irregular visits (time) data, missing data are challenges in analysing longitudinal data. Hence, it is vital to select a more inclusive statistical approach that can overcome all challenges with the longitudinal data.

The mixed-effect model is considered to be a more flexible and accommodative statistical method and is suggested by Food and Drug Administration (FDA) for observational and clinical studies (Garcia & Marder, 2017).

Applications of the mixed effect model have become an attractive tool to evaluate disease progression in neurodegenerative disorders. The mixed-effect model explains the regression relationship between covariates and repeated measures. It contains both fixed and random effects. Random effects can capture the correlation of repeated measures, which can be used to estimate the group-specific effects and elaborate group-specific or within-group trends over time. Mixed effect models are utilised mainly in HD, e.g., Tabrizi and colleagues (Sarah J Tabrizi et al., 2013) used linear mixed effect model to explain longitudinal variations of several outcomes over 36 months period. In addition, Long et al. (2014) also used a linear mixed effect model to estimate motor impairments timing in the progression of HD.

3.2 General Approaches for Longitudinal Data

Several statistical approaches are implemented to analyse the longitudinal data depending upon different criteria, such as several time points and repeated measures (multivariate). The change score analysis method is implemented when there are only two-time points. This statistical approach is a direct method to analyse the difference between the measured entity at each time point. For example, Sturrock et al. (2015) used this approach to evaluate longitudinal in vivo brain metabolite profiles in HD over 24 months. Govinda R. Poudel et al. (2015) used this method to analyse the longitudinal changes in white matter microstructure in HD over 18 months.

3.2.1 Repeated Measures using ANOVA

One way analysis of variance (ANOVA) approach helps to remove correlation problem (Garcia & Marder, 2017) and is suitable for both change score analysis and repeated measures (Gibbons, Hedeker, & DuToit, 2010). This method includes time and disease criteria and an interaction term (time x disease criteria) to assess group differences over time. The statistically significant interaction term (time x disease criteria) represents the effect of time varies between

disease criteria. However, the ANOVA approach implemented with missing data generates biased parameter estimation (Shaw & Mitchell-Olds, 1993).

3.2.2 Multivariate Analysis of Variance (MANOVA)

The multivariate ANOVA (MANOVA) approach makes more flexible variance-covariance estimation (Zeger & Liang, 1992); however, these two methods have many similarities. For example, both ANOVA and MANOVA hypotheses that time intervals are equally distributed over space, normally distributed data, and each statistical approach requires complete data, i.e., missing data is not accepted for any subjects in any period of observation.

3.2.3 Limitation of Repeated Measures ANOVA and MANOVA

These limitations in approaches yield modern methods for modelling disease progression in neuroimaging longitudinal data. Namely, generalized estimating equations model (Liang & Zeger, 1986) and mixed-effects regression (Laird & Ware, 1982) are suggested and used in several study (Maroof, Gross, & Brandt, 2011; Sarah J Tabrizi et al., 2013). These methods allow both time-varying predictors (e.g., age, brain volume) and time-invariant predictors (e.g., gender, genotype) and solve the problem of missing data and irregular timed information.

In this study, we exclude the generalized estimation equation model apart from having various advantages, as it is not designed or modelled to analyse the correlation structure of repeated measures (Fitzmaurice, Davidian, Verbeke, & Molenberghs, 2008). Hence, the mixed-effect regression model is the best statistical approach for my study. In HD, the mixed-effect regression model is widely used for the statistical modelling of correlated longitudinal data. It has already proved its statistical computing power in analysis of prospective, observational, multi-center longitudinal studies such as COHORT (Dorsey & Investigators, 2012), PHAROS (Biglan et al., 2016), PREDICT (Jane S Paulsen et al., 2014) and TRACK-HD (Sarah J Tabrizi et al., 2013). Mixed effect regression models are widely implemented yet come with the primary

limitation of complex computational modelling involving time-consuming numerical integration over random effects, especially for non-linear modelling. However, in this study, we hypothesis disease progression in HD as a linear function of time; this drawback can be avoidable. Hence, we implemented a Linear mixed-effect model (LMER) to estimate and predict disease progression in HD for 24 months on TRACK-ON HD cohort (Kloppel et al., 2015). This approach would be the first to analyse TRACK-ON HD longitudinal data set to predict atrophy progression in HD, along with NDM. Repeated measures ANOVA and MANOVA, as discussed has some limitations which are pointed below (Vock et al., 2012):

1. Observation time for each subject should be at the same time points. However, it is unrealistic to achieve practically due to various reason. For example, in our dataset, some participants had participated for three years while some other had only participated two years.
2. ANOVA assumes that "the correlation among all measured data on the given subject is same regardless of how data were measured in real time". This completely ignore the random variation between subjects and within subjects' correlation variation.
3. Both ANOVA and MANOVA assumes covariance matrix of measured data within each subject is similar to all subjects. In this study, people were randomly assigned to two different groups, patients' group, and healthy controls. Hence, it is inappropriate to assume same covariance matrix.
4. There are other prominent issues with regards to covariates which fails to categories between time-varying and time-invariant covariates.

These limitation in approaches yields to modern methods for modelling disease progression in neuroimaging longitudinal data. Namely, generalized estimating equations model (Liang & Zeger, 1986) and mixed effects regression (Laird & Ware, 1982) are suggested and used in several study (Maroof et al., 2011; Sarah J Tabrizi et al., 2013). These methods allows both

time-varying predictors (e.g., age, brain volume) and time- invariant predictors (e.g., gender, genotype) as well as solving the problem of missing data and irregular timed information.

This study exclude generalized estimation equation model apart from having various advantages, as it is not designed or modelled to analyze the correlation structure of repeated measures (Fitzmaurice et al., 2008). Hence, mixed effect regression model is the best statistical approach for my study. In HD, mixed effect regression model is widely used for statistical modelling of correlated longitudinal data. It has already proved its statistical computing power in analysis of prospective, observational, multi-center longitudinal studies such as COHORT (Dorsey & Investigators, 2012), PHAROS (Biglan et al., 2016), PREDICT (Jane S Paulsen et al., 2014) and TRACK-HD (Sarah J Tabrizi et al., 2013). Mixed effect regression models are widely implemented yet come with the primary limitation of complex computational modelling involving time-consuming numerical integration over random effects, especially for non-linear modelling. However, in this study we hypothesize disease progression in HD as linear function of time, this drawback can be avoidable. Hence, we implemented Linear mixed- effect model (LMER) to estimate and predict disease progression in HD over a period of 24 month on TRACK-ON HD cohort (Kloppel et al., 2015). As far as we believe, this approach would be the first to analyse TRACK-ON HD longitudinal data set to predict atrophy progression in HD, along with NDM.

3.3 Linear Mixed-Effects Model (LME)

LME model is the advanced statistical approach to analyse longitudinal data. It is capable to model the longitudinal data with between subject and within subject correlations with inclusivity of covariables. we used an LME model to analyse the volume data from 82 brain regions across participants. One of the main reasons for using an LME model for our longitudinal study cohort is that it can be used to represent complex features of longitudinal data (Davis, 2002). LME models allow quantification of the variability in outcomes between and

within-subjects. The allow adjusting for covariates, both time-dependent and time-invariant. They can also account for missing data if the data are MAR (missing at random). The representation of the model into fixed-effects and random-effects is referred to by the term "mixed effects". These models can be specified so that some regression parameters are fixed or assumed to be the same for all subjects (e.g., the slope of a predictor), and others are random or distinct to every subject (e.g., intercepts) (Verbeke, 1997). An LME model (Davis, 2002; Laird & Ware, 1982; Verbeke, 1997) that includes both random and fixed effect parameters mathematically expressed as follows:

$$Y_i = X_i\beta + Z_i b_i + \epsilon, \quad i = 1, \ldots, N \qquad \textbf{Equation 1}$$

In the above equation,

i represents each subject, whereby we have a total N number of subjects.

Y_i is the response vector for subject i which has the dimension of n_i.

X_i and Z_i are known values (e.g., explanatory variables), and which have dimensional matrices of (n_i x p) and (n_i x q) respectively.

β denotes the fixed- effects of p-dimensional vector

b_i represents the random-effects of q-dimensional vector

ε_i is a error component of n_i dimensions.

Furthermore, this model has following assumptions:

1. The random effect $\mathbf{b}_i$ and within-subject error $\boldsymbol{\varepsilon}_I$ are independent for different subjects and independent of each other for same subject. i.e.,

   Cov (bi, bj) = 0 if i =/= j,

   Cov (εi, εj) = 0 if i =/= j and,

   Cov (bi, εi) = 0

2. $b_i \sim$ MV N_q (0, D), where D is a general (q x q) covariance matric with (i, j) element

$\sigma_{ij} = \sigma_{ji}$.

3. $\varepsilon_i \sim MVN_{n_i}(0, \Sigma_i)$, where Σ_i is an $n_i \times n_i$ covariance matrix.

The LME model assumes that the error terms and random effects are normally distributed, with mean zero, general covariance matrix D, and covariance of $\sigma^2\mathbf{I}$, where **I** represent the identity matrix. We have introduced interaction effect between group and time in our model.

3.3 LME Assumption

3.3.1 Random effect assumption

In statistical practice, histograms plotted from Bayesian estimates are generally used to check the normality assumption for the random effects (Pinheiro & Bates, 2002). We are fitting *lme4* package in R (D. Bates, Mächler, Bolker, & Walker, 2014) platform to mathematically compute the model. In *lme4* package *qqnorm* can be used to get normal plot of estimated random effects for checking marginal normality and identifying outliers.

3.3.2 Residual terms assumption

We come across two different residuals in the mixed model, marginal and conditional residual (Pinheiro & Bates, 2002). Marginal residuals are the predictors of marginal error i.e., deviation of a subject from group mean, and the conditional residuals are the predictors of conditional error i.e., deviation from each measurement within a subject from the mean of same subject in a period of time.

3.4 Fitting LME Model in R

Out of various packages available, we use *lme4* package version 1.1-27.1(D. Bates et al., 2014) in this study in R platform. Some codes used in the thesis are listed in appendix. It is described more in detail in Chapter 4.

Chapter 4: Linear Mixed Effects Modelling of Longitudinal Degeneration in Premanifest HD

The main focus of this chapter is to address the first aim of this research project. This project uses the structural MRI scans from a longitudinal study in pre-HD - the Track-On HD. The MRI data were statistically analysed using linear mixed-effects (LME) models to derive the spatial distribution of degeneration in pre-HD patients comparing with healthy controls. The spatial maps are used as measured atrophy to inform the development of NDM in the next chapter.

4.1 Introduction

The CAG trinucleotide unnatural repetition in the HTT causes the HD, which results in formation of the mutant huntingtin protein (mHTT) and progressive neurodegeneration (MacDonald et al., 1993). Because of the monogenic nature of the disease, HD provides an excellent model of progressive neurodegeneration that is independent of the ageing process. In particular, individuals can be studied even before the appearance of clinical symptoms (pre-manifest; pre-HD). Clinical diagnosis of the onset of HD depends on the assessment of motor symptoms. However, progressive decline in motor function, cognitive abilities, and mood observed are before clinical diagnosis. The average onset of HD is around 40 years of age, with a formal clinical assurance requiring motor signs in a person with a positive family history. Genetic testing is also often conducted in individuals with a family history of HD, which provides 100% specificity to the clinical diagnosis.

An important marker of HD progression is the widespread degeneration of the brain that is independent of the ageing process. Various studies have researched the degeneration in HD by utilising neuroimaging procedures like MRI. These studies map brain volumes in pre-HD

individuals compared to a healthy control cohort (Garcia & Marder, 2017; G. R. Poudel, Harding, Egan, & Georgiou-Karistianis, 2019; Rodrigues et al., 2020; S. J. Tabrizi et al., 2009; Sarah J. Tabrizi et al., 2011; Van Raamsdonk, Pearson, Murphy, Hayden, & Leavitt, 2006). These studies have revealed structural and microstructural changes in the grey and white matter regions, such as the caudate, putamen, occipital regions, and the cortico-striatal tracts in pre-HD several years before disease onset. Other studies have mapped the subtle alterations in functional and structural brain networks within the cortico-striatal loops in pre-HD (Domínguez et al., 2017; G. R. Poudel, Harding, Egan, & Georgiou-Karistianis, 2019; Govinda R. Poudel, Julie C. Stout, et al., 2014).

Furthermore, selective microstructural loss of white matter tracts extending from the striatum to the prefrontal and motor cortices have also been observed in pre-HD far from and close to onset (Govinda R. Poudel, Julie C. Stout, et al., 2014). Although these studies provide sufficient evidence to suggest early degeneration in individuals with the HD gene, there is emerging evidence that degeneration proliferates through brain networks, spreading from the striatum and affecting the cortical surface (G. R. Poudel, Harding, Egan, & Georgiou-Karistianis, 2019). Several longitudinal studies are starting to map the potential spread of degeneration throughout the brain in HD.

The PREDICT-HD is considered to be one of the first and biggest multi-site, longitudinal cohort studies of HD to investigate degeneration in both pre-HD and symptomatic HD (symp-HD)(Van Raamsdonk et al., 2006). Using MRI scans, PREDICT-HD tracked brain volumes, cognitive, motor, and psychiatric symptoms in pre-HD and manifest HD patients over ten years (2001 to 2011). The analysis of MRI scans from many individuals (N=1314) suggested the largest and most significant changes observed in regional brain volumes, including the putamen and caudate. In another multi-site MRI research in HD (TRACK and Track-On HD)(Sarah J. Tabrizi et al., 2011), neuroimaging changes reflecting the underlying neurodegenerative processes observed for twelve months in both pre-manifest and symptomatic

HD groups. The findings suggested that the pre-HD individuals closer to onset showed significantly greater whole-brain degeneration and ventricular size increase than healthy controls. The degeneration of the whole brain and increase in ventricular size was also observed in within-group comparison in pre-HD far from the onset, but this was not statistically significant compared to controls. Importantly, consistent with the previous PREDICT-HD study, the degeneration in the putamen and caudate was faster in pre-HD both far from and close to onset (Sarah J. Tabrizi et al., 2011). Importantly, TRACK-HD was the first study to show the possibility of observation of brain markers before any measurable clinical decline. Corroborated by smaller-scale longitudinal studies such as IMAGE-HD (Domínguez et al., 2013; G. R. Poudel, Harding, Egan, & Georgiou-Karistianis, 2019) shows the evidence of striatal degeneration in pre-HD. The IMAGE-HD study has likewise uncovered that caudate decay is the primary marker of degeneration in both premanifest and indicative phases of HD. The IMAGE-HD study also revealed that caudate atrophy is the most significant marker of degeneration in both premanifest and symptomatic stages of HD (Domínguez et al., 2013; G. R. Poudel, Harding, Egan, & Georgiou-Karistianis, 2019).

Despite the progress in mapping whole-brain and subcortical degeneration in premanifest HD, robust spatial mapping of the degeneration in the HD brain across different brain regions during the premanifest stage of the disease is lacking. In a recent review, Tan et al. (Estevez-Fraga, Scahill, Rees, Tabrizi, & Gregory, 2021) found that there is a dire need to map the progressions on cortical surfaces in HD and its further research. The accessibility of large neuroimaging datasets from new studies such as Track-On HD has made it possible to conduct new cortical and sub-cortical examinations in HD (Qi & Arfanakis, 2021). Furthermore, the use of advanced image processing on MRI scans, followed by robust statistical modelling, should reveal subtle changes which might have been otherwise missed. For example, a recent study used longitudinal data from all three longitudinal studies (PREDICT-HD, TRACK-HD, and

IMAGE-HD) and used LME models to reveal imaging biomarkers that might be relevant for future clinical trials (Rodrigues et al., 2020).

4.2 Specific aims

We aimed to characterise the longitudinal changes in the cortical and subcortical brain volumes in premanifest HD (pre-HD) compared to healthy controls. We hypothesised that premanifest HD shows widespread degeneration in the cortical (motor) and sub-cortical (striatum) brain regions over 24-months, compared to healthy controls.

4.3 Methods

4.3.1 Participants

The data used in this study are from the participants who were recruited as a part of Track-On HD. Track-On HD is the follow-up study of TRACK-HD (S. J. Tabrizi et al., 2009). In the TRACK-ON study, participants were followed up every 12 months, up to 24 months (i.e., three visits). A sample of N=239 participants was enrolled from the Track-On HD study, out of whom 106 were premanifest HD (pre-HD), 22 were early HD, and 111 individuals were age- and sex-matched healthy controls without HD. Four international multi-site scanners were used for collecting the data. In this study, we only used the data from pre-HD and healthy controls. Furthermore, we excluded 22 early HD. The participants were genetically tested and required to have a CAG repeat length greater than or equal to 40 and a disease burden score greater than 250 (Klöppel et al., 2015). These data were made available by CHDI (Cure Huntington's Disease Initiative) Foundation.

The information obtained contains clinical and demographic patient data; cognitive, neuropsychiatric, oculomotor and quantitative motor data, brain imaging (MRI), blood, tissue and hereditary markers. The participants were selected from four international cities - London,

Paris, Leiden, and Vancouver. The information was gathered from the study participants yearly between 2012 and 2014.

Enrolment methods, consideration standards, and MRI convention have been published elsewhere (Klöppel et al., 2015; S. J. Tabrizi et al., 2009; Sarah J. Tabrizi et al., 2011). See Table 3 for the demographic data.

Table 3 Demographic data of Pre-HD and control participants

	Healthy participants	**Pre-HD (n=106)**
Age	23 to 65.7	18.6 to 64.1
Male/Female	34/55	49/57
Disease burden score	----------	293.2
CAG repeat length	----------	39 to 52

**Data are in range/average numbers*

Note. **CAG: (number of repeats >40) *Disease burden score = Age X* (CAG *length – 35.5)* CAG*: cytosine-adenine-guanine*

4.4 Neuroimaging Data Acquisition (MRI)

MRI images were collected using Philips Achieva and Siemens TIM Trio 3T MRI scanners. The scans performed at four internationals sites were London, Paris, Leiden and Vancouver. Structural MRIs were acquired using T1-weighted imaging with the following parameters: TE 30 ms, FOV 212 mm, flip angle 80 degrees, forty-eight slices in ascending order with slice thickness: 2.8 mm, gap: 1.5 mm, in-plane resolution of 3.3 x 3 mm and bandwidth of 1960 Hz per Px. Previously published research (Klöppel et al., 2015) describes the detailed MRI data acquisition process.

The process of data collection and storage was previously explained in the report of the TRACK-HD study (Tabrizi et al., 2009). To ensure high data quality during the acquisition of 3T MRI data, standardised acquisition protocols were developed to follow at all four sites (Tabrizi et al., 2009, Kloppel et al., 2015). These protocols included both T1-weighted volumetric and T2-weighted sequences. To ensure good quality data, pre-imaging preparation phases were conducted which lasted six months. Four phases of QA were conducted, including discussion with the advisory group and the receipt of a full range of sequences, performing qualitative and quantitative review on the MRI image data, determining the stability of the sequences received and conducting final optimization and testing of the shortlisted MRI image data sequences. Furthermore, image quality was compared during quality control and different scores were given to determine whether T1 images were of similar quality or T1 weighted images were of higher quality. Additionally, the FreeSurfer neuroimaging tool was used for each image quality check.

4.5 Structural MRI Data Processing

The T1-weighted MRI scans were processed using the image processing pipeline presented in figure 4. Each subject's high-resolution MRI data image was utilised to segment and measure grey matter volumes according to the Desikan-Killiany Atlas. In addition, the FreeSurfer was utilised for parcellation of the T1-weighted imaging (MRI) information into 82 subcortical and cortical cerebrum regions, as indicated by the Desikan-Killiany atlas. FreeSurfer analysis was conducted on the MASSIVE HPC website using the longitudinal stream "recon-all" function (http://www.massive.org.au).

FreeSurfer is open-source software for assessing and analysing basic and viable neuroimaging data from cross-sectional or longitudinal examinations. FreeSurfer version 5.3.0 estimates regional neurodegeneration concerning total grey matter volume for 82 cortical and sub-cortical brain regions. Each of these brain regions is specifically known as a region of interest (ROI). All ROIs associated with the cerebellum were excluded from this analysis. An

automated longitudinal stream method to extract brain regional volumes estimates in FreeSurfer (Reuter, Schmansky, Rosas, & Fischl, 2012).

The longitudinal stream includes various processing steps as follows: a) skull stripping, b) Volumetric Labelling, c) Intensity normalisation, d) white matter segmentation, e) surface Atlas registration, f) Surface extraction, and e) Gyral labelling (Reuter et al., 2012). In addition, all MRI images went through standardised quality control methodologies. As a result, all participants included in this study had good image quality with a complete segmentation success rate.

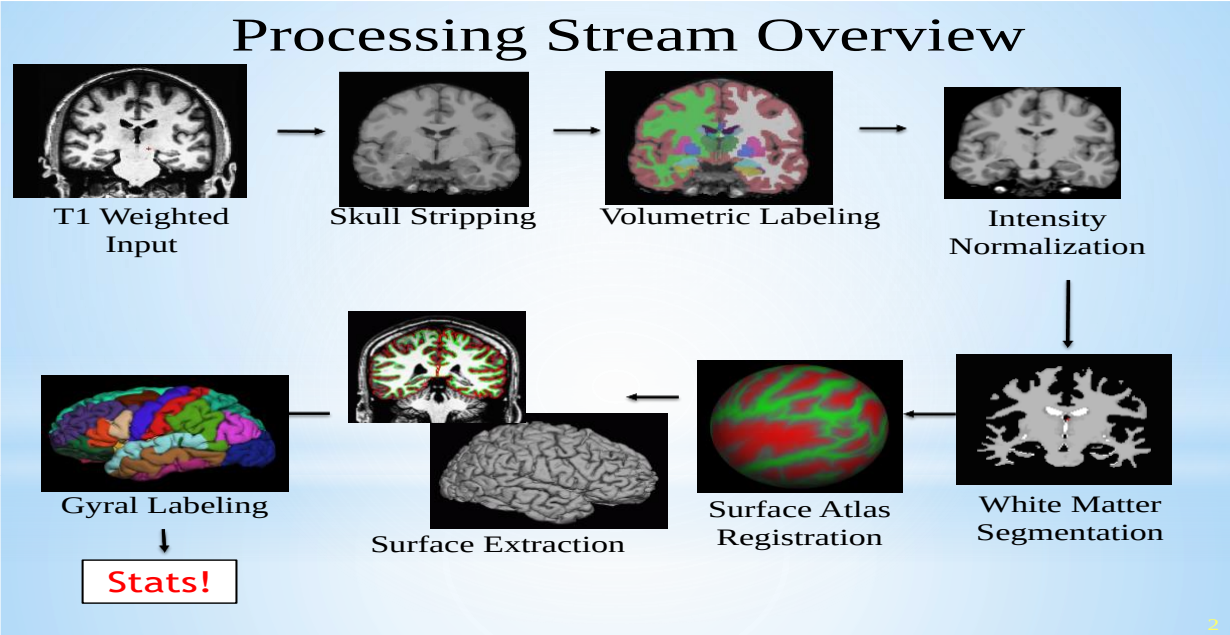

Figure 10: The graphical representation for neuroimaging pre-processing in the study.

Note. Free-surfer version 5.3.0 software was used to run the analysis (Reuter et al., 2012).

4.4.1 Workflow Summary

Below, we provide the steps used in longitudinal processing of MRI data.

Step 1. First, all data at different time points are cross-sectionally processed with default workflow using recon-all, e.g.:

recon-all -all -s <tpNid> -i path_to_t1_dcm; here t1 is one of the time points.

Step 2. Data is processed again with recone-all creating an unbiased template from all the time points for each subject, e.g.:

recon-all -base <templateid> -tp <tp1id> -tp <tp2id> ... -all

Step 3. "-long" is used for processing all timepoints longitudinally, e.g.:

recon-all -long <tp1id> <templateid> -all

The detailed, step-by-step method used in our study is described in FreeSurfer.

4.6 Data Preparation for Longitudinal Analysis

The volumetric data obtained from the longitudinal stream processing in FreeSurfer was initially in mm3, where values were in the order of 106 in magnitude for all the ROI brain regions. We then normalised all the ROI volumes within each subject by dividing ROI volume from each brain region by estimated total intracranial volume (eTIV) for all time points. After normalisation, every volume measurement in the analysis cohort was taken forward for longitudinal statistical modelling using a linear mixed model in R.

4.7 Statistical Analysis

We first inspected our longitudinal data through graphical displays. Next, we checked if our data are normally distributed across time. To check for normality, we visualised the raw data using distribution plots and Q-Q plots. The Q-Q plot was generated by graphing the two quantiles of data against one another. For most brain regions, the two sets of quantiles appeared to be from the same Gaussian distribution, as there was a straight line for all the Q-Q plots. The Q-Q plots and distribution plots of the raw data are shown in figure 10. From this plot, we can assess the overall trend of the raw data (increment, decrement or constant).

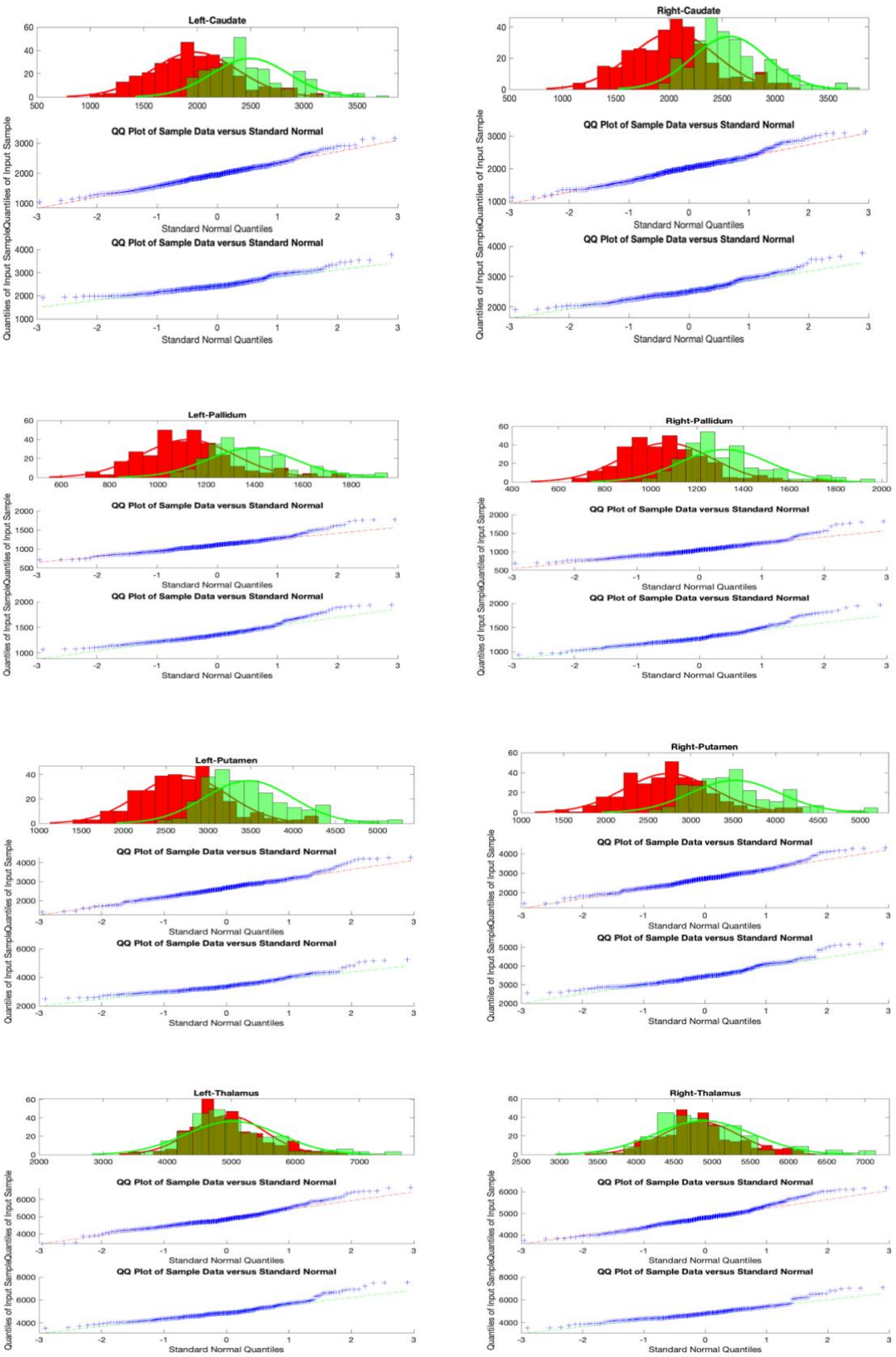

Figure 11 Distribution (histogram) and QQ-plot for raw volume data of some of the example brain regions in healthy controls (green) and patients (red).

4.9 LME implementation in R

We started the longitudinal modelling by defining the random and fixed effects in our LME model. In the LME model, "fixed-effects" are the explanatory (aka, predictor) variables of interest – namely, time of assessment and group (pre-HD vs. healthy controls). To estimate the differences in change of brain region volume trajectories across the two groups (pre-HD and healthy controls), we included a Group by Time interaction term in the MLE model (denoted as "group x timepoints"). This term was modelled as a fixed effect for each of the 82 brain regions of the subjects. Subjects represented the random effect in the model, expressed as (1 | subject.ID) in the MLE equation. This indicates different intercepts for each subject, i.e., that subjects were assumed to have different baseline response values (specific brain region volumes).

We used R to implement the LME model. Although we started with a more complex model incorporating linear and quadratic components, the quadratic component was removed as it did not appear to offer any improvements (based on Akaike Information Criterion values). Statistically significant ($p<.05$) interaction terms were probed by estimating the effect of time on the response variable for each of the groups separately (pre-HD and healthy controls).

The pseudocode for the implementation of the LME model is provided below.

```
for (i in 7:88){
NDMmodL<-lmer(dataHD[,i] ~ fgroup*timepoints +fgender + age + (1|Subject.ID),
data=dataHDL, REML=FALSE)
TimeInteractionL<- confint(glht(NDMmodL, linfct = c("fgroup1:timepoints = 0")))
```

In the above model, dataHDL[,i] represents each subject's 82 brain regions (ROI). As stated above, the group by time interaction effect for each of the 82 brain regions was estimated. Gender and age were included as covariates because they may explain residual variance in the response variables. The restricted maximum likelihood (REML) estimation method was used to

derive estimates of the variance components instead of the maximum likelihood because the latter has been shown to produce biased variance estimates. The model estimated the group by time interaction effect, one by one, for all 82 brain regions, keeping subjects' ID as a random effect.

We modelled a linear mixed model (estimation using REML) to predict dataHD[,i] (brain regions) with fgroup, timepoints, fgender and age (formula: ~ dataHD[,i] ~ fgroup*timepoints + fgender + age). The model included subject.ID as random effect (formula: ~1 | Subject.ID). This model measures whether the interaction effect of timepoints on fgroup [1] was statistically significant. Any interaction effect at $p<0.05$ is considered significant.

4.10 Results

4.10.1 Longitudinal brain degeneration in pre-HD compared to controls

Table 4, 5 and 6 provide a summary of statistical outputs from linear mixed models of the brain volume data in the left and right hemisphere of the cortex and sub-cortical regions. In the left side of the brain, most of the cortical brain regions showed negligible effects in terms of longitudinal volume change. Significant degeneration ($p<0.05$) was observed in the left lateralorbitofrontal, parsorbitalis, and superiortemporal brain regions as compared to controls. In the right hemisphere, there were no brain regions showing significant atrophy over time.

Within the sub-cortical regions, several structures showed significant atrophy over time in pre-HD. The most significant sub-cortical areas were in the left and right putamen and left and right caudate, with the left amygdala showing the largest longitudinal volume loss (As shown in Table 7).

Table 4 Comparison of volumes in Pre-HD and controls in Left Hemisphere of cortical regions of brain.

Difference in volume changes between Controls and pre-HD subjects						
Brain regions (Left Hemisphere)	**Beta(estimate)**	**CI (95%)**		**t value**	**z value**	**p value**
		lower	**Upper**			
bankssts	-6.95	-26.53	12.64	-0.70	-1.92	0.49
caudalanteriorcingulate	2.28	-15.23	19.79	0.26	0.49	0.80
caudalmiddlefrontal	-10.90	-69.31	47.51	-0.37	-1.54	0.72
cuneus	12.19	-21.62	46.00	0.71	-3.49	0.48
entorhinal	15.45	-18.78	49.69	0.89	-0.15	0.38
fusiform	-42.93	-114.58	28.73	-1.18	-3.95	0.24
inferiorparietal	-10.02	-127.35	107.30	-0.17	-2.99	0.87
inferiortemporal	-29.07	-128.15	70.02	-0.58	-3.76	0.57
isthmuscingulate	14.70	-3.89	33.29	1.55	-0.62	0.12
lateraloccipital	0.52	-114.45	115.49	0.01	-5.29	0.99
lateralorbitofrontal	-63.15	-124.66	-1.64	-2.02	-2.93	0.05

Difference in volume changes between Controls and pre-HD subjects						
Brain regions (Left Hemisphere)	**Beta(estimate)**	**CI (95%)**		**t value**	**z value**	**p value**
		lower	**Upper**			
lingual	-15.08	-68.90	38.74	-0.55	-3.86	0.58
medialorbitofrontal	-14.25	-81.76	53.27	-0.41	-0.32	0.68
middletemporal	-55.41	-143.40	32.58	-1.24	-4.20	0.22
parahippocampal	0.96	-14.77	16.69	0.12	-2.00	0.90
paracentral	-4.41	-48.16	39.35	-0.20	-1.31	0.84
parsopercularis	-16.81	-55.54	21.91	-0.85	-2.73	0.40
parsorbitalis	**-47.04**	**-77.31**	**-16.78**	**-3.05**	**-2.66**	**0.00**
parstriangularis	-17.29	-55.70	21.11	-0.88	-2.99	0.38
pericalcarine	23.10	-11.38	57.59	1.32	-1.17	0.19
postcentral	-47.47	-144.57	49.62	-0.96	-2.44	0.34
posteriorcingulate	13.79	-12.33	39.92	1.04	0.53	0.30
precentral	-53.32	-191.45	84.80	-0.76	-2.39	0.45

Difference in volume changes between Controls and pre-HD subjects						
Brain regions (Left Hemisphere)	**Beta(estimate)**	**CI (95%)**		**t value**	**z value**	**p value**
		lower	**Upper**			
precuneus	12.13	-85.98	110.25	0.24	-1.18	0.81
rostralanteriorcingulate	4.18	-23.78	32.13	0.29	0.82	0.77
rostralmiddlefrontal	-56.90	-205.98	92.18	-0.75	-1.32	0.46
superiorfrontal	-43.39	-254.39	167.61	-0.40	-0.85	0.69
superiorparietal	-14.59	-166.48	137.30	-0.19	-2.58	0.85
superiortemporal	**-97.50**	**-188.02**	**-6.98**	**-2.12**	**-4.25**	**0.04**
supramarginal	-14.54	-114.46	85.38	-0.29	-1.99	0.78
frontalpole	0.18	-17.74	18.11	0.02	-0.17	0.98
temporalpole	5.04	-31.69	41.78	0.27	-2.25	0.79
transversetemporal	0.90	-12.52	14.32	0.13	-2.60	0.90
insula	-5.12	-47.29	37.04	-0.24	-0.09	0.81

Note. *Brain regions showing significant differences in volume changes between the two groups of subjects are highlighted in green.*

Table 5 Comparison of volumes in Pre-HD and controls in Right Hemisphere of cortical regions of brain.

	Difference in volume changes between Controls and pre-HD subjects					
Brain regions (Right Hemisphere)	**Beta(estimate)**	**CI (95%)**		**t value**	**z value**	**p value**
		lower	**upper**			
bankssts	1.71	-17.05	20.47	0.18	0.55	0.86
caudalanteriorcingulate	8.46	-11.59	28.50	0.83	-0.48	0.41
caudalmiddlefrontal	16.80	-43.60	77.21	0.55	-0.03	0.59
cuneus	-2.53	-41.48	36.43	-0.13	-2.31	0.90
entorhinal	-1.09	-34.08	31.89	-0.07	1.52	0.95
fusiform	-22.54	-84.62	39.54	-0.71	-2.25	0.48
inferiorparietal	-39.03	-169.59	91.53	-0.59	-0.87	0.56
inferiortemporal	-56.71	-139.82	26.41	-1.34	-1.16	0.18
isthmuscingulate	1.66	-15.74	19.06	0.19	-1.57	0.85
lateraloccipital	-87.97	-208.30	32.36	-1.44	-3.87	0.15
lateralorbitofrontal	-44.73	-113.48	24.02	-1.28	-2.69	0.20
lingual	0.78	-61.31	62.86	0.02	-1.55	0.98

Difference in volume changes between Controls and pre-HD subjects						
Brain regions (Right Hemisphere)	**Beta(estimate)**	**CI (95%)**		**t value**	**z value**	**p value**
		lower	**upper**			
medialorbitofrontal	12.75	-58.48	83.98	0.35	-0.27	0.73
middletemporal	-53.13	-132.02	25.75	-1.32	-1.75	0.19
parahippocampal	4.44	-11.94	20.82	0.53	0.29	0.60
paracentral	-12.27	-57.26	32.72	-0.54	-0.96	0.59
parsopercularis	-13.03	-46.43	20.37	-0.77	-0.17	0.45
parsorbitalis	-7.06	-38.85	24.72	-0.44	-1.81	0.66
parstriangularis	-15.50	-57.37	26.38	-0.73	-0.92	0.47
pericalcarine	14.73	-27.17	56.63	0.69	-0.33	0.49
postcentral	-12.59	-110.80	85.61	-0.25	-1.28	0.80
posteriorcingulate	4.26	-20.70	29.22	0.34	-0.99	0.74
precentral	-42.23	-186.51	102.06	-0.58	-0.87	0.57
precuneus	-25.81	-117.51	65.90	-0.55	-0.92	0.58
rostralanteriorcingulate	-9.69	-35.57	16.19	-0.74	0.81	0.46

Difference in volume changes between Controls and pre-HD subjects						
Brain regions (Right Hemisphere)	**Beta(estimate)**	**CI (95%)**		**t value**	**z value**	**p value**
		lower	**upper**			
rostralmiddlefrontal	-32.93	-202.59	136.74	-0.38	-0.15	0.70
superiorfrontal	20.58	-181.81	222.97	0.20	-0.11	0.84
superiorparietal	-54.23	-206.48	98.03	-0.70	-1.62	0.49
superiortemporal	-38.29	-127.24	50.66	-0.85	-1.08	0.40
supramarginal	-8.08	-93.44	77.28	-0.19	-1.34	0.85
frontalpole	5.30	-14.68	25.28	0.52	-0.07	0.60
temporalpole	-6.33	-41.98	29.32	-0.35	-2.32	0.73
transversetemporal	-7.50	-19.78	4.79	-1.20	-4.84	0.23
insula	-3.01	-45.52	39.50	-0.14	-0.30	0.89

Note. *Brain regions showing significant differences in volume changes between the two groups of subjects are highlighted in green.*

Table 6 *Comparison of volumes in Pre-HD and controls in Sub-Cortical brain regions.*

Difference in volume changes between Controls and pre-HD subjects						
Brain regions	**Beta(estimate)**	**CI (95%)**		**t value**	**z value**	**p value**
		lower	**upper**			
Left-Thalamus	**-40.58**	**-81.42**	**0.26**	**-1.95**	**-3.28**	**0.05**
Left-Caudate	**-44.64**	**-69.98**	**-19.29**	**-3.46**	**-10.52**	**0.00**
Left-Putamen	**-40.31**	**-70.78**	**-9.83**	**-2.60**	**-7.43**	**0.01**
Left-Pallidum	-4.48	-19.66	10.70	-0.58	-0.67	0.56
Left-Hippocampus	-12.77	-36.78	11.25	-1.04	-1.23	0.30
Left-Amygdala	**-21.44**	**-40.52**	**-2.36**	**-2.21**	**-2.50**	**0.03**
Left-Accumbens-area	-6.64	-21.30	8.01	-0.89	-0.78	0.38
Right-Thalamus	-38.61	-80.86	3.65	-1.80	-1.94	0.07
Right Caudate	**-33.58**	**-61.82**	**-5.35**	**-2.34**	**-8.52**	**0.02**
Right-Putamen	**-44.00**	**-72.20**	**-15.80**	**-3.07**	**-6.72**	**0.00**
Right-Pallidum	-2.25	-17.75	13.25	-0.29	-1.54	0.78

Difference in volume changes between Controls and pre-HD subjects						
Brain regions	**Beta(estimate)**	**CI (95%)**		**t value**	**z value**	**p value**
		lower	**upper**			
Right-Hippocampus	2.35	-20.21	24.90	0.20	-2.07	0.84
Right-Amygdala	-4.27	-22.07	13.52	-0.47	-2.45	0.64
Right-Accumbens-area	-8.40	-18.30	1.49	-1.67	-3.45	0.10

Note. *Brain regions showing significant differences in volume changes between the two groups of subjects are highlighted in green.*

4.10.2 Spatial distribution of degeneration in the pre-HD brain

Figure 11 shows the spatial distribution of degeneration across the 82 sub-cortico regions regarding the Desikan-Killiany atlas. Compared to healthy controls, the colour coding shows z-scores for group-by-time interaction effects from the longitudinal volume loss of pre-HD. The spatial map reveals that the sub-cortical network is most susceptible to longitudinal degeneration of atrophy in HD comparing healthy participant's brain. Table 7 list out all cortical and sub-cortical regions showing highest rate of volume loss comparing HD and healthy controls. Caudate, putamen and amygdala showed the maximum rate of sub-cortical volume loss while largest rate of longitudinal degeneration are noticed in ateralorbitofrontal, parsorbitalis and superiortemporal regions of cortical brain.

Table 7 Comparison of regional volumes in HD and healthy controls. Only regions showing loss of volumes at $p<0.05$ are shown in the table

Brain regions	**Beta(estimate)**	**CI (95%)**		**z_value**	**p_value**
		lower	**upper**		
Left-Caudate	-44.64	-69.98	-19.29	-10.52	0.00
Left-Putamen	-40.31	-70.78	-9.83	-7.43	0.01
Left-Amygdala	-21.44	-40.52	-2.36	-2.50	0.03
Right Caudate	-33.58	-61.82	-5.35	-8.52	0.02
Right-Putamen	-44.00	-72.20	-15.80	-6.72	0.00
lateralorbitofrontal	-63.15	-124.66	-1.64	-2.93	0.05
parsorbitalis	-47.04	-77.31	-16.78	-2.66	0.00
superiortemporal	-97.50	-188.02	-6.98	-4.25	0.04

Furthermore, the degeneration of the cortex appears to be left-lateralised, with the strongest atrophy observed only in the left side of the brain. It can be noted that the left part of the caudate and putamen have a slightly higher effect of atrophy distribution compared to the right part.

Figure 12 Visualisation of the spatial degeneration in Pre-HD compared to controls.

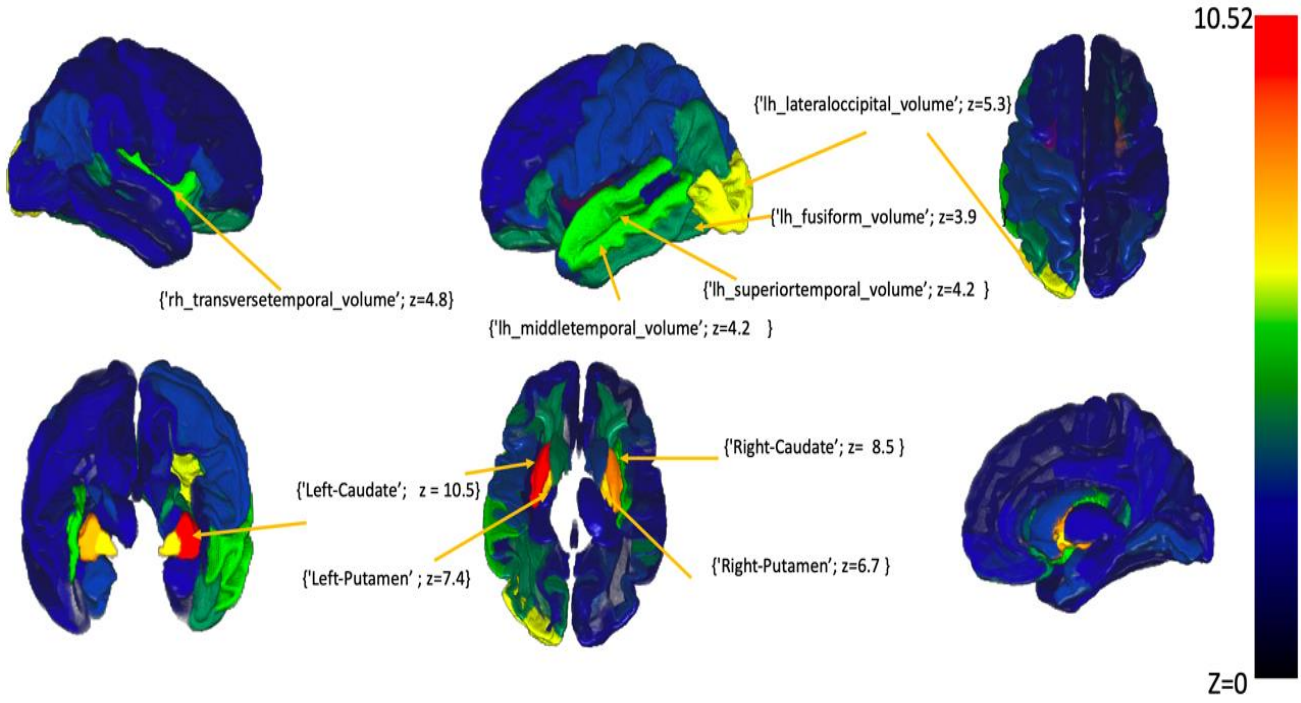

Note. The distribution is provided for 82 ROIs with reference to the IIT atlas (Desikan-Killiany atlas). The colour code indicates the z-values (of group-by-time interaction effect) such that red, yellow denotes maximum observed atrophy over time.

Figure 12 further depicts the decrease in volume in pre-HD over time compared to controls. For illustration, we take two example regions from the cortical and subcortical parts of the brain. The visualisation of the baseline adjusted volume of the caudate and left lateral occipital cortex shows apparent group-by-time interaction effects. On average, the volume loss in the caudate over 24 months is approximately 6%, whereas, in the left lateral occipital cortex, the volume loss over the same period is approximately 2.5%. Overall, this plot indicates the spatial distribution of atrophy in the cortical and sub-cortical regions across time in pre-HD

compared to controls. The rate of atrophy in the caudate is higher and looks consistent from the baseline time point, with gradual decrement as time passes. However, the left lateral occipital cortex shows a slow rate of change from the baseline to the time point (i.e., 12 months) and a sudden decrement after that.

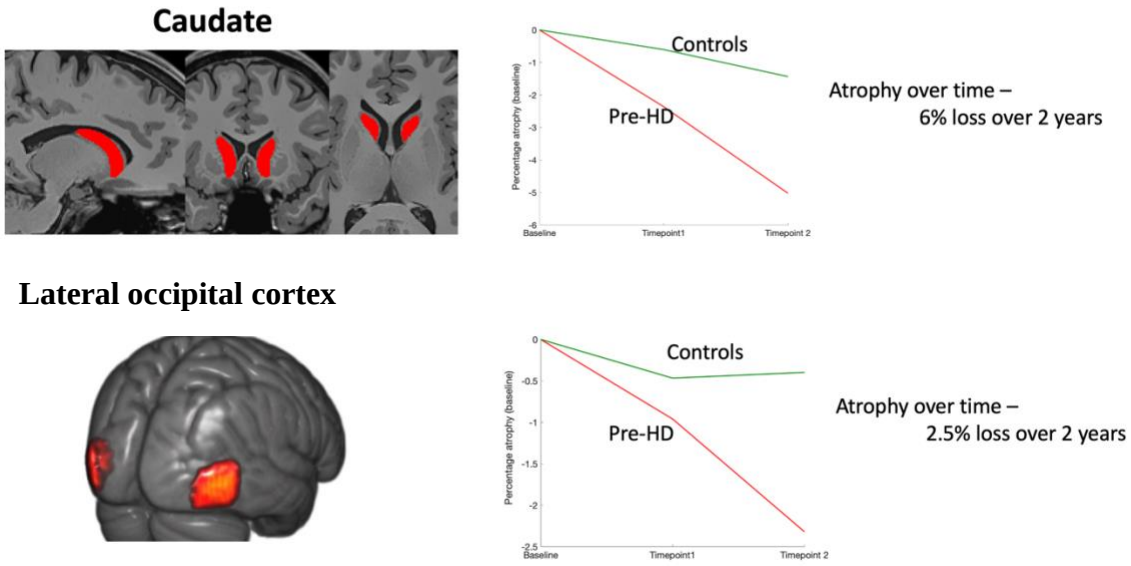

Figure 13 Plots of average baseline adjusted volumes of the Caudate and Lateral Occipital Cortex in Pre-HD and Control**.**

Note. The baseline adjusted volumes reveal change over time in volume in pre-HD and Controls.

4.11 Discussion

This study investigated cortical and subcortical degeneration in pre-HD compared to controls within a two-year timeframe. We used an LME model to compare the rate of atrophy in pre-HD against a group of age-matched healthy controls. The findings suggest that brain degeneration can be observed in both the subcortical and cortical regions in pre-HD. However, the rate of atrophy is much higher in subcortical regions such as the caudate and putamen. The

caudate shows, on average, 6% atrophy over 24 months in pre-HD. Cortically, the highest atrophy is observed in the visual cortex (lateral occipital) and temporal cortices (superior and middle temporal). These findings highlight the need for mapping degeneration across the whole brain in pre-HD so that the epicentres and pathways of degeneration in HD can be traced accurately.

We have overcome the challenges encountered in the statistical analysis of longitudinal neuroimaging data by implementing an LME model in this research. Longitudinal data are correlated, have different baseline timing, and usually have missing measurements. After thorough research and review of the literature, we found that the LME model overcomes the factors mentioned above, compared to other models such as repeated measure ANOVA and t-tests (Garcia & Marder, 2017). The statistical power of the LME model to handle irregular timing and missing data from longitudinal neuroimaging data has increased its popularity among researchers in longitudinal studies of neurodegenerative diseases. LME models have been previously used in various studies, such as COHORT (Dorsey & Investigators, 2012), PHAROS (Biglan et al., 2016), PREDICT (J. S. Paulsen et al., 2008) and TRACK-HD (Sarah J Tabrizi et al., 2013). The LME model has helped to study behavioural function, cognitive analysis, and movement disorder, utilising the data from COHORT, which includes three assessments across time (Dorsey & Investigators, 2012). Most of the above studies faced similar challenges related to missing data and irregular scan timing. We had the same issue initially as we were analysing our longitudinal data using paired t-tests to quantify and test the statistical significance of the change in atrophy. However, to implement this statistical method, we had to eliminate many subjects in both pre-HD and healthy controls due to irregularity in consecutive scanning. Very few subjects had three consecutive scans over three years. The use of the LME model has eliminated these obstacles and has allowed us to include almost all the quality matched data.

Our findings in sub-cortical degeneration are consistent with the findings reported in previous studies in pre-HD (Wijeratne et al., 2020) (Aylward et al., 2000) (Govinda R. Poudel et al., 2020). We observed that the highest sub-cortical atrophy is observed in the caudate, putamen, and thalamus. The caudate showed on average up to 6% volume loss over two years. These findings suggest that the caudate may serve as an imaging biomarker for HD. In a recent cross-sectional study of subcortical volumes in HD, the caudate volume has been highlighted as one of the most significant regions (Wijeratne et al., 2020). The most significant volume loss in the striatum in pre-HD compared to controls, after controlling for the effects of age and gender, further supports the notion of selective vulnerability of medium spiny neurons in HD (Ehrlich, 2012). The medium spiny neurons in the caudate have predominantly afferent glutamatergic input from the cortex, and predominantly dopaminergic input from the substantia nigra. Hence, the aggregate effects of total dopaminergic and glutamatergic input may result in the selective vulnerability of medium spiny neurons to the neurotoxic effects of mutant huntingtin protein (Ehrlich, 2012).

In the cortex, we discovered localised cortical degeneration in the occipital and temporal lobes, consistent with previous cross-sectional cortical thickness studies (Rosas et al., 2008). We observed the highest progression of atrophy in the visual cortex (lateral occipital) and temporal cortex (superior and middle temporal), consistent with previous studies which suggested occipital-lobe abnormalities in HD (Klöppel et al., 2008; Rosas et al., 2006). We found the cerebellar cortical region to be relatively unaffected, especially at early baseline stages, which was also found in neuropathological studies (Vonsattel & DiFiglia, 1998), although in contrast, other studies showed a wide progression in the cortical region in later stages of manifest HD (Heinsen et al., 1994; Selemon, Rajkowska, & Goldman-Rakic, 2004; Wagster, Hedreen, Peyser, Folstein, & Ross, 1994). Our initial results indicate the rate of volume change in the left lateral occipital cortex over two years to be about 2.5% loss, with no significant volume loss in the right cortical regions. The rate of longitudinal volume change was seen to be faster in later stages than at

baseline. Typical, age-related volume loss was identified in the control group, smaller than the degeneration associated with HD, which shows that cortical degeneration in HD can start years before it can be clinically detected.

Several limitations were needed to be considered. First, we do not analyse the association between imaging changes and behavioural or cognitive issues in the current study. Secondly, previous research has found significant associations between brain imaging markers and neurobehavioral outcomes (Gregory et al., 2018; Govinda R. Poudel, Julie C. Stout, et al., 2014; S. J. Tabrizi et al., 2009). However, as the current study was focused on determining the spatial maps of degeneration, correlation with behavioural measures was out of scope. Furthermore, the study is limited to the investigation of pre-manifest individuals.

In summary, this study performed a comprehensive analysis of volume changes in the 82 brain regions of premanifest HD individuals compared to healthy controls. The model used revealed that the most significant degeneration over two years occurs in the caudate and putamen (controlling for the effect of age and gender). Contrary to expectations, cortical brain regions did not show widespread degeneration in pre-HD. Based on these findings, we suggest that volumetric markers, such as caudate and putamen volumes could be considered a primary endpoint in future clinical trials. Furthermore, the findings suggest that cortical degeneration may occur later in the disease process than subcortical degeneration. Thus, monitoring both cortical and sub-cortical volumetric changes, alongside primary and secondary clinical endpoints, may provide more comprehensive tracking of neurodegeneration in HD.

Chapter 5: Predicting Neurodegeneration in pre-HD Using NDM

The previous chapter demonstrated that neuropathological changes in HD typically develop in the brain by following a specific anatomical pattern, which most likely initiates in the striatum and then spreads to the cortical motor, frontal, and occipital regions. This chapter addresses the second aim of this project and focuses on describing the implementation and application of the NDM for predicting longitudinal degeneration in pre-HD compared to healthy controls. Finally, we will use the empirical data obtained from the previous chapter (Chapter 3) to test the predictive ability of NDM in HD.

5.1 Introduction

The pathogenesis of HD is largely explained by the accumulation of intracellular or extracellular protein aggregates known as mutant Huntingtin (mHTT). Transgenic mice models suggest that mHTT aggregates can cross cellular membranes, which potentially contribute to its spread (Pecho-Vrieseling et al., 2014). It is likely that once initiated; neuropathological changes might spread in a 'prion-like' (cell-to-cell transmission) manner via axonal pathways. Therefore, progression may be facilitated by the brain's structural pathways (structural connectome) in humans. With network-sensitive brain imaging techniques and model-driven analysis of the human connectome, recent developments have allowed macroscopic mapping of susceptible pathways and the establishment of biophysically driven models of degeneration spread in the human brain.

NDM represents a bio-physical model that has been used to show the spread of mutant protein in various neurodegenerative diseases (Sneha Pandya et al., 2017; S. Pandya et al., 2019;

Govinda R. Poudel et al., 2020; Ashish Raj et al., 2012; A. Raj et al., 2015). The NDM models the spread of atrophy through brain networks to capture the spatial patterns of pathology, which has been applied in AD (A. Raj et al., 2015), frontotemporal dementia (Ashish Raj et al., 2012), PD (Freeze, Acosta, Pandya, Zhao, & Raj, 2018; Freeze, Pandya, Zeighami, & Raj, 2019b; S. Pandya et al., 2019), corticobasal syndrome and progressive supranuclear palsy (Sneha Pandya et al., 2017).

Ashish Raj and Powell (2021) recently experimented with NDM in both directional and non-directional cases to recapitulate the atrophy in HD. This research used a large dataset of 635 subjects from the TRACK-HD study to propose multiple hypotheses, including an anterograde network transmission model. Using NDM as a computational tool, the study suggested strong evidence of network spread in HD. Furthermore, it suggested that significant striatal degeneration is seen in the earliest pre-HD subjects. Finally, it also described the relation between healthy control gene expression and the patterns of regional degeneration. In sum, this most recent study has shown the robust effectiveness of NDM and its flexibility in understanding the progressive nature of HD and its spread mechanism.

G. R. Poudel, Harding, Egan, and Georgiou-Karistianis (2019) encapsulated the trans-neuronal spread of atrophy in the whole brain regions by modelling it as a diffusion process. Their study located the seeds of degeneration in the accumbens and thalamus regions of the subcortical brain. As part of the study, 26 symptomatic HD, T1-weighted and diffusion-weighted (DWI) data were collected at baseline. After implementing an NDM, the outcome indicated that the regions most affected were in the subcortical parts of the brain regions. In addition, the caudate, pallidum, putamen, and accumbens were part of regions with more significant volume loss. Overall, the study suggested that NDM can help understand the atrophy distribution and neuronal disconnection in HD.

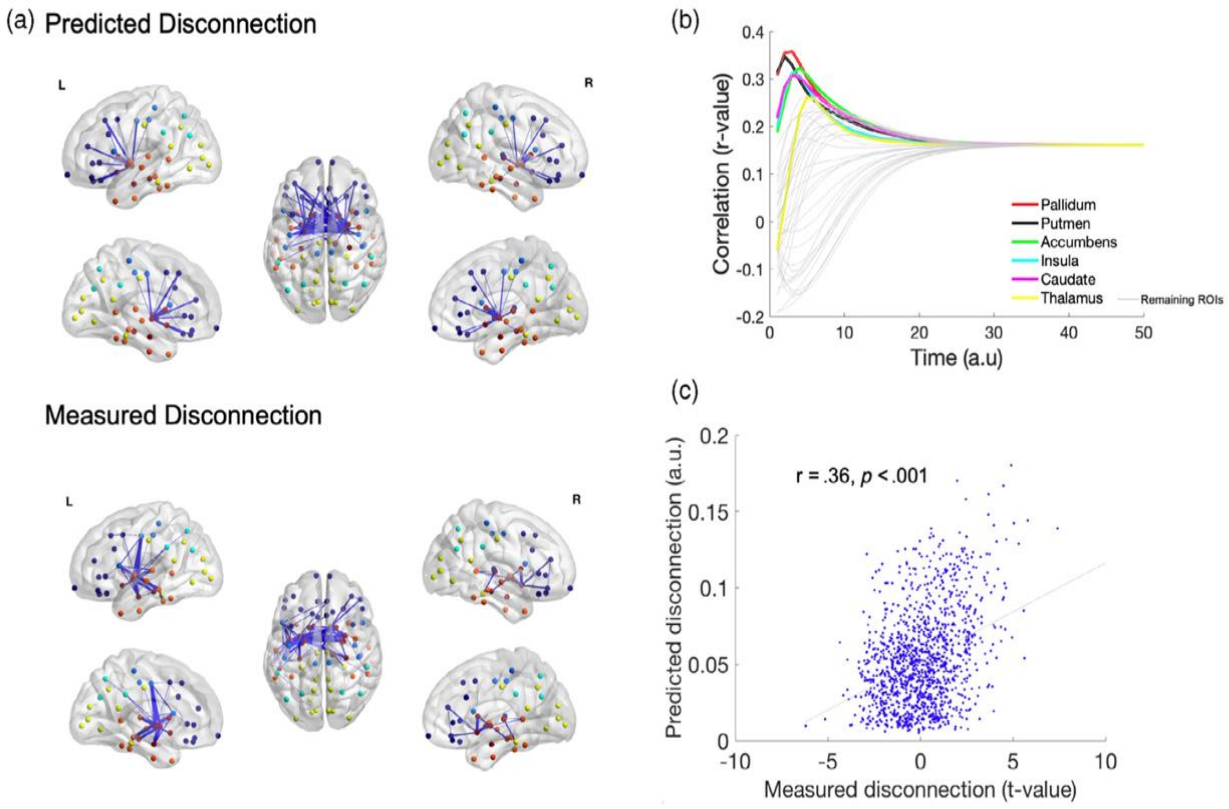

Figure 14 Use of NDM to determine white matter disconnection in HD compared to controls (G. R. Poudel, Harding, Egan, & Georgiou-Karistianis, 2019)

Figure 13 shows the results of Poudel et al. (2019)'s NDM. Strong disconnection was measured in the pallidum, putamen, and accumbens parts of the subcortical region of the brain. Similarly, other research studies have successfully implemented NDM to elucidate the relationship between structural and functional brain connections in network expansion (Abdelnour et al., 2014).

Whilst the two studies described above have previously implemented NDM in HD, they have been limited by their ability to monitor atrophy in the premanifest stage and longitudinal multimodal neuroimaging datasets of HD. In this project, we use the spatial maps of atrophy generated from pre-HD individuals to determine whether NDM can predict the atrophy pattern during HD's premanifest stage. Furthermore, we hypothesize that network diffusion can predict changes in brain volumes in pre-HD.

5.2 Materials and Methods

5.2.1 Participants

This study uses the results from the LME modelling conducted in Chapter 3 as input data. The LME analysed T1-weighted MRI data from 195 participants (N=89 age-matched healthy controls and 106 as pre-HD participants), as outlined in Chapter 3. These MRI data were made available from the Track-On HD study cohort.

5.2.2 Data descriptors

The output from the LME model run in Chapter 3 was organized such that there was a single standardized effect size (Z-value) for each brain region forming an 82 x 1 vector representing the amount of degeneration in 82 brain regions in pre-HD compared to controls. In addition, these data were organized such that a more significant value reflected greater atrophy. Finally, these data were imported into MATLAB for analysis using MATLAB R2020b.

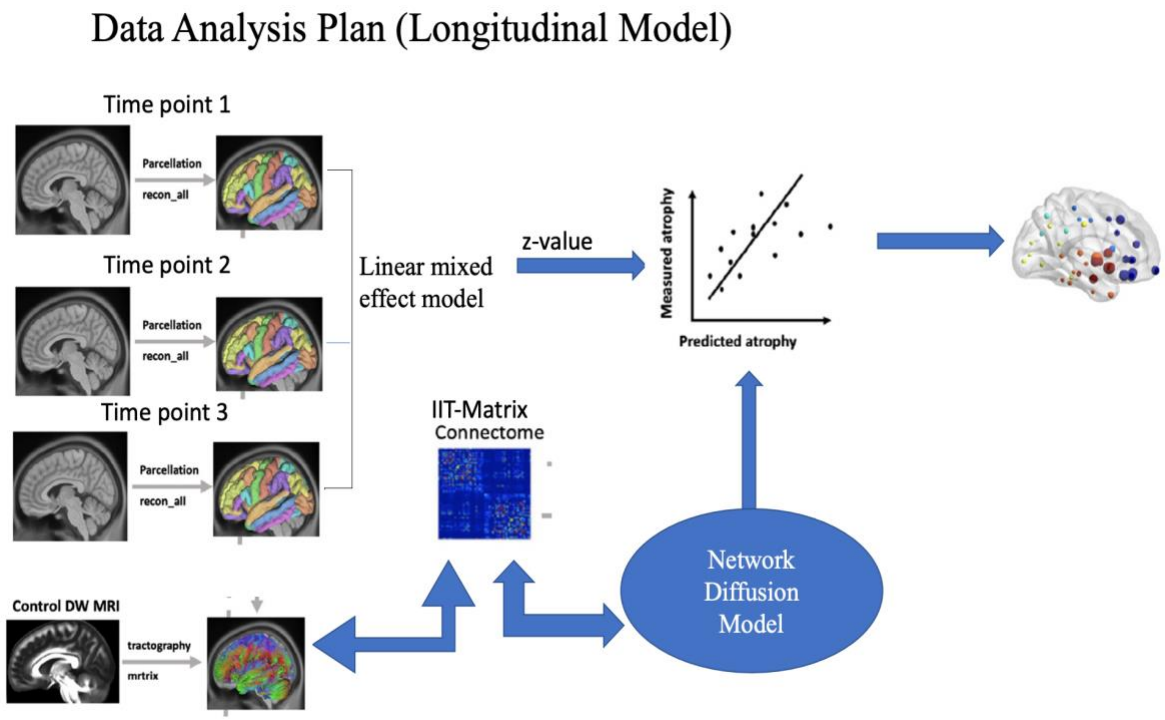

Figure 15: The graphical representation for neuroimaging pre-processing and NDM analysis in the study.

5.2.3 Healthy Brain Connectome

We used the Illinois Institute of Technology's (IIT) Human Brain Atlas (version V.5.0) for structural mapping connectivity. The structural connectome used in this research is available at the NITRC website (http://www.nitrc.org/projects/iit). High goal dispersion-weighted MRI information from 72 youthful sound subjects was utilized to gauge the availability between the nodes by developing the connectome recently proposed by Iturria-Medina et al. (2007). Anatomical connection density was calculated by dividing the initial connection strength value by the summation of paired region surface areas used to quantify the connectivity strength in our study, thus normalizing the variable cortical and sub-cortical regions' sizes. The IIT Human Brain Atlas is used in the current study to build a white matter connectome. The DWI data were collected using Turboprop diffusion MRI, which is relatively clean and does not suffer from image distortions and artefacts commonly observed in conventional echo-planar imaging (EPI).

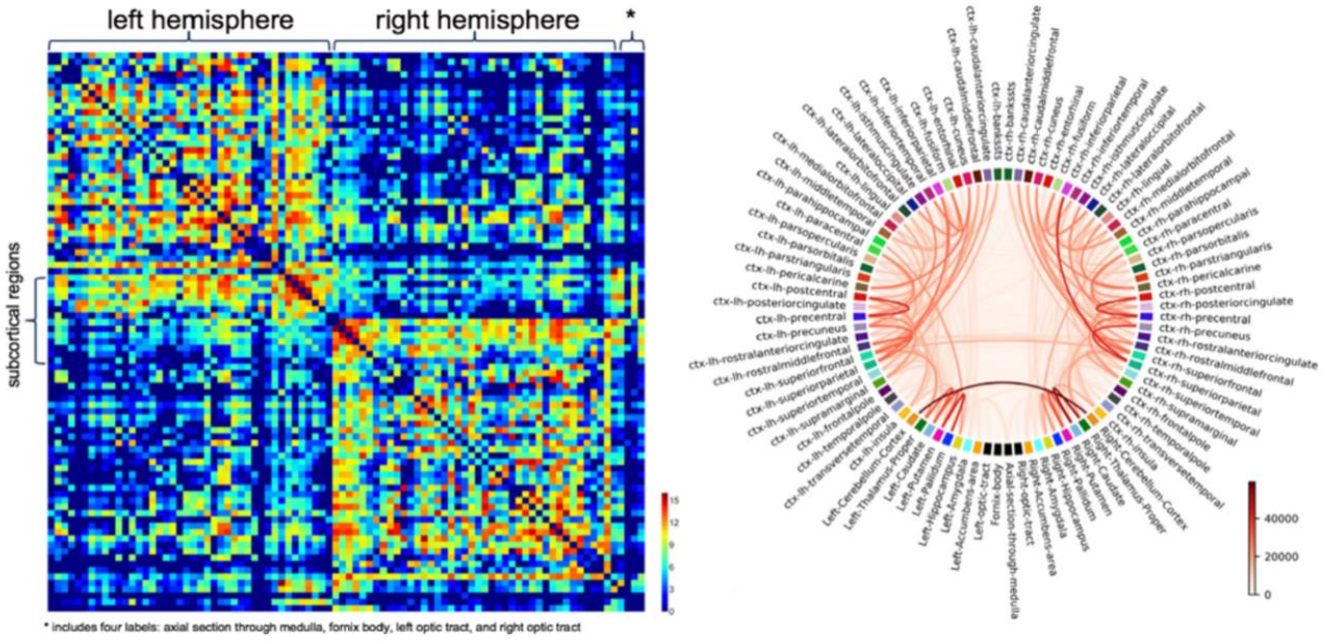

Figure 16 Visualisation of structural connectivity obtained from IIT Human Brain Atlas.

Note: The colour bar represents the number of streamlines connecting two regions. Circular layout of the connectivity matrix is also provided. This figure has been adapted from (Qi & Arfanakis, 2021).

5.3 Mathematical Modelling of NDM

We implemented NDM on the healthy brain connectome described above and used it to predict the degeneration pattern measured using LME. The basic concepts of network diffusive mechanism were taken from the network heat equation, which can be expressed as the progression of any pathology (in this case, mHTT molecules) from a high concentration to a lower concentration until the equilibrium state is accomplished (G. R. Poudel, Harding, Egan, & Georgiou-Karistianis, 2019). Finally, we adapted the same model proposed by Ashish Raj et al. (2012) in our longitudinal data to determine the pre-HD progression pattern.

We modelled pre-HD longitudinal progression as hypothesised brain network G = (V, ε), where V represents the nodes (gray matter structures) and ε represents the connection strength between the nodes (white matter pathways connections between the nodes). From Ashish Raj et al. (2012), the progression of atrophy from region R1 to region R2 is given by,

$$\frac{dx1}{dt} = \boldsymbol{\beta c1,2(x2 - x1)} \qquad \textbf{Equation 2}$$

where *x2* and *x1* are atrophy concentrations of the respective regions R2 and R1.

$\boldsymbol{\beta}$ is a diffusion coefficient.

Now, we can represent all regions of the brain *i* into vectors as x(t) = [x_i(t)]; the equation 4-1 can be represented as,

$$\frac{dx1}{dt} = -\boldsymbol{\beta L x(t)} \qquad \textbf{Equation 3}$$

where L is the normalised graph Laplacian matrix which is symmetric, and its eigenvectors are orthogonal. From matrix algebra, equation 3 is satisfied by,

$$\boldsymbol{x(t) = e^{-\alpha H} x(0)} \qquad \textbf{Equation 4}$$

where *x*(t) is the response variable at any given time *t*, starting from an initial distribution of pathology given by *x* (0) at time baseline.

x(t) can be estimated as diffusion process

$$x(t) = \sum_{i=1}^{N} [\![(e^{-\alpha t} u_i^t]\!] f(0)) u_i \qquad \textbf{Equation 5}$$

where U = [u_1, u_2, u_3, ...u_n] represent eigenvectors of the Laplacian matrix.

4.3.1 Eigenmode Analysis

According to Raj et. al., the eigendecomposition of the graph Laplacian term (H) in equation 5 provides eigenvectors, which help elucidate the dynamics of network diffusion on a graph. The first eigenvector of healthy connection denotes ageing-related changes in the brain volume, whereas the second and third eigenmodes are linked to dementia and Alzheimer's disease. Poudel et. al (G. R. Poudel, Harding, Egan, & Georgiou-Karistianis, 2019) suggested that the fourth and fifth eigenmode may reflect network spread in movement disorders. Thus, eigenmode decomposition of the graph Laplacian was performed using MATLAB. The fourth and fifth eigenvectors were then correlated against the measured atrophy obtained from Chapter 3. Correlation values with $p<0.05$ were considered statistically significant.

5.3.2 Repetitive diffusion in network to observe longitudinal progression of atrophy

A repeated network diffusion is performed to recognize the likely focal points of disorders in the brain from where the spread start. In the repeated seeding simulation, NDM is run by repeatedly setting each of the 82 brain regions as a seed region. Running NDM from each brain region helps identify the trajectory of diffusion across the network given a seed. This trajectory is represented as xt in equation 4-3. Thus, we ran an NDM model with x0= ei for each node i, where ei represents the unit vector whose value is 1 at ith region and else zero at the time ranging from 1 to 40. Network diffusion was simulated bilaterally using 41 different initial seed brain regions, generating 82 element vectors at each time point. For each region, the corresponding Pearson's correlation value R was calculated at time t, producing the R(t) value, resulting in 41 x 40 correlation-time matrices. For each seeding region, we noted the highest R-value to measure the most probable region of source for longitudinal degeneration of the pathology. These R(t) values were plotted as an R-t curve, as shown in Figure 16.

5.4 Results

5.4.1 Spatial progression of atrophy in the pre-HD brain.

The spatial progression of longitudinal atrophy in the pre-HD brain has been reported in Chapter 3. The most significant longitudinal volume loss was seen in the subcortical region of the brain with the caudate, putamen, and amygdala. Similarly, the lateral occipital, pars orbitalis, and superior temporal cortices showed cortically the largest longitudinal volume loss. These changes expressed as z-values associated with each of the 82 brain regions are used to measure atrophy in the NDM analysis.

5.4.2 Association between eigenmode and atrophy in pre-HD

Figure 15 shows the distribution of eigenvalues of the healthy connectome of graph Laplacian and its association with measured atrophy. The graph of the eigenvalues elucidates that most of the dynamics of diffusion in a healthy connectome can be explained by the first few (<10) eigenvectors. Figure 4-3 shows that the relationship between the fourth eigenmode and measured atrophy in pre-HD is significant ($r=0.37$, $p=0.0006$).

5.4.3. Repeated diffusion

Figure 16 shows the correlation-time curves between predicted degeneration and measured atrophy obtained from NDM simulation. Repeated diffusion processes were performed in 82 brain regions to identify the potential initial point of atrophy degeneration in the brain connectome. The curves show that only a few regions (the pallidum, thalamus, and putamen) show maximum longitudinal degeneration in the sub-cortical region. In contrast, the temporal pole and inferior temporal show a moderate longitudinal pattern of atrophy in pre-HD in the cortical region of the brain.

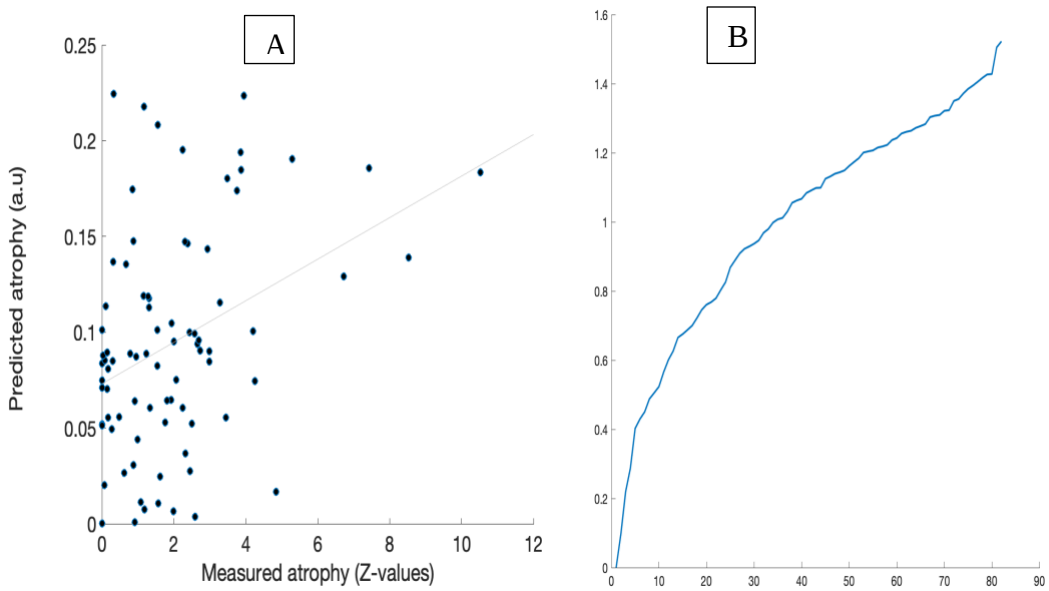

Figure 17 Association between eigenmode and atrophy at fourth eigenmode decomposition.

Note. A shows the scatter plot between measured atrophy obtained from empirical longitudinal data analysed in the LME model implying group by time interaction in fourth eigenmode decomposition. B is the representation of eigenvalue distribution across the brain regions.

Figure 17 shows the spatial distribution of the brain regions showing the most significant association between measured and predicted atrophy. The highest association was noticed when diffusion was initiated from the Pallidum ($r = 0.488$, $p < 0.0001$) and thalamus ($r = 0.40$, $p < 0.0001$).

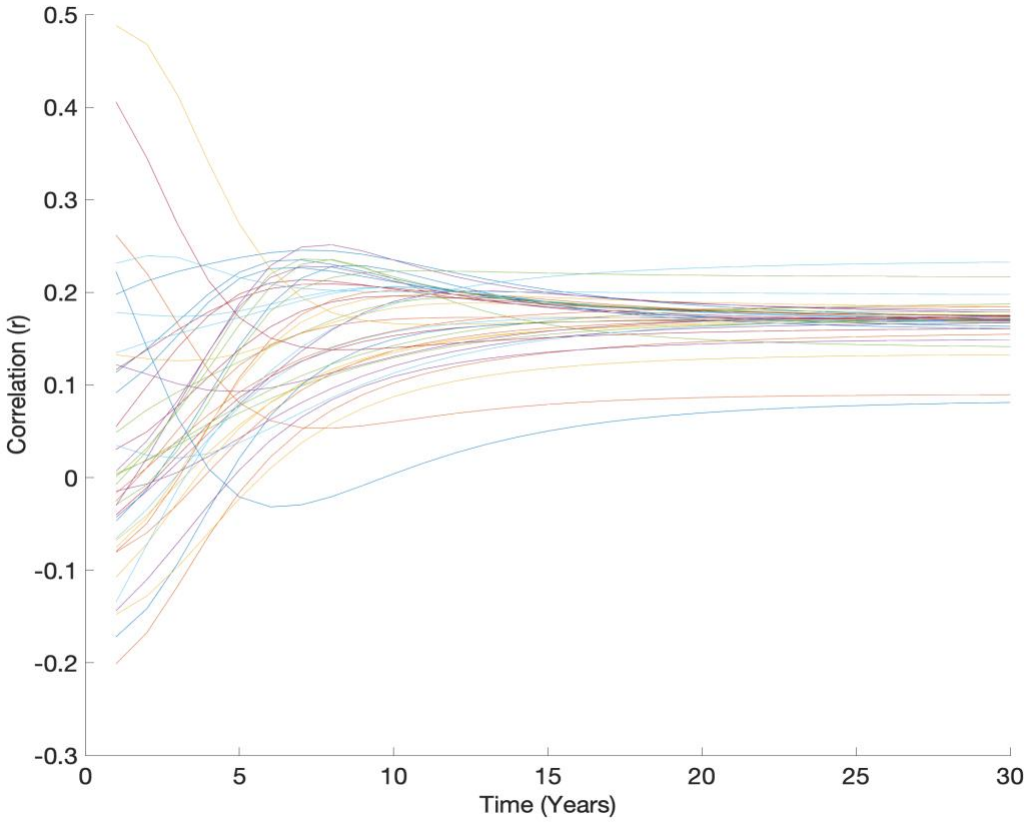

Figure 18 Temporal profile of correlation between measured atrophy and NDM predicted atrophy over time.

Note. Each curve represents 41 bilateral brain regions (82 cortical and sub-cortical regions of the brain). The correlation-time curve represented the diffusion process when diffusion was initiated from the brain regions within the Desikan-Kelliany atlas. The X-axis represents time in years, and Y-axis shows the correlation (Pearson's) values.

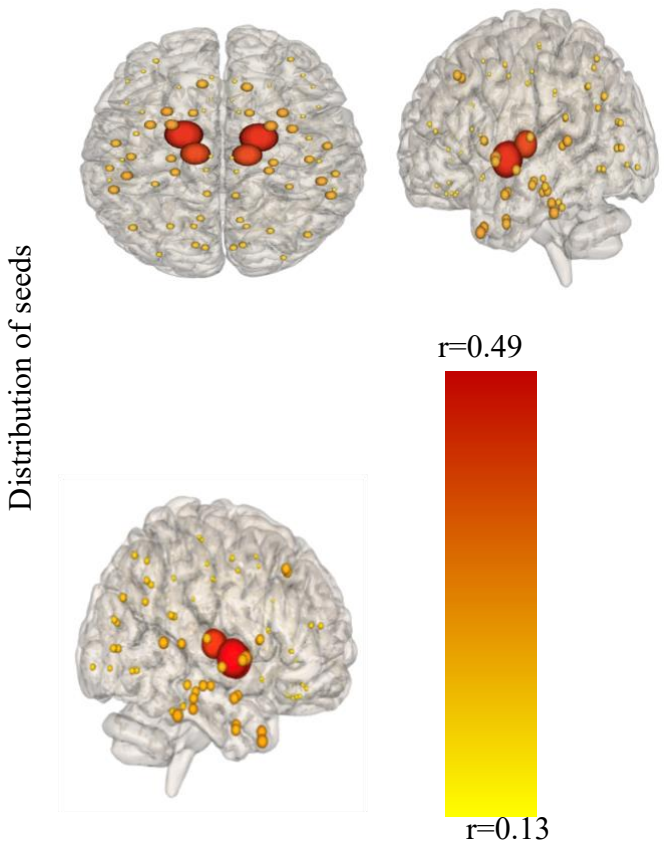

Brain Region	R-value (Pearson's r)
Pallidum	0.4881, p < 0.0001
Thalamus	0.4055, p < 0.0001
Putamen	0.2618, p=0.02
temporalpole	0.2514, p=0.02
inferiortemporal	0.2456, p=0.02

Figure 19 The spatial distribution of potential seeds of degeneration in pre-HD individuals.

Note. The spherical nodes represent the location of brain regions. The colour bar and the size of the nodes represent maximum observed correlation values. The pallidum, putamen, and thalamus show the largest correlations. The correlated value (R-value) is colour coded by lobe. Thus, we can observe the longitudinal pattern of degeneration initiated from the sub-cortical region of the brain, with the putamen and thalamus showing the strongest correlation between measured and predicted atrophy. We also can note the longitudinal pattern of moderate associations in the cortical region of the brain.

5.5 Discussion

This study demonstrated that longitudinal progression of neurodegeneration in premanifest HD could be modelled as a diffusion process across the brain connectome. Using NDM, we recapitulated the pattern of longitudinal regional volume loss in the cortical and subcortical regions of the brain in pre-HD. This research project is the first study to use NDM to model 24-month changes in cortical and subcortical regional volumes compared to healthy controls in pre-HD. The application of NDM helps identify the longitudinal pattern of degeneration across the brain regions. Initiating the diffusion process from the pallidum, thalamus, and putamen of the subcortical region of the brain shows the strongest association with longitudinal degeneration in pre-HD. These findings demonstrate that, while NDM can predict some of the degeneration over time, it could not characterize the full degeneration in HD.

This study has incorporated graph theory principles, representing the brain as a network of nodes and edges, and implemented NDM to elucidate the longitudinal progression of atrophy in pre-HD. The eigendecomposition of graph Laplacian was able to capture the dynamics of diffusion on the healthy brain connectome and capture an underlying process of diffusion on the network (Ashish Raj & Powell, 2021). Interestingly, the fourth eigenmode of the healthy connectome was significantly associated with the atrophy over two years in pre-HD. This finding is consistent with studies that have suggested that progressive neurodegeneration may be captured in the eigenmodes (Ashish Raj et al., 2012; A. Raj et al., 2015). The fourth eigenmode, in particular, reflects a diffusion process accumulating in the cortico-striatal networks, which are the most vulnerable networks in HD. A similar outcome was achieved by G. R. Poudel, Harding, Egan, and Georgiou-Karistianis (2019) in their cross-sectional study of symptomatic HD implementing the network diffusion principle. Although they further elucidated that the cortical and subcortical regions may reflect a distinct course of degeneration, we did not see divergent associations in the cortical or subcortical regions. While the exact process of atrophy progression

is still the subject of research, the study of mouse models of HD suggests that neuro-synaptic propagation could be a cause of disease progression (Pecho-Vrieseling et al., 2014). This mechanism of disease spread through the diffusion of synaptic processes in the brain network can provide a neuro-biomarker basis for atrophy progression in HD (G. R. Poudel, Harding, Egan, & Georgiou-Karistianis, 2019).

By simulating NDM for each brain region, we further demonstrated which brain regions are most likely to act as seeds of pathology spread in HD. Maximum correlation between measured and predicted longitudinal atrophy was observed when the putamen, pallidum, and thalamus were used as seed regions in the NDM analysis. Specifically, the pallidum and putamen showed a much more robust and stable spatial pattern of degeneration. This finding is consistent with previous studies where the striatum, putamen, accumbens, and caudate show the initial structural changes and volume loss in HD (van den Bogaard et al., 2011). The indication of longitudinal loss of volumes in the subcortical region of the brain in pre-HD also reflects the associated motor and cognitive abnormalities observed before onset. Several studies in HD have also suggested strong evidence of maximum degeneration in the sensorimotor regions, which are strongly connected with the striatum (Bohanna, Georgiou-Karistianis, & Egan, 2011; Rosas et al., 2008). However, these motor regions did not appear to be the epicentres.

Furthermore, a strong correlation between measured and predicted longitudinal atrophy was identified in the thalamus. These findings were somewhat surprising as the thalamus is not considered to be vulnerable in pre-HD (G. R. Poudel, Harding, Egan, & Georgiou-Karistianis, 2019). However, the thalamus, being a hub region connecting various cortical and subcortical structures, may act as an epicentre of disease spread in HD (van den Bogaard et al., 2011). As a result of this hubness, which drives interhemispheric connectivity between the cortical and subcortical structures and its proximity to the striatum, the thalamus may serve as a region essential for spatial degeneration atrophy in pre-HD. More research is needed to establish the

biophysical mechanisms underpinning the role of the thalamus in spreading disease in the HD brain.

Several factors must be considered in relation to the results. The NDM works on the linear passive diffusion process principle. Hence, it models the longitudinal progression of atrophy as the linear passive diffusion process; however, many other studies have suggested neurobiological progress as an active process incorporating synaptic vesicles as trans-synaptic progression (Govinda R. Poudel et al., 2020). Hence, non-linear active modelling should be the next step in analysing available data to understand the spread mechanism of atrophy better. Also, using a dedicated and specific connectome (micro-connectome) in a current model can improve the efficacy of the result. We have utilized longitudinal data up to 24 months in time from the baseline. More extended periods of data collection would be essential in providing a robust identification of the spread mechanism in the network.

In conclusion, we showed that some of the longitudinal atrophy in pre-HD might be explained by network diffusion. Thus, NDM may be a tool to explore further where and how the pathology spreads in the brain of neurodegenerative disorders during the premanifest stage. However, future work needs to improve on the predictive ability of NDM by incorporating active transport mechanisms, genetic factors, and functional connectivity into the model.

Chapter 6: General Discussion and Conclusion

The purpose of this thesis was to investigate whether the pattern of degeneration in the premanifest stage of Huntington's disease can be modelled as a network diffusion process. We used the graph theory algorithm (NDM) proposed by Raj et al. (Ashish Raj, 2015) to understand the spatial patterns of degeneration. First, a brief review and analysis of previous studies were conducted. Next, a statistical tool was selected to study and compare the volume change rate between a group of healthy controls and patients. In this case, we used a linear mixed effect model (LME) to characterize the longitudinal changes in the hemisphere of the brain in premanifest HDs compared to healthy controls. Finally, we implemented an NDM for predicting the longitudinal changes in brain volume in premanifest HD.

6.1 Summary by chapter

In Chapter provides a brief introduction of the clinical characteristics of HD and its current prevalence worldwide. Then, we explained how the trans-neuronal spread of pathology distribution takes place in HD. Trans-synaptic exchange of atrophy has been previously studied and examined in mouse models (Pecho-Vrieseling et al., 2014). Other studies also suggested that the distribution mechanism follows a typical pattern of cortico-striatal spatial progression in HD (Jansen et al., 2017; Mitchell et al., 1999). This chapter helped to understand the pathological characteristics from a clinical perspective, i.e., identified affected brain regions through in-vitro study, providing a framework for our comprehensive study.

With advanced computational and imaging techniques such as MRI, we can now visualize the actual degeneration. We have introduced neuroimaging studies conducted to identify the pattern of degeneration in HD. A few large-scale neuroimaging studies in HD have identified the pattern of the spread of degeneration in the HD brain. Structural MRI studies have established that degeneration in the striatum (caudate and putamen) is the crucial neuropathological feature of HD (Govinda R. Poudel, Julie C. Stout, et al., 2014; Sturrock et al.,

2015; S. J. Tabrizi et al., 2009; Sarah J. Tabrizi et al., 2011; Vemuri & Jack, 2010), with other areas outside the striatum showing significant deterioration with disease progression.

However, we can only quantify the atrophy in brain regions through neuroimaging. Therefore, identifying or predicting the pattern of degeneration in the brain is not possible only by neuroimaging. We have addressed this issue by briefly explaining network spread models, whereby the brain is viewed as a complex network of nodes and edges. In this study, we proposed an NDM model previously used to spread Alzheimer's disease pathology and other neurodegenerative disorders. Finally, we stated my aims to conclude the first chapter.

In Chapter 2, we reviewed the findings from cellular, animal models, and human neuroimaging to understand the spatial distribution, protein aggregation mechanism, and atrophy patterns in HD. Findings suggested that HD shows distinct patterns during progressive degeneration from higher atrophied regions to neighbouring regions. The extensive inter-neuronal spread in brain regions was evident from several in-vivo studies (Ren et al., 2009; Trevino et al., 2012). Further review revealed evidence that the HD brain network structures were altered as compared to healthy controls. Change in structure, specifically in the cortical regions, was seen through imaging modalities such as MRI. Structural MRI studies have determined the various microstructural changes in white matter (Govinda R. Poudel, Julie C. Stout, et al., 2014), thalamus, hippocampus and other regions of the brain in HD patients (Georgiou-Karistianis et al., 2013). These microstructural changes were more evident in studies like TRACK-HD, PREDICT-HD, and IMAGE-HD. Other cross-sectional studies found that the most affected brain regions in HD patients were sub-cortical regions such as the putamen, caudate and thalamus (S. J. Tabrizi et al., 2009). The evidence of microstructural changes in brain regions from several studies listed above made it possible to map the epicentres and trajectory of degeneration progression by network spread models.

We also provided a review of studies that suggested that spread models can predict disease progression, which is structured and driven by a mechanistic process. Whilst the brain

has been recognized as a complex network since the early days of neuroscience, mathematical models of how the disease may spread through this network have been made possible by developing network diffusion models (NDM). Since their first introduction by Raj and colleagues (Raj et. al., 2012), NDM has been successfully implemented in various disorders, such as Alzheimer's disease, Parkinson's and Huntington's disease, to understand and predict the spatial distribution and characteristics of pathology. Interestingly, this model effectively identifies the spread of pathology and has been suggested to help predict future atrophy patterns. For example, this powerful computational tool has helped determine the pattern of grey matter decay and white matter detachment in HD (G. R. Poudel, Harding, Egan, & Georgiou-Karistianis, 2019). Furthermore, NDM proves to be more accurate in predicting correlation structures when implemented to the structural networks.

Chapter 3 and 4 described Study I, which used linear mixed effect models to estimate degeneration in 82 brain regions in pre-HD compared to controls. This chapter mainly focuses on the longitudinal study findings on the progression of HD in the brain. While investigating the findings of past researchers and scholars, this section was able to point out the advantages of adopting a longitudinal rather than cross-sectional design to investigate the progression of the disease. An investigation of past research studies showed that longitudinal and cross-sectional designs had been used in equal measure. A longitudinal design was implemented in the present study, and its advantages over the cross-sectional design must be highlighted.

In study 1, we used a linear mixed-effects model (LME) to statistically analyze the change in volume of 82 brain regions in pre-HD compared to controls. We were able to characterize the changes in volume over 24 months using data from three assessments (baseline, 12 months and 24 months). We found that volume change was most significant in the sub-cortical brain regions, including the caudate and putamen, which suffered ~ 6% volume loss over 24-months. Cortically, the highest atrophy was observed in the visual cortex (lateral occipital) and temporal cortices (superior and middle temporal). We concluded that the findings highlighted the need to

map degeneration across the whole brain in pre-HD so that HD's epicentres and pathways of degeneration can be traced accurately.

Chapter 4 described the implementation of NDM to elucidate whether network spread can be used to model the spread of pathology via the structural connectome created from both healthy controls and patients (pre-symptomatic HD). Diffusion is the process of the flow of particles (e.g., misfolded proteins, prions) to the lower concentration region from the higher concentration region. This process of diffusion is continued until equilibrium is achieved. As discussed earlier, this diffusion process is mathematically modelled and used across various structures by a set of elements and their interconnections. This model is actively used in social networks and human brain connectome (G. R. Poudel, Harding, Egan, & Georgiou-Karistianis, 2019).

We used empirical data obtained from Study 1 (Chapter 3) to test the predictive ability of the network diffusion model. To determine the advantage of the network diffusion model (NDM), which is proposed in the study, we apply it to predict atrophy patterns in the brain regions and compare it to the measured output from the LME. We found that NDM was only able to predict the atrophy pattern moderately.

6.2 Discussion

6.2.1 Cortico-striatal degeneration before clinical manifestation in HD

There is growing international awareness that a clear understanding of the natural course of disease and its manifestation is necessary to be able to develop therapeutic interventions. Furthermore, the intervention and management need to occur at the earliest stage possible. However, the lack of clear biomarkers associated with earliest degeneration in HD has made it difficult to manage HD as early as possible. In the current study, we demonstrate that degeneration of striatum is likely to be an earliest biomarker in HD pathogenesis.

The main strength of the current study was to be able to delineate the change in brain volume over time within 12 to 24 months during the premanifest stage. Findings provide evidence that the changes in brain volume, as measured by imaging, is linear in pre-HD. Furthermore, there is distinct decline in the striatum volume within 24-months, which is not observed in healthy controls. The changes in cortical brain regions were not very strong, suggesting that cortical degeneration may become more apparent when HD is closer to diagnosis.

In the cortical region, there were differences in the longitudinal changes in brain volume within occipital cortex and temporal cortices in pre-HD compared to controls. Previous studies have suggested that occipital lobe shows the earliest and the fastest rates of atrophy on pre-HD (Johnson et. al., 2021). The parietal brain regions can also degenerate in the premanifest HD, only in the individuals which are closer to onset (Johnson et. al., 2021). It is important note that most of the neurocognitive, neuropsychiatric symptoms in pre-HD manifest only when atrophy spreads to cortical regions. We provide a framework for regional brain degeneration which may be linked to behavioural and clinical changes in HD closer to onset.

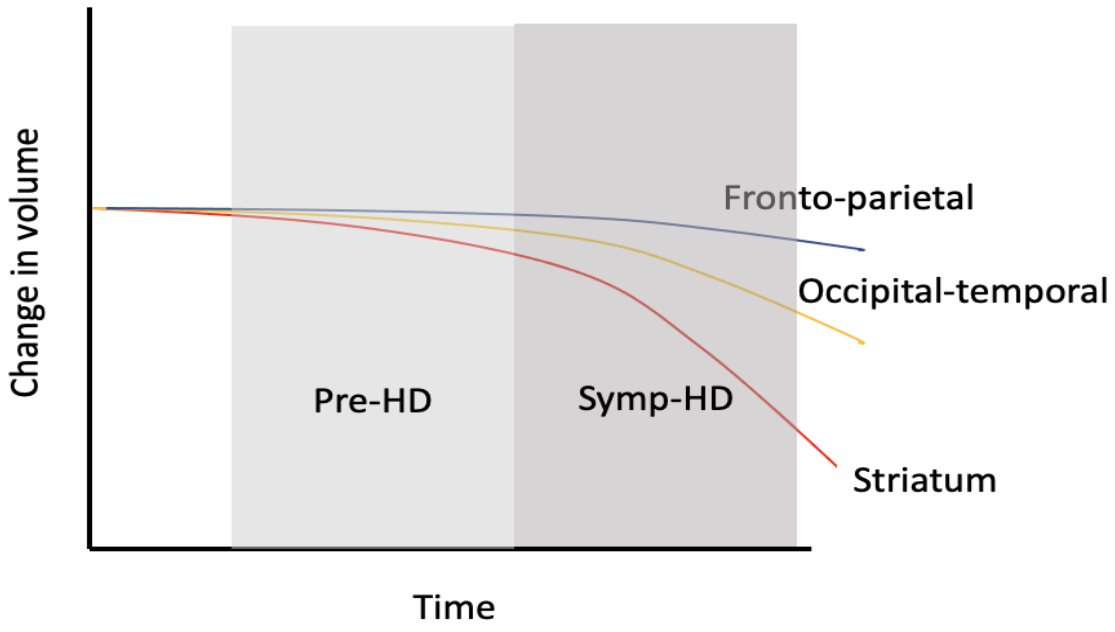

Figure 20 A framework showing the trajectory of degeneration in HD over time, based on the findings from the current study.

6.2.2 Relationship with network degeneration hypothesis

The pattern of degeneration observed in pre-HD can be explained by network spread model. The healthy connectome comprises the best state of the neuronal cell wiring of a brain, which sits between the significantly assembled/deficiently joined regular spread network and the insufficiently clustered and highly organized random graph (Fulcher & Fornito, 2016). The network spread was determined based on eigen-modes of graph Laplacian of healthy brain network and diffusivity of mutant HTT proteins through axonal network. Trans-neuronal patterns and their consistency are dominant across these eigenmodes throughout the network. Similarities across these networks may show pathways of disease spreads, or groupings of eigenmodes may be associated with HD stage or subject-specific similarities and differentiations.

Recent network studies show brain networks are altered in neurodegeneration (Domínguez et al., 2013; He, Chen, & Evans, 2008; Lo et al., 2010). Distinctive spatial trans-neuronal patterns are suggested in HD and AD (Govinda R. Poudel, Julie C. Stout, et al., 2014; Ashish Raj et al., 2012; Zhou et al., 2010). Seeley, Crawford, Zhou, Miller, and Greicius (2009) suggested that spatial patterns belong to the default mode and conspicuous networks, respectively. While the relationship between neurodegeneration and connectivity networks shows convincing results, the underlying cause of neural activity remains unexplained (Seeley et al., 2009). The neural activity of different functional networks can is determined by selective vulnerability of structural, metabolic and physiological aspects of neural network (Saxena & Caroni, 2011). In HD, selective vulnerability is suggested to be involved in the connectivity properties of striatal spiny neurons (Cepeda, Wu, André, Cummings, & Levine, 2007).

Interestingly, the network diffusion model implemented in this study can explain the findings mentioned above, excluding the requirement of selective vulnerability, regional specificity, or shared functional load. The eigenmode and connectivity networks are merely homologous, which are the outcome of the eigendecomposition of brain networks. The NDM model implies that many eigenvalues diffuse very quickly, and a small number of eigenvalues

diffuse slower over time, dominating the diffusion process. However, this does not suggest that the selective vulnerability hypothesis is incorrect (Ashish Raj et al., 2012). NDM model accommodates a concept of disease progression that is entirely consistent with known findings but excluding selective vulnerability.

6.2.3 Relationship to Prion-like spread in HD

The NDM model likely represents macroscopic consequence of the prion-like (protein misfolding) during disease progression in HD. In HD, the mutation results in mutant Htt (mHtt) misfolding and aggregation (Shacham, Sharma, & Lederkremer, 2019). Furthermore, there is overwhelming neuropathological evidence that apart from HD, other neurodegenerative disease proteins such as tau, alpha-synuclein, beta-amyloid and TDP-43, exhibits the capacity to misfold and spread through neural networks via trans-synaptic nature (Hobbs et al., 2009; Palop & Mucke, 2010; Govinda R. Poudel et al., 2020; A. Raj et al., 2015). These results demonstrate the dependency of brain regions to identify neurodegenerative diseases, including HD. Hence, the NDM model contributes to the qualitative understanding of trans-synaptic propagation of misfolded protein into a quantitative model.

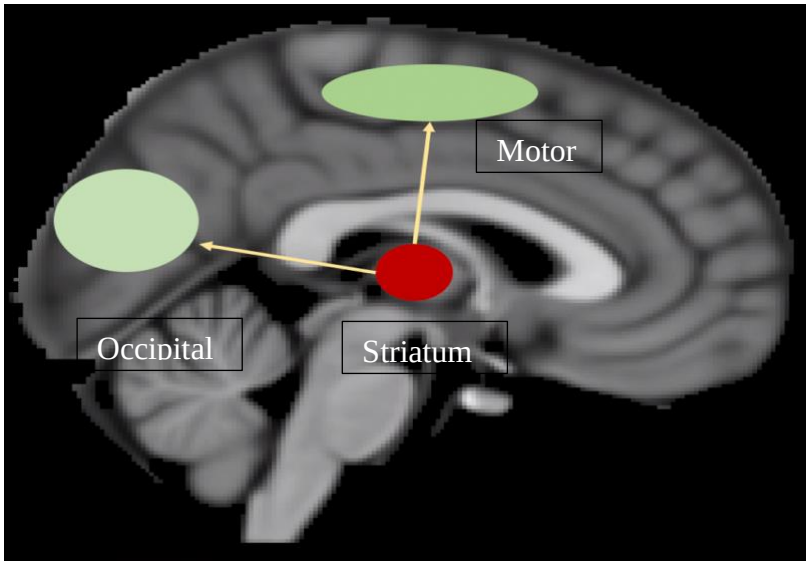

Figure 21 Likely pathways of spread of degeneration in HD.

In contrast to previous research in HD and other neurodegenerative diseases, this study specifically used NDM to emulate the longitudinal atrophy in HD. The NDM relies on mathematical modelling of diffusion process on structural connectome. Therefore, the model itself has an intrinsic temporal component, which has not been studied in previous work.

Fig 22 shows the likely pattern of network-based degenerations in HD compared to healthy control. HD, when compared with the standard control, shows longitudinal spread throughout the region of inter-hemisphere covering the areas such as frontal, motor, parietal cortices, and correct-striatal regions. These findings align with previous network studies in HD (G. R. Poudel, Harding, Egan, & Georgiou-Karistianis, 2019; Govinda R. Poudel et al., 2015; Ashish Raj & Powell, 2021).

Furthermore, when NDM was stimulated for each brain region, the highest number of correlations among the atrophy, i.e., measured and predicted ones, has been seen for the striatum region. Putamen had shown a stable pattern of network diffusion in the case of HD. Several studies have suggested that neuronal loss, along with the structural changes found in the brain's sub-cortical areas, has been taken as the early-stage progression of HD (van den Bogaard et al., 2011). Cognitive and motor disbalances in HD has been recorded as an immediate effect of these changes occurring in subcortical regions (Bäckman, Robins-Wahlin, Lundin, Ginovart, & Farde, 1997). Some studies suggest that longitudinal disease progression from the striatum region, overall covering significant areas of the cortex, is much more similar to the atrophy of cortical regions. In contrast, the sensorimotor regions have been included as the most affected regions showing longitudinal degenerations, which have a similar connectivity case with striatum G. R. Poudel, Harding, Egan, & Georgiou-Karistianis, 2019).

To sum up, longitudinal atrophy in HD throughout the brain structure can be reflected by NDM as a diffusion process in the brain as a network connectome. Implementation of NDM in disorders such as PD, ALS and AD has demonstrated the same pattern of longitudinal progression (Bhattarai et al., 2021; S. Pandya et al., 2019; Govinda R. Poudel et al., 2020; Ashish

Raj & Powell, 2021). Furthermore, when diffusion is ingested through the brain regions such as the pallidum and the thalamus, it follows the same pattern of longitudinal degeneration in the cortical brain of HD. Thus, predictions of the longitudinal atrophy in the HD brain have been effectively mapped throughout the brain connectome using NDM, providing the trans-synaptic framework to test HD's longitudinal disease progression hypothesis.

6.2.4 Relationship to white matter degeneration in HD.

In the current study, we used normative brain connectome and NDM to predict degeneration of grey matter in HD brain. Previous studies have demonstrated that NDM may also explain white matter disconnection in HD (Poudel et. al., 2019). Furthermore, pre-HD shows degeneration of white matter network connecting hub regions of the brain (McColgan, Seunarine, Razi, Cole, Gregory, Durr, Roos, Stout, Landwehrmeyer, & Scahill, 2015). It has also been suggested that the topological length of white matter connections with longer length are affected earlier (McColgan et al., 2017). Primarily corticostriatal connections first reveal the decrease in network connectivity followed by inter-hemispheric and intra-hemispheric connectivity, which are in line with previous studies (Govinda R Poudel et al., 2014). Our findings of potential trans-axonal distribution of atrophy requires asks for further investigation regarding this process may impact the white matter itself.

6.3 Overall implication of the findings

The primary implication of the findings from the current thesis is to demonstrate that the progression of neurodegeneration in HD during premanifest stage can be shaped by the organisation of the structural connectome in the brain. Our findings suggest that neurodegenerative changes in HD may begin in the vulnerable brain hubs and then spreads to specific neural circuits via trans-neuronal propagation constrained by the structural and functional organization of the brain. We have built upon our computational imaging strengths

and develop models that best predict the pattern of atrophy spread over time. Advanced graph theoretical methods, as well as mathematical propagation models, were used to investigate whether structural reorganization in the brain predicts longitudinal progression of atrophy in HD.

This is the first study to show that network diffusion can, indeed, be used as model to predict how and where the pathology may spread in HD brain. Although previous studies have shown cell-to-cell propagation of abnormal protein in animal model, relatively little was known regarding how structural organization may shape the progression of atrophy in the human brain. This knowledge is critical to inform future drug discovery efforts where neuroimaging methods maybe used to assess efficacy of potential therapeutic compounds in targeting vulnerable neural circuits in HD.

The most unique aspects of the current study, which advance on the previous work are 1) the application of NDM on longitudinal data 2) and the use of NDM during the premanifest stage of the disease. While previous work has employed this technique on a cross-sectional symptomatic-HD cohort (Poudel et. al., 2019), longitudinal data is necessary to make sense of disease progression and model the change over time. Previous longitudinal studies have only focused on statistical modelling of the volumetric changes over time (Dorsey & Investigators, 2012, Biglan et al., 2016), PREDICT (Aulsen et al., 2008, Tabrizi et al., 2013), which limits the ability to make predictions about nature spatial spread in the brain. The NDM model is a unique mathematical model which allowed us to make inferences about how the disease might be spreading in the HD brain.

The use of relatively large neuroimaging dataset in this rare disease population allowed us to specifically investigate whether neurodegeneration in HD propagates via structural networks. The use of the data from pre-manifest stage of the disease, who are several years away from the onset of the disease, allowed us to demonstrate that macroscopic consequences of cell-to-cell transfer may alter the brain early.

6.4 Limitations and Future Directions

The outcomes from our study can be summarized into two main findings. First, volumetric analysis of longitudinal MRI data from premanifest HD patients from the TRACK-ON HD study uncovers progressive pathological degeneration in brain regions of both hemispheres. Second, a network diffusion model implemented to the structural brain connectome demonstrated the longitudinal pattern of spatial degeneration in premanifest HD. However, this study has several limitations. The study's sample size was relatively small. The small sample size may have influenced the precision of estimates and the power of the study of conclusion drawn. Furthermore, the period of longitudinal monitoring was relatively short (only 24 months). The short time-frame may have reduced the sensitivity of detecting longitudinal changes in brain volume in pre-manifest individuals. Previous studies have suggested the volumetric changes in the striatum are evident within a year (Gregory et al., 2018; Poudel, Stout, et al., 2014; Tabrizi et al., 2009). However, cortical degeneration is a relatively slow process in HD, which may not have been captured fully in the current study. As the focus of the study was on computational modelling, we also excluded the correlation study between imaging changes and behavioral or cognitive issues. Previous studies have found extensive correlation between brain imaging markers and neurobehavioral outcomes (Gregory et al., 2018; Poudel, Stout, et al., 2014; Tabrizi et al., 2009). Period of monitoring was only twenty-four months, which may influence cause and effect of the outcome.

The predictive power of the diffusion model approach and mathematical analysis presented here has not yet been fully evaluated. The validity of the network diffusion model is related to the accuracy of the processing pipelines considered. We considered only the volumetric measurements (structural change) of the brain. Hence, inclusion of further details such as functional change in the brain may capture more vivid outcomes and validate the research aims. Our research results are based on a normative brain model of the human

connectome which may influence our findings. Specifically, these findings may not be necessarily useful in the context of other neurodegenerative diseases. Furthermore, we also analysed the data using group level-modelling and this approach cannot be used to make inferences on a personalised level. Another important question that arises is how these subnets are related to the patient's phenotype and other patient-specific characteristics. Subject characteristics other than brain imaging data (e.g. sex, age, education, genotype, depressive symptoms, cardiovascular disease, etc.) were not considered. Additionally, the implications of subnet identification for HD can be extended to other neurodegenerative diseases. When these important factors can be combined to form a comprehensive model, the ultimate end goal is to create a disease state and progression classifier, given all patient scans and connectivity data.

Despite the above limitations, we provide an advance computational model for characterizing and tracking the progression of brain changes in HD. This new knowledge regarding how the disease spreads within the brain network in the premanifest stage of HD will be critical in the field of monogenic neurodegenerative disorders. It will also help characterize various phenotypes within HD. The applications of such a framework in patient intervention and management are numerous, with the potential to provide non-invasive diagnostic, prognostic information, and sensitive measures of treatment efficacy.

The methodological innovations outlined in this application can build hybrid data-driven models by incorporating machine learning tools with bio-physical models such as NDM. This can help the development of personalized techniques for predicting future degeneration from baseline MRI scans. These personalized, predictive technologies will be suitable for a range of neurodegenerative diseases such as Huntington's and Alzheimer's disease and can potentially be applied to clinical work. Ultimately, the successful integration of these contributions represents a significant development in neurodegeneration research and will significantly improve the prognostic and predictive outcomes for patients.

6.4 Concluding Remarks

The overall aim of this thesis was to test the hypothesis that network diffusion model could be used to predict neurodegenerative changes in HD during the pre-manifest stage of the disease. Based on the findings from our empirical work, we showed that NDM can only moderately predict macroscopic consequences of disease in HD. However, the predictive arability of NDM used in this study is yet to be fully evaluated.

Appendices

Appendix A. Ethics Applications Report

ETHICS APPLICATIONS REPORT

Madan Kc (S00270745)

ECODE				
2019-380N	Application Title	Network Diffusion Model for Predicting Progressive Neurodegeneration Using Magnetic Resonance Imaging (MRI).		
	Status	Approved	Applied date	17/12/2019
	Risk Level	Deidentified Data	Date Approved	6/01/2020
	School	Mary MacKillop Institute for Health Research	Start	30/01/2020
	Investigators		End	31/01/2021

Appendix B. MATLAB script for Graph Theoretical Analysis

```
%%% MATLAB Code for Network Diffusion Model  %%%



ztestdata=readtable('../MATLAB/zstatL.xlsx');
all_label=ztestdata.Brain_regions(1:82);
atropy=-1*ztestdata.z_value(1:82)';
atropy(atropy<0)=0;
%Running NDM
beta=1;
time=1:40;

IITconnect=load('../MATLAB/IIT_connectivity_matrix.txt');
indx=[1:34,36:83];
conmat=IITconnect(indx,indx);

lh_seed=[1:41]; %This are roi locations corresponding to left and right hand side of the brain
rh_seed=[49:82,42:48];
c_indx=[1:34 49:82]; %Node index for cortical parcels
s_indx=[35:48]; % Node index for subcortical parcels


[eig_val,V]=generateLaplacian(conmat); % Generate lapacian vectors

[r_val_Patients,xt_Patients_all, atr_all]=runSeedingNDM_ss(eig_val,V,time,beta,atropy,lh_seed,rh_seed); % Run
seeding analysis for all bilateeral seeds
[vm_Patients, im_Patients]=sort(max(r_val_Patients),'descend'); % sort according to the correlation analysis
%fig_h1=generateRTCurves(r_val_Patients,time,[im_Patients(1:4)


xlabel('Time (a.u)', 'Fontsize', 24);
ylabel('Correlation (r-value)','Fontsize', 24);
%plot(time, r_val_Patients)
%title('GROUP BY TIME Correlation')
%xlabel('time')
%ylabel('correlation')

%Regions showing maxium correlation
all_label(im_Patients(1:5))

%indx=[1:34,36:83];
generateFSVolumes("aparc+aseg_mrtrix",indx,atropy,'brainresult_zscore.nii')

%

%end



%Generate Laplacian Matrix%

function [eig_val V]=generateLaplacian(mat)
```

```
%Generate degree normalised laplacian matrix from connectivity matrix
Deg=diag(sum(mat,2));
L=Deg-mat;

norm_vol=generateDegreeMatrix(diag(Deg));
L=L./norm_vol;

[V,Di]=eig(L);
eig_val=diag(Di);


% Generate Degree Matrix%

function [VolMat]=generateDegreeMatrix(Vol)
%Generate a degree matrix based on the input degree vector
sz=length(Vol);
VolMat=zeros(sz,sz);
for i=1:sz
  cn1=Vol(i);
   for j=1:sz
      cn2=Vol(j);
      VolMat(i,j)=sqrt(cn1*cn2);
   end
end

%Generate FS Volumes  %%

 function generateFSVolumes(atlasbrain,indx,atrophy,outbrain)

% A function that can read an atlas and change the values as per
   V=niftiread(atlasbrain);
   infos=niftiinfo(atlasbrain);

   all_indx=unique(V);

   Vs=V;
   n_indx=setdiff(all_indx,indx);


   for i=1:length(n_indx)

      Vs(find(Vs==n_indx(i)))=0;

   end

   for i=1:length(indx)

      Vs(find(Vs==indx(i)))=atrophy(i);

   end

   niftiwrite(Vs,outbrain,infos);

% Seeding Process in NDM %%

function [r_val xt_all atr_all]=runSeedingNDM(eig_val,V,time,beta,atropy,lh_seed,rh_seed)
% A function to run seeding analysis for bilateeral seeds specified in
% lh_seed and rh-seed
```

```
r_val=[];
xt_all=[];
atr_all=[];
atr_all=[];
ns=1:length(atropy);
for i=1:length(atropy)/2;
    xt=[];
    C0=zeros(1,length(eig_val))';
    C0(lh_seed(i))=1;
    C0(rh_seed(i))=1;
    u_ns=setdiff(ns,[lh_seed(i),rh_seed(i)]);
    [xt]=RunNDM(V,eig_val,C0,time,beta);
    r_val(:,i)=corr(xt(u_ns,:),atropy(u_ns)','type','Pearson');
    xt_all(:,:,i)=xt(u_ns,:);
    atr_all(:,i)=atropy(u_ns)';

    %xt_all(:,:,i)=xt(u_ns,:);
    %atr_all(:,:,i)=atropy(u_ns)';

End
```

Appendix C. R script for Statistical Analysis Using LMER

```r
library(lme4)
library (lmerTest) # Mixed model package by Douglas Bates, comes w/ pvalues!
library (texreg) #Helps us make tables of the mixed models
library (afex) # Easy ANOVA package to compare model fits
library (plyr) # Data manipulator package
library (ggplot2) # GGplot package for visualizing data
library(dplyr)
library(ggpubr)
library(multcomp)
library(effects)
library(psycho)
library(devtools)
library(report)
library(emmeans)
library(sjPlot)
library(sjmisc)
library(ggplot2)
library(prediction)


dataHDL<-read.csv("R_data_NDM_NORM_2021_v1.2.csv", sep = ",")
cat("The dataset has", dim(dataHDL)[1], "records, each with", dim(dataHDL)[2],
    "attributes.")
str(dataHDL)
head(dataHDL)
attach(dataHDL)

fgroup<-factor(group)
fgender<-factor(gender)
summary(dataHDL)

for (i in 7:88){
NDMmodL<-lmer(dataHD[,i] ~ fgroup*timepoints +fgender + age + (1|Subject.ID), data=dataHDL, REML=FALSE)
TimeInteractionL<- confint(glht(NDMmodL, linfct = c("fgroup1:timepoints = 0")))
summary(TimeInteractionL)
#results<-report(NDMmodL)
#qqnorm(resid(NDMmodL,xlab="residual",main=i))
#qqline(resid(NDMmodL))
#hist(resid(NDMmodL))
}
plot_model(NDMmodL, type = "int")


for (i in 7:88){
NDMmodQ<-lmer(dataHD[,i] ~ fgroup*I(timepoints^2) + fgender + age + (1|Subject.ID), data=dataHD, REML=FALSE)
summary(NDMmodQ)
TimeInteractionQ<- confint(glht(NDMmod1, linfct = c("fgroup1:I(timepoints^2) = 0")))
print(summary(TimeInteractionQ))
}
for (i in 7:88) {
NDMmodC<-lmer(dataHD[,i] ~ fgroup*timepoints + fgroup*I(timepoints^2) + fgender + age + (1|Subject.ID), data=dataHD, REML=FALSE)
summary(NDMmodC)
TimeInteractionC<- confint(glht(NDMmod1, linfct = c("fgroup1:timepoints + fgroup1:I(timepoints^2) = 0")))
print(summary(TimeInteractionC))
}
```

REFERENCES

Abdelnour, F., Voss, H. U., & Raj, A. (2014). Network diffusion accurately models the relationship between structural and functional brain connectivity networks. *Neuroimage, 90*, 335-347. doi:https://doi.org/10.1016/j.neuroimage.2013.12.039

Agosta, F., Galantucci, S., & Filippi, M. (2017). Advanced magnetic resonance imaging of neurodegenerative diseases. *Neurol Sci, 38*(1), 41-51. doi:10.1007/s10072-016-2764-x

AIHW. (2018). *Australian Burden of Disease Study 2015: fatal burden preliminary estimates*. Canberra: AIHW Retrieved from https://www.aihw.gov.au/reports/burden-of-disease/fatal-burden-2015-preliminary-estimates/contents/summary

Ambrose, C. M., Duyao, M. P., Barnes, G., Bates, G. P., Lin, C. S., Srinidhi, J., . . . MacDonald, M. E. (1994). Structure and expression of the Huntington's disease gene: evidence against simple inactivation due to an expanded CAG repeat. *Somat Cell Mol Genet, 20*(1), 27-38. doi:10.1007/bf02257483

Andrich, J., Arning, L., Wieczorek, S., Kraus, P. H., Gold, R., & Saft, C. (2008). Huntington's disease as caused by 34 CAG repeats. *Mov Disord, 23*(6), 879-881. doi:10.1002/mds.21958

Aylward, E. H., Codori, A. M., Rosenblatt, A., Sherr, M., Brandt, J., Stine, O. C., . . . Ross, C. A. (2000). Rate of caudate atrophy in presymptomatic and symptomatic stages of Huntington's disease. *Movement disorders: official journal of the Movement Disorder Society, 15*(3), 552-560.

Baig, S. S., Strong, M., & Quarrell, O. W. (2016). The global prevalence of Huntington's disease: a systematic review and discussion. *Neurodegener Dis Manag, 6*(4), 331-343. doi:10.2217/nmt-2016-0008

Bates, D., Mächler, M., Bolker, B., & Walker, S. (2014). Fitting linear mixed-effects models using lme4. *arXiv preprint arXiv:1406.5823*.

Bates, G. P., Mangiarini, L., Mahal, A., & Davies, S. W. (1997). Transgenic models of Huntington's disease. *Hum Mol Genet, 6*(10), 1633-1637. doi:10.1093/hmg/6.10.1633

Baxendale, S., Abdulla, S., Elgar, G., Buck, D., Berks, M., Micklem, G., . . . Lehrach, H. (1995). Comparative sequence analysis of the human and pufferfish Huntington's disease genes. *Nature Genetics, 10*(1), 67-76. doi:10.1038/ng0595-67

Bhattarai, A., Chen, Z., Chua, P., Talman, P., Mathers, S., Chapman, C., . . . Egan, G. F. (2021). Network diffusion model predicts neurodegeneration in limb-onset amyotrophic lateral sclerosis. *bioRxiv*, 2021.2007.2002.450445. doi:10.1101/2021.07.02.450445

Biglan, K. M., Shoulson, I., Kieburtz, K., Oakes, D., Kayson, E., Shinaman, M. A., . . . Hersch, S. (2016). Clinical-Genetic associations in the prospective Huntington at risk observational study (PHAROS): implications for clinical trials. *JAMA neurology, 73*(1), 102-110.

Blamire, A. M. (2018). MR approaches in neurodegenerative disorders. *Prog Nucl Magn Reson Spectrosc, 108*, 1-16. doi:10.1016/j.pnmrs.2018.11.001

Bohanna, I., Georgiou-Karistianis, N., & Egan, G. F. (2011). Connectivity-based segmentation of the striatum in Huntington's disease: Vulnerability of motor pathways. *Neurobiology of Disease, 42*(3), 475-481. doi:https://doi.org/10.1016/j.nbd.2011.02.010

Brundin, P., Melki, R., & Kopito, R. (2010). Prion-like transmission of protein aggregates in neurodegenerative diseases. *Nature Reviews Molecular Cell Biology, 11*(4), 301-307. doi:10.1038/nrm2873

Carbonell, F., Iturria-Medina, Y., & Evans, A. (2018). Mathematical Modeling of Protein Misfolding Mechanisms in Neurological Diseases: A Historical Overview. *Front. Neurol., 9*. doi:10.3389/fneur.2018.00037

Cicchetti, F., Lacroix, S., Cisbani, G., Vallières, N., Saint-Pierre, M., St-Amour, I., . . . Freeman, T. B. (2014). Mutant huntingtin is present in neuronal grafts in huntington disease patients. *Annals of Neurology, 76*(1), 31-42. doi:10.1002/ana.24174

Daniel, T. B., & Barry, G. (2015). Transcellular spreading of huntingtin aggregates in the Drosophila brain. *Proceedings of the National Academy of Sciences, 112*(39), E5427. doi:10.1073/pnas.1516217112

Davis, C. S. (2002). *Statistical methods for the analysis of repeated measurements*: Springer Science & Business Media.

Domínguez, D. J., Egan, G. F., Gray, M. A., Poudel, G. R., Churchyard, A., Chua, P., . . . Georgiou-Karistianis, N. (2013). Multi-modal neuroimaging in premanifest and early Huntington's disease: 18 month longitudinal data from the IMAGE-HD study. *PloS one, 8*(9), e74131. doi:10.1371/journal.pone.0074131

Domínguez, D. J., Poudel, G., Stout, J. C., Gray, M., Chua, P., Borowsky, B., . . . Georgiou-Karistianis, N. (2017). Longitudinal changes in the fronto-striatal network are associated with executive dysfunction and behavioral dysregulation in Huntington's disease: 30 months IMAGE-HD data. *Cortex, 92*, 139-149. doi:10.1016/j.cortex.2017.04.001

Dorsey, E. R., & Investigators, H. S. G. C. (2012). Characterization of a large group of individuals with Huntington disease and their relatives enrolled in the COHORT study. *PloS one, 7*(2), e29522.

Douaud, G., Gaura, V., Ribeiro, M. J., Lethimonnier, F., Maroy, R., Verny, C., . . . Remy, P. (2006). Distribution of grey matter atrophy in Huntington's disease patients: a combined ROI-based and voxel-based morphometric study. *Neuroimage, 32*(4), 1562-1575. doi:10.1016/j.neuroimage.2006.05.057

Duyao, M., Ambrose, C., Myers, R., Novelletto, A., Persichetti, F., Frontali, M., . . . et al. (1993). Trinucleotide repeat length instability and age of onset in Huntington's disease. *Nat Genet, 4*(4), 387-392. doi:10.1038/ng0893-387

Ehrlich, M. E. (2012). Huntington's disease and the striatal medium spiny neuron: cell-autonomous and non-cell-autonomous mechanisms of disease. *Neurotherapeutics, 9*(2), 270-284. doi:10.1007/s13311-012-0112-2

Estevez-Fraga, C., Scahill, R., Rees, G., Tabrizi, S. J., & Gregory, S. (2021). Diffusion imaging in Huntington's disease: comprehensive review. *Journal of Neurology, Neurosurgery & Psychiatry, 92*(1), 62-69. doi:10.1136/jnnp-2020-324377

Faria, A. V., Ratnanather, J. T., Tward, D. J., Lee, D. S., van den Noort, F., Wu, D., . . . Miller, M. I. (2016). Linking white matter and deep gray matter alterations in premanifest Huntington disease. *Neuroimage Clin, 11*, 450-460. doi:10.1016/j.nicl.2016.02.014

Fitzmaurice, G., Davidian, M., Verbeke, G., & Molenberghs, G. (2008). *Longitudinal data analysis*: CRC press.

Freeze, B., Acosta, D., Pandya, S., Zhao, Y., & Raj, A. (2018). Regional expression of genes mediating trans-synaptic alpha-synuclein transfer predicts regional atrophy in Parkinson disease. *NeuroImage: Clinical, 18*, 456-466.

Freeze, B., Pandya, S., Zeighami, Y., & Raj, A. (2019a). Regional transcriptional architecture of Parkinson's disease pathogenesis and network spread. *Brain : a journal of neurology, 142*(10), 3072. doi:10.1093/brain/awz223

Freeze, B., Pandya, S., Zeighami, Y., & Raj, A. (2019b). Regional transcriptional architecture of Parkinson's disease pathogenesis and network spread. *Brain, 142*(10), 3072-3085.

Frisoni, G. B., Fox, N. C., Jack, C. R., Jr., Scheltens, P., & Thompson, P. M. (2010). The clinical use of structural MRI in Alzheimer disease. *Nature reviews. Neurology, 6*(2), 67-77. doi:10.1038/nrneurol.2009.215

Fulcher, B. D., & Fornito, A. (2016). A transcriptional signature of hub connectivity in the mouse connectome. *Proceedings of the National Academy of Sciences, 113*(5), 1435. doi:10.1073/pnas.1513302113

Garcia, T. P., & Marder, K. (2017). Statistical Approaches to Longitudinal Data Analysis in Neurodegenerative Diseases: Huntington's Disease as a Model. *Curr Neurol Neurosci Rep, 17*(2), 14. doi:10.1007/s11910-017-0723-4

Georgiou-Karistianis, N., Scahill, R., Tabrizi, S. J., Squitieri, F., & Aylward, E. (2013). Structural MRI in Huntington's disease and recommendations for its potential use in clinical trials. *Neuroscience and Biobehavioral Reviews, 37*(3), 480-490. doi:10.1016/j.neubiorev.2013.01.022

Gibbons, R. D., Hedeker, D., & DuToit, S. (2010). Advances in analysis of longitudinal data. *Annu Rev Clin Psychol, 6*, 79-107. doi:10.1146/annurev.clinpsy.032408.153550

Greer, M. L., Pujo-Menjouet, L., & Webb, G. F. (2006). A mathematical analysis of the dynamics of prion proliferation. *Journal of Theoretical Biology, 242*(3), 598-606. doi:10.1016/j.jtbi.2006.04.010

Gregory, S., Long, J. D., Kloppel, S., Razi, A., Scheller, E., Minkova, L., . . . Rees, G. (2018). Testing a longitudinal compensation model in premanifest Huntington's disease. *Brain, 141*(7), 2156-2166. doi:10.1093/brain/awy122

Gusella, J. F., Wexler, N. S., Conneally, P. M., Naylor, S. L., Anderson, M. A., Tanzi, R. E., . . . et al. (1983). A polymorphic DNA marker genetically linked to Huntington's disease. *Nature, 306*(5940), 234-238. doi:10.1038/306234a0

Halliday, G. M., McRitchie, D. A., Macdonald, V., Double, K. L., Trent, R. J., & McCusker, E. (1998). Regional Specificity of Brain Atrophy in Huntington's Disease. *Experimental Neurology, 154*(2), 663-672. doi:https://doi.org/10.1006/exnr.1998.6919

He, Y., Chen, Z., & Evans, A. (2008). Structural insights into aberrant topological patterns of large-scale cortical networks in Alzheimer's disease. *Journal of Neuroscience, 28*(18), 4756-4766.

Heinsen, H., Strik, M., Bauer, M., Luther, K., Ulmar, G., Gangnus, D., . . . Götz, M. (1994). Cortical and striatal neurone number in Huntington's disease. *Acta Neuropathol, 88*(4), 320-333. doi:10.1007/bf00310376

Hobbs, N. Z., Henley, S. M., Ridgway, G. R., Wild, E. J., Barker, R. A., Scahill, R. I., . . . Tabrizi, S. J. (2010). The progression of regional atrophy in premanifest and early Huntington's disease: a longitudinal voxel-based morphometry study. *J Neurol Neurosurg Psychiatry, 81*(7), 756-763. doi:10.1136/jnnp.2009.190702

Hobbs, N. Z., Henley, S. M., Ridgway, G. R., Wild, E. J., Barker, R. A., Scahill, R. I., . . . Tabrizi, S. J. (2010). The progression of regional atrophy in premanifest and early Huntington's disease: a longitudinal voxel-based morphometry study. *Journal of Neurology, Neurosurgery & Psychiatry, 81*(7), 756-763.

Hobbs, N. Z., Henley, S. M., Wild, E. J., Leung, K. K., Frost, C., Barker, R. A., . . . Fox, N. C. (2009). Automated quantification of caudate atrophy by local registration of serial MRI: evaluation and application in Huntington's disease. *Neuroimage, 47*(4), 1659-1665. doi:10.1016/j.neuroimage.2009.06.003

Iturria-Medina, Y., Canales-Rodríguez, E. J., Melie-García, L., Valdés-Hernández, P. A., Martínez-Montes, E., Alemán-Gómez, Y., & Sánchez-Bornot, J. M. (2007). Characterizing brain anatomical connections using diffusion weighted MRI and graph theory. *Neuroimage, 36*(3), 645-660. doi:10.1016/j.neuroimage.2007.02.012

Jansen, A. H., Batenburg, K. L., Pecho-Vrieseling, E., & Reits, E. A. (2017). Visualization of prion-like transfer in Huntington's disease models. *Biochim Biophys Acta Mol Basis Dis, 1863*(3), 793-800. doi:10.1016/j.bbadis.2016.12.015

Jech, R., Klempír, J., Vymazal, J., Zidovská, J., Klempírová, O., Růzicka, E., & Roth, J. (2007). Variation of selective gray and white matter atrophy in Huntington's disease. *Mov Disord, 22*(12), 1783-1789. doi:10.1002/mds.21620

Jedynak, B. M., Lang, A., Liu, B., Katz, E., Zhang, Y., Wyman, B. T., . . . Prince, J. L. (2012). A computational neurodegenerative disease progression score: Method and results with the Alzheimer's disease neuroimaging initiative cohort. *Neuroimage, 63*(3), 1478-1486. doi:10.1016/j.neuroimage.2012.07.059

Jelescu, I. O., & Budde, M. D. (2017). Design and Validation of Diffusion MRI Models of White Matter. *Frontiers in Physics, 5*(61). doi:10.3389/fphy.2017.00061

Jeon, I., Cicchetti, F., Cisbani, G., Lee, S., Li, E., Bae, J., . . . Song, J. (2016). Human-to-mouse prion-like propagation of mutant huntingtin protein.(Original Paper). *Acta Neuropathologica, 132*(4), 577. doi:10.1007/s00401-016-1582-9

Karlovich, C. A., John, R. M., Ramirez, L., Stainier, D. Y., & Myers, R. M. (1998). Characterization of the Huntington's disease (HD) gene homologue in the zebrafish Danio rerio. *Gene, 217*(1-2), 117-125. doi:10.1016/s0378-1119(98)00342-4

Kenney, C., Powell, S., & Jankovic, J. (2007). Autopsy-proven Huntington's disease with 29 trinucleotide repeats. *Mov Disord, 22*(1), 127-130. doi:10.1002/mds.21195

Klöppel, S., Draganski, B., Golding, C. V., Chu, C., Nagy, Z., Cook, P. A., . . . Parker, G. J. (2008). White matter connections reflect changes in voluntary-guided saccades in pre-symptomatic Huntington's disease. *Brain, 131*(1), 196-204.

Kloppel, S., Gregory, S., Scheller, E., Minkova, L., Razi, A., Durr, A., . . . Track-On, i. (2015). Compensation in Preclinical Huntington's Disease: Evidence From the Track-On HD Study. *EBioMedicine, 2*(10), 1420-1429. doi:10.1016/j.ebiom.2015.08.002

Klöppel, S., Gregory, S., Scheller, E., Minkova, L., Razi, A., Durr, A., . . . Tabrizi, S. J. (2015). Compensation in Preclinical Huntington's Disease: Evidence From the Track-On HD Study. *EBioMedicine, 2*(10), 1420-1429. doi:https://doi.org/10.1016/j.ebiom.2015.08.002

Koikkalainen, J., Rhodius-Meester, H., Tolonen, A., Barkhof, F., Tijms, B., Lemstra, A. W., . . . Jyrki. (2016). Differential diagnosis of neurodegenerative diseases using structural MRI data. *NeuroImage: Clinical, 11*(C), 435-449. doi:10.1016/j.nicl.2016.02.019

Laird, N. M., & Ware, J. H. (1982). Random-effects models for longitudinal data. *Biometrics*, 963-974.

Li, Z., Karlovich, C. A., Fish, M. P., Scott, M. P., & Myers, R. M. (1999). A putative Drosophila homolog of the Huntington's disease gene. *Hum Mol Genet, 8*(9), 1807-1815. doi:10.1093/hmg/8.9.1807

Liang, K.-Y., & Zeger, S. L. (1986). Longitudinal data analysis using generalized linear models. *Biometrika, 73*(1), 13-22.

Lo, C.-Y., Wang, P.-N., Chou, K.-H., Wang, J., He, Y., & Lin, C.-P. (2010). Diffusion tensor tractography reveals abnormal topological organization in structural cortical networks in Alzheimer's disease. *Journal of Neuroscience, 30*(50), 16876-16885.

Long, J. D., Paulsen, J. S., Marder, K., Zhang, Y., Kim, J.-I., Mills, J. A., & Group, t. R. o. t. P.-H. H. s. S. (2014). Tracking motor impairments in the progression of Huntington's disease. *Movement Disorders, 29*(3), 311-319. doi:https://doi.org/10.1002/mds.25657

MacDonald, M. E., Ambrose, C. M., Duyao, M. P., Myers, R. H., Lin, C., Srinidhi, L., . . . Harper, P. S. (1993). A novel gene containing a trinucleotide repeat that is expanded and unstable on Huntington's disease chromosomes. *Cell, 72*(6), 971-983. doi:https://doi.org/10.1016/0092-8674(93)90585-E

Mangiarini, L., Sathasivam, K., Seller, M., Cozens, B., Harper, A., Hetherington, C., . . . Bates, G. P. (1996). Exon 1 of the HD Gene with an Expanded CAG Repeat Is Sufficient to Cause a Progressive Neurological Phenotype in Transgenic Mice. *Cell, 87*(3), 493-506. doi:10.1016/S0092-8674(00)81369-0

Maroof, D. A., Gross, A. L., & Brandt, J. (2011). Modeling longitudinal change in motor and cognitive processing speed in presymptomatic Huntington's disease. *Journal of clinical and experimental neuropsychology, 33*(8), 901-909.

Masnata, M., & Cicchetti, F. (2017). The Evidence for the Spread and Seeding Capacities of the Mutant Huntingtin Protein in Systems and Their Therapeutic Implications. *Frontiers in neuroscience, 11*, 647. doi:10.3389/fnins.2017.00647

Matsuyama, N., Hadano, S., Onoe, K., Osuga, H., Showguchi-Miyata, J., Gondo, Y., & Ikeda, J.-E. (2000). Identification and Characterization of the Miniature Pig Huntington's Disease Gene Homolog: Evidence for Conservation and Polymorphism in the CAG Triplet Repeat. *Genomics, 69*(1), 72-85. doi:https://doi.org/10.1006/geno.2000.6317

Matthaus, F. (2009). The spread of prion disease in the brain - Models of reaction and transport on network. *Journal of Biological Systems, 17*(04), 623-641. doi:10.1142/s0218339009003010

Matthäus, F. (2006). Diffusion versus network models as descriptions for the spread of prion diseases in the brain. *Journal of Theoretical Biology, 240*(1), 104-113. doi:10.1016/j.jtbi.2005.08.030

McColgan, P., Seunarine, K. K., Gregory, S., Razi, A., Papoutsi, M., Long, J. D., . . . Roos, R. A. (2017). Topological length of white matter connections predicts their rate of atrophy in premanifest Huntington's disease. *JCI insight, 2*(8).

McColgan, P., Seunarine, K. K., Razi, A., Cole, J. H., Gregory, S., Durr, A., . . . Track, H. D. I. (2015). Selective vulnerability of Rich Club brain regions is an organizational principle of structural connectivity loss in Huntington's disease. *Brain : a journal of neurology, 138*(Pt 11), 3327-3344. doi:10.1093/brain/awv259

McKiernan, E. F., & O'brien, J. T. (2017). 7t mri for neurodegenerative dementias in vivo: A systematic review of the literature. *Journal of Neurology, Neurosurgery & Psychiatry, 88*(7), 564.

McNeil, S. M., Novelletto, A., Srinidhi, J., Barnes, G., Kornbluth, I., Altherr, M. R., . . . Myers, R. H. (1997). Reduced penetrance of the Huntington's disease mutation. *Hum Mol Genet, 6*(5), 775-779. doi:10.1093/hmg/6.5.775

Mitchell, I., Cooper, A., & Griffiths, M. (1999). The selective vulnerability of striatopallidal neurons. *Prog. Neurobiol., 59*(6), 691-719. doi:10.1016/S0301-0082(99)00019-2

Moradi, Elaheh, Pepe, Antonietta, Gaser, Christian, . . . Jussi. (2015). Machine learning framework for early MRI-based Alzheimer's conversion prediction in MCI subjects. *Neuroimage, 104*, 398-412. doi:10.1016/j.neuroimage.2014.10.002

Müller, H.-P., & Kassubek, J. (2013). Diffusion tensor magnetic resonance imaging in the analysis of neurodegenerative diseases. *Journal of visualized experiments : JoVE*(77), 50427. doi:10.3791/50427

Neil P. Oxtoby , & Daniel C. Alexander. (2017). Imaging plus X: multimodal models of neurodegenerative disease. *Current Opinion in Neurology 30*. doi:10.1097/WCO.0000000000000460

Oxtoby, N., P,, Young, A., L,, Marinescu, Razvan, Valentin, & Alexander, D., C,. (2017). Data-driven models of disease progression and applications to alzheimer disease: Event-based model and differential quation models of biomarkers changes in ADNI. *Alzheimer's & Dementia: The Journal of the Alzheimer's Association, 13*(7), P1323-P1325. doi:10.1016/j.jalz.2017.06.2031

Palop, J. J., & Mucke, L. (2010). Amyloid-β–induced neuronal dysfunction in Alzheimer's disease: from synapses toward neural networks. *Nature neuroscience, 13*(7), 812-818.

Pandya, S., Mezias, C., & Raj, A. (2017). Predictive Model of Spread of Progressive Supranuclear Palsy Using Directional Network Diffusion. *Frontiers in Neurology, 8*(692). doi:10.3389/fneur.2017.00692

Pandya, S., Zeighami, Y., Freeze, B., Dadar, M., Collins, D. L., Dagher, A., & Raj, A. (2019). Predictive model of spread of Parkinson's pathology using network diffusion. *Neuroimage, 192*, 178-194. doi:10.1016/j.neuroimage.2019.03.001

Paulsen, J. S., Langbehn, D. R., Stout, J. C., Aylward, E., Ross, C. A., Nance, M., . . . Coordinators of the Huntington Study, G. (2008). Detection of Huntington's disease decades before diagnosis: the Predict-HD study. *J Neurol Neurosurg Psychiatry, 79*(8), 874-880. doi:10.1136/jnnp.2007.128728

Paulsen, J. S., Long, J. D., Johnson, H. J., Aylward, E. H., Ross, C. A., Williams, J. K., . . . Harrington, D. L. (2014). Clinical and biomarker changes in premanifest Huntington disease show trial feasibility: a decade of the PREDICT-HD study. *Frontiers in aging neuroscience, 6*, 78.

Payne, R. J., & Krakauer, D. C. (1998). The spatial dynamics of prion disease. *Proc Biol Sci, 265*(1412), 2341-2346. doi:10.1098/rspb.1998.0581

Pearce, M. M., Spartz, E., Hong, W., Luo, L., & Kopito, R. (2015). Prion-like transmission of neuronal huntingtin aggregates to phagocytic glia in the Drosophila brain. *Nature Communications, 6*(1), 6768. doi:10.1038/ncomms7768

Pecho-Vrieseling, E., Rieker, C., Fuchs, S., Bleckmann, D., Esposito, M. S., Botta, P., . . . Di Giorgio, F. P. (2014). Transneuronal propagation of mutant huntingtin contributes to non-cell autonomous pathology in neurons. *Nature neuroscience, 17*(8), 1064. doi:10.1038/nn.3761

Pinheiro, J., & Bates, D. (2002). *Mixed-Effect Models in S and S-plus* (Vol. 96).

Poudel, G. R., Dominguez D, J. F., Verhelst, H., Vander Linden, C., Deblaere, K., Jones, D. K., . . . Caeyenberghs, K. (2020). Network diffusion modeling predicts neurodegeneration in traumatic brain injury. *Annals of Clinical and Translational Neurology, 7*(3), 270-279. doi:10.1002/acn3.50984

Poudel, G. R., Egan, G. F., Churchyard, A., Chua, P., Stout, J. C., & Georgiou-Karistianis, N. (2014). Abnormal synchrony of resting state networks in premanifest and symptomatic Huntington disease: the IMAGE-HD study.(Research Paper)(Clinical report). *Journal of Psychiatry and Neuroscience, 39*(2), 87.

Poudel, G. R., Harding, I. H., Egan, G. F., & Georgiou-Karistianis, N. (2019). Network spread determines severity of degeneration and disconnection in Huntington's disease. *Hum Brain Mapp, 40*(14), 4192-4201. doi:10.1002/hbm.24695

Poudel, G. R., Harding, I. H., Egan, G. F., & Georgiou-Karistianis, N. (2019). Network spread determines severity of degeneration and disconnection in Huntington's disease. *Human Brain Mapping, 40*(14), 4192-4201. doi:10.1002/hbm.24695

Poudel, G. R., Stout, J. C., Domínguez D, J. F., Churchyard, A., Chua, P., Egan, G. F., & Georgiou-Karistianis, N. (2015). Longitudinal change in white matter microstructure in Huntington's disease: The IMAGE-HD study. *Neurobiology of Disease, 74*, 406-412. doi:https://doi.org/10.1016/j.nbd.2014.12.009

Poudel, G. R., Stout, J. C., Domínguez D, J. F., Churchyard, A., Chua, P., Egan, G. F., & Georgiou-Karistianis, N. (2015). Longitudinal change in white matter microstructure in Huntington's disease: The IMAGE-HD study. *Neurobiology of Disease, 74*(1), 406-412. doi:10.1016/j.nbd.2014.12.009

Poudel, G. R., Stout, J. C., Domínguez D, J. F., Salmon, L., Churchyard, A., Chua, P., . . . Egan, G. F. (2014). White matter connectivity reflects clinical and cognitive status in Huntington's disease. *Neurobiology of Disease, 65*, 180-187. doi:10.1016/j.nbd.2014.01.013

Poudel, G. R., Stout, J. C., Salmon, L., Churchyard, A., Chua, P., Georgiou-Karistianis, N., & Egan, G. F. (2014). White matter connectivity reflects clinical and cognitive status in Huntington's disease. *Neurobiology of Disease, 65*, 180-187.

Qi, X., & Arfanakis, K. (2021). Regionconnect: Rapidly extracting standardized brain connectivity information in voxel-wise neuroimaging studies. *Neuroimage, 225*, 117462. doi:https://doi.org/10.1016/j.neuroimage.2020.117462

Raj, A. (2015). Graph models of brain diseases. *2015*, 1552-1555. doi:10.1109/ISBI.2015.7164174

Raj, A., & Iturria-Medina, Y. (2019). Editorial: Network Spread Models of Neurodegenerative Diseases. *Frontiers in Neurology, 9*(1159). doi:10.3389/fneur.2018.01159

Raj, A., Kuceyeski, A., & Weiner, M. (2012). A Network Diffusion Model of Disease Progression in Dementia. *Neuron, 73*(6), 1204-1215. doi:10.1016/j.neuron.2011.12.040

Raj, A., Locastro, E., Kuceyeski, A., Tosun, D., Relkin, N., & Weiner, M. (2015). Network Diffusion Model of Progression Predicts Longitudinal Patterns of Atrophy and Metabolism in Alzheimer's Disease. *Cell Reports, 10*(3), 359-369. doi:10.1016/j.celrep.2014.12.034

Raj, A., & Powell, F. (2018). Models of Network Spread and Network Degeneration in Brain Disorders. *Biological Psychiatry: Cognitive Neuroscience and Neuroimaging, 3*(9), 788-797. doi:https://doi.org/10.1016/j.bpsc.2018.07.012

Raj, A., & Powell, F. (2021). Network model of pathology spread recapitulates neurodegeneration and selective vulnerability in Huntington's Disease. *Neuroimage, 235*, 118008. doi:https://doi.org/10.1016/j.neuroimage.2021.118008

Read, A. P. (1993). Huntington's disease: testing the test. *Nat Genet, 4*(4), 329-330. doi:10.1038/ng0893-329

Reiner, A., Dragatsis, I., & Dietrich, P. (2011). Genetics and neuropathology of Huntington's disease. *Int Rev Neurobiol, 98*, 325-372. doi:10.1016/b978-0-12-381328-2.00014-6

Ren, P.-H., Lauckner, J. E., Kachirskaia, I., Heuser, J. E., Melki, R., & Kopito, R. R. (2009). Cytoplasmic penetration and persistent infection of mammalian cells by polyglutamine aggregates. *Nature Cell Biology, 11*(2), 219-225. doi:10.1038/ncb1830

Reuter, M., Schmansky, N. J., Rosas, H. D., & Fischl, B. (2012). Within-subject template estimation for unbiased longitudinal image analysis. *Neuroimage, 61*(4), 1402-1418. doi:10.1016/j.neuroimage.2012.02.084

Risacher, S. L., & Saykin, A. J. (2013). Neuroimaging biomarkers of neurodegenerative diseases and dementia. *Semin Neurol, 33*(4), 386-416. doi:10.1055/s-0033-1359312

Rodrigues, F. B., Byrne, L. M., Tortelli, R., Johnson, E. B., Wijeratne, P. A., Arridge, M., . . . Wild, E. J. (2020). Mutant huntingtin and neurofilament light have distinct longitudinal dynamics in Huntington's disease. *Sci Transl Med, 12*(574). doi:10.1126/scitranslmed.abc2888

Roos, R. A., Pruyt, J. F., de Vries, J., & Bots, G. T. (1985). Neuronal distribution in the putamen in Huntington's disease. *J Neurol Neurosurg Psychiatry, 48*(5), 422-425. doi:10.1136/jnnp.48.5.422

Rosas, H. D., Salat, D. H., Lee, S. Y., Zaleta, A. K., Pappu, V., Fischl, B., . . . Hersch, S. M. (2008). Cerebral cortex and the clinical expression of Huntington's disease: complexity and heterogeneity. *Brain, 131*(4), 1057-1068.

Rosas, H. D., Tuch, D. S., Hevelone, N. D., Zaleta, A. K., Vangel, M., Hersch, S. M., & Salat, D. H. (2006). Diffusion tensor imaging in presymptomatic and early Huntington's disease: Selective white matter pathology and its relationship to clinical measures. *Movement disorders: official journal of the Movement Disorder Society, 21*(9), 1317-1325.

Santa-Cecilia, F., Leite, C., Del-Bel, E., & Raisman-Vozari, R. (2019). The Neuroprotective Effect of Doxycycline on Neurodegenerative Diseases. *Neurotoxicity Research, 35*(4), 981-986. doi:10.1007/s12640-019-00015-z

Saxena, S., & Caroni, P. (2011). Selective neuronal vulnerability in neurodegenerative diseases: from stressor thresholds to degeneration. *Neuron, 71*(1), 35-48.

Seeley, W. W., Crawford, R. K., Zhou, J., Miller, B. L., & Greicius, M. D. (2009). Neurodegenerative diseases target large-scale human brain networks. *Neuron, 62*(1), 42-52.

Selemon, L. D., Rajkowska, G., & Goldman-Rakic, P. S. (2004). Evidence for progression in frontal cortical pathology in late-stage Huntington's disease. *J Comp Neurol, 468*(2), 190-204. doi:10.1002/cne.10938

Seppi, K., Schocke, M. F., Mair, K. J., Esterhammer, R., Weirich-Schwaiger, H., Utermann, B., . . . Wenning, G. K. (2006). Diffusion-weighted imaging in Huntington's disease. *Mov Disord, 21*(7), 1043-1047. doi:10.1002/mds.20868

Shaw, R. G., & Mitchell-Olds, T. (1993). ANOVA for unbalanced data: an overview. *Ecology, 74*(6), 1638-1645.

Shimizu, S., Hirose, D., Hatanaka, H., Takenoshita, N., Kaneko, Y., Ogawa, Y., . . . Hanyu, H. (2018). Role of Neuroimaging as a Biomarker for Neurodegenerative Diseases. *Front Neurol, 9*, 265. doi:10.3389/fneur.2018.00265

Solberg, O. K., Filkuková, P., Frich, J. C., & Feragen, K. J. B. (2018). Age at Death and Causes of Death in Patients with Huntington Disease in Norway in 1986-2015. *J Huntingtons Dis, 7*(1), 77-86. doi:10.3233/jhd-170270

Sturrock, A., Laule, C., Wyper, K., Milner, R. A., Decolongon, J., Santos, R. D., . . . Leavitt, B. R. (2015). A longitudinal study of magnetic resonance spectroscopy Huntington's disease biomarkers. *Movement Disorders, 30*(3), 393-401. doi:10.1002/mds.26118

Tabrizi, S. J., Langbehn, D. R., Leavitt, B. R., Roos, R. A., Durr, A., Craufurd, D., . . . Stout, J. C. (2009). Biological and clinical manifestations of Huntington's disease in the longitudinal TRACK-HD study: cross-sectional analysis of baseline data. *Lancet Neurol, 8*(9), 791-801. doi:10.1016/s1474-4422(09)70170-x

Tabrizi, S. J., Scahill, R. I., Durr, A., Roos, R. A., Leavitt, B. R., Jones, R., . . . Stout, J. C. (2011). Biological and clinical changes in premanifest and early stage Huntington's disease in the TRACK-HD study: the 12-month longitudinal analysis. *The Lancet Neurology, 10*(1), 31-42. doi:10.1016/S1474-4422(10)70276-3

Tabrizi, S. J., Scahill, R. I., Owen, G., Durr, A., Leavitt, B. R., Roos, R. A., . . . Johnson, H. (2013). Predictors of phenotypic progression and disease onset in premanifest and early-stage Huntington's disease in the TRACK-HD study: analysis of 36-month observational data. *The Lancet Neurology, 12*(7), 637-649.

Torok, J., Maia, P. D., Powell, F., Pandya, S., & Raj, A. (2018). A method for inferring regional origins of neurodegeneration. *Brain, 141*(3), 863-876. doi:10.1093/brain/awx371

Trevino, R., Lauckner, J., Sourigues, Y., Pearce, M. M., Bousset, L., Melki, R., & Kopito, R. (2012). Fibrillar Structure and Charge Determine the Interaction of Polyglutamine

Protein Aggregates with the Cell Surface. *J. Biol. Chem., 287*(35), 29722-29728. doi:10.1074/jbc.M112.372474

van den Bogaard, S. J. A., Dumas, E. M., Acharya, T. P., Johnson, H., Langbehn, D. R., Scahill, R. I., . . . Group, T.-H. I. (2011). Early atrophy of pallidum and accumbens nucleus in Huntington's disease. *Journal of Neurology, 258*(3), 412-420. doi:10.1007/s00415-010-5768-0

Van Raamsdonk, J. M., Pearson, J., Murphy, Z., Hayden, M. R., & Leavitt, B. R. (2006). Wild-type huntingtin ameliorates striatal neuronal atrophy but does not prevent other abnormalities in the YAC128 mouse model of Huntington disease. *BMC Neuroscience, 7*(1), 80. doi:10.1186/1471-2202-7-80

Vemuri, P., & Jack, C. R. (2010). Role of structural MRI in Alzheimer's disease. *Alzheimer's Research & Therapy, 2*(4), 23. doi:10.1186/alzrt47

Verbeke, G. (1997). Linear mixed models for longitudinal data. In *Linear mixed models in practice* (pp. 63-153): Springer.

Vock, D. M., Davidian, M., Tsiatis, A. A., & Muir, A. J. (2012). Mixed model analysis of censored longitudinal data with flexible random-effects density. *Biostatistics, 13*(1), 61-73. doi:10.1093/biostatistics/kxr026

Vonsattel, J. P. (2008). Huntington disease models and human neuropathology: similarities and differences. *Acta Neuropathol, 115*(1), 55-69. doi:10.1007/s00401-007-0306-6

Vonsattel, J. P., & DiFiglia, M. (1998). Huntington disease. *J Neuropathol Exp Neurol, 57*(5), 369-384. doi:10.1097/00005072-199805000-00001

Wagster, M. V., Hedreen, J. C., Peyser, C. E., Folstein, S. E., & Ross, C. A. (1994). Selective loss of [3H]kainic acid and [3H]AMPA binding in layer VI of frontal cortex in Huntington's disease. *Exp Neurol, 127*(1), 70-75. doi:10.1006/exnr.1994.1081

Wang, Z., Zhu, X., Adeli, E., Zhu, Y., Nie, F., Munsell, B., & Wu, G. (2017). Multi-modal classification of neurodegenerative disease by progressive graph-based transductive learning. *Medical Image Analysis, 39*, 218-230. doi:10.1016/j.media.2017.05.003

Weston, P. S. J., Simpson, I. J. A., Ryan, N. S., Ourselin, S., & Fox, N. C. (2015). Diffusion imaging changes in grey matter in Alzheimer's disease: a potential marker of early neurodegeneration. *Alzheimer's Research & Therapy, 7*(1), 47. doi:10.1186/s13195-015-0132-3

Wijeratne, P. A., Johnson, E. B., Eshaghi, A., Aksman, L., Gregory, S., Johnson, H. J., . . . Alexander, D. C. (2020). Robust Markers and Sample Sizes for Multicenter Trials of Huntington Disease. *Annals of Neurology, 87*(5), 751-762. doi:https://doi.org/10.1002/ana.25709

Wyss-Coray, T. (2016). Ageing, neurodegeneration and brain rejuvenation. *Nature, 539*(7628), 180-186. doi:10.1038/nature20411

Zeger, S. L., & Liang, K.-Y. (1992). An overview of methods for the analysis of longitudinal data. *Statistics in Medicine, 11*(14-15), 1825-1839. doi:https://doi.org/10.1002/sim.4780111406

Zhang, X., Mormino, E. C., Sun, N., Sperling, R. A., Sabuncu, M. R., & Yeo, B. T. T. (2016). Bayesian model reveals latent atrophy factors with dissociable cognitive trajectories in Alzheimer's disease. *Proceedings of the National Academy of Sciences of the United States of America, 113*(42), E6535. doi:10.1073/pnas.1611073113